BIOMIMETIC MICROPATTERNING OF ELECTROSPUN SCAFFOLDS FOR TISSUE ENGINEERING

by

Eric Meade Jeffries

Bachelor of Science, University of Pittsburgh, 2009

Submitted to the Graduate Faculty of

Swanson School of Engineering in partial fulfillment

of the requirements for the degree of

Doctor of Philosophy

University of Pittsburgh

2014

UNIVERSITY OF PITTSBURGH

SWANSON SCHOOL OF ENGINEERING

This dissertation was presented

by

Eric Meade Jeffries

It was defended on

July 11, 2014

and approved by

Martin Oudega, Ph.D. Assistant Professor, Physical Medicine & Rehabilitation

William Wagner, Ph.D. Professor, Bioengineering

Douglas Weber, Ph.D. Assistant Professor, Bioengineering

Dissertation Director: Yadong Wang, Ph.D. Professor, Bioengineering

BIOMIMETIC MICROPATTERNING OF ELECTROSPUN SCAFFOLDS FOR TISSUE ENGINEERING

Eric M. Jeffries, PhD

University of Pittsburgh, 2014

The nanostructure of the extracellular matrix (ECM) can direct cell attachment, alignment, and organization. Similarly, ECM micropatterns such as tubes and branched networks organize cells into larger functional units. To mimic this complex cellular microenvironment in tissue engineered scaffolds, we need new fabrication methods capable of constructing structures on both the nano- and micro-scale. Furthermore, these methods should be compatible with a variety of biomaterials to allow tailoring of mechanical and degradation properties. Electrospinning is a useful technique for creating fibrous scaffolds, but there have been few reports introducing micropatterns.

This dissertation describes the development of a new versatile fabrication approach that combines electrospinning with a fused deposition modeling (FDM) 3D printer to create micropatterns that mimic tissues. We hypothesized that these structures would improve cell migration and positioning within electrospun scaffolds. We tested this hypothesis by patterning scaffolds for peripheral nerves and microvascular networks. We first demonstrate the feasibility of templated electrospinning for generating linear channels in fibrous nerve guides that mimic the endoneurial/fascicular tubes of nerve and promote faster Schwann cell infiltration. This micropatterning technique was combined with FDM production of branched templates to create microvascular networks within fibrous scaffolds. Finally, material properties were improved by developing a technique to fabricates scaffolds with electrospun poly(glycerol sebacate)(PGS).

TABLE OF CONTENTS

LIST OF TABLES

LIST OF FIGURES

PREFACE

I would first like to thank my advisor, Dr. Yadong Wang, for giving me the opportunity to participate in exciting research and for providing me with an enjoyable graduate experience. You are a great mentor and I consider it a blessing to have worked under your guidance. I would like to thank my graduate committee members: Dr. Martin Oudega, Dr. William Wagner, and Dr. Doug Weber for their direction and support throughout my doctoral program.

I would like to thank all members of the Biomaterials Foundry. I have learned so much from everyone sharing their expertise and am grateful for all of your time and support. Working with all of you has really motivated and encouraged me throughout this entire process and I am fortunate to call so many of my colleagues my friends.

Finally, I would like to thank my family who initiated my technical interests and offered continual encouragement throughout my life. Thank you for teaching me the value of hard work and determination.

1.0 INTRODUCTION

Tissue engineering has made significant progress in developing clinical therapies for flat (skin), hollow (bladder), and avascular (cartilage) tissues.[1-3] However, successful tissue engineering of larger organs has been more elusive for several reasons:

1) A hierarchical 3D structure must be reconstructed and populated by appropriate cell type.[4] These structures include linear channels (eg: fascicles in nerve, muscle, and tendon; Haversian canals in bone) and branched networks (eg: biliary ducts in the liver, respiratory airways of the lungs, and collection ducts in kidneys)

2) Vascular support is necessary since cells cannot survive on diffusion alone in solid organs greater than 2-3mm^3 volume.[4-6]

3) Porosity must be balanced with mechanical/degradation properties to resist physiological loads while permitting resorption and remodeling.[7]

Due to the small scale of many biological structures, microfabrication has been useful in investigating the role of topographical cues on cell morphology, differentiation, and adhesion.[8] However, most microfabrication (MF) and solid free-form fabrication (SFF) methods were not designed with the porosity and degradability necessary for tissue engineering applications. Similarly, many tissue engineering approaches cannot match the high resolution and spatial control of microfabrication. Thus, significant hurdles remain for successfully creating biomimetic scaffolds for large organ repair.

1.1 SIGNIFICANCE

Organ transplantation remains the standard treatment for failure of vital organs. However, since the number of candidates on waiting lists (Figure 1) far exceeds the allograft donors, thousands die before receiving a transplant.[9] The kidney wait list is the largest and has increased steadily over the past decade to almost 60,000 candidates currently.[10] Liver has the second largest waiting list and remains close to 15,000.[10] Lung and heart waiting lists have shown the most rapid increases in the past 5 years.[10] While the number of candidates awaiting a particular organ fluctuates by year, the overall trend of organ shortage continues to grow. This trend is expected to worsen as the average life span grows. One promising solution is the use of tissue engineering to circumvent the donor shortage and avoid the need of immunosuppressants.[11]

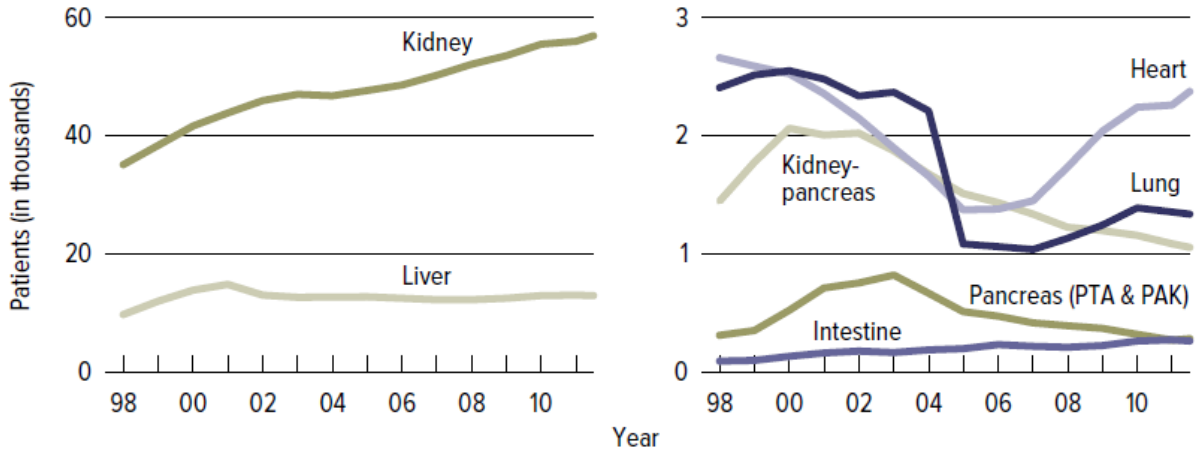

Figure 1. Patients on Organ Waiting List by Year. Reproduced from [10]

1.2 TISSUE ENGINEERING

The term *tissue engineering* was coined in the early 1990s as "an interdisciplinary field that applies engineering and life sciences toward the development of biological substitutes for the repair or regeneration of tissue or organ functions."[12] Tissue engineering approaches combine scaffolds, cells, and stimulatory cues to promote healing. This dissertation focuses on the development of new fabrication methods to produce scaffolds that closely resemble the structures and physical properties of the tissues they aim to replace.

Tissue engineering scaffolds 1) define a space for regeneration, 2) serve as a temporary substitute for function and 3) provide a substrate for cell adhesion and ingrowth.[13] Cells can be pre-seeded before implantation or recruited from the host after implantation.[11] Scaffolds can also act to release or retain bioactive molecules to guide regeneration. A fundamental challenge of scaffold design lies in mimicking the complex cellular microenvironment.[11, 14] Facets of this microenvironment include porosity, biodegradability, cell-material interactions, and mechanical properties.[13] Porosity is critical for permitting cell infiltration and nutrient diffusion.[1] Biodegradability is necessary to allow constructive remodeling and should match the rate of extracellular matrix (ECM) deposition to maintain structural stability while avoiding extended inflammation or encapsulation.[15] Mechanical properties of the scaffold can influence a range of cellular activities including attachment, migration, gene expression, and differentiation, thus influencing the remodeling response.[16-18] Some applications, especially bone and muscle, require load-bearing functions where the scaffold must provide mechanical forces until the remodeled tissue can undertake this function. As a result, scaffold design must balance between mechanical support and degradation rate.[19]

Methods to generate scaffolds with complex architecture have generally taken two approaches: decellularization or scaffold fabrication. Decellularization removes cellular debris from autologous or xenogeneic sources while retaining bioactive components of the extracellular matrix (collagen, fibronectin, elastin) and growth factors. Research in this field has produced decellularization protocols for many tissues and successfully regenerated flat tissues such as skin and bladder.[20] However, decellularization of larger organs is more likely to leave residual DNA and cellular debris.[2] Aggressive protocols can be used, but these chemicals can easily damage fragile ECM molecules. [2, 21-25] Recellularization of parenchymal cells into their proper locations is also more difficult in larger organs. Furthermore, disruption of the vascular network during decellularization also disrupts the vascular network, exposing collagen which can induce thrombogenesis unless endothelialized.[5, 26, 27] Other challenges of decellularization include retaining growth factor bioactivity during sterilization and achieving reproducibility.[1, 25] Because of these limitations, our work focused on scaffold fabrication approaches.

1.3 SCAFFOLD FABRICATION

Fabrication methods can be grouped into three categories: conventional, microfabrication (MF), and solid freeform fabrication (SFF) methods. Conventional processing methods can produce porous or fibrous scaffolds with most biomaterials. While techniques have been developed to control microstructure (eg. channels,[28] pores,[29] fibers[30]), the random nature of these processes make it difficult to controllably create micropatterns.[31] In contrast, MF and SFF can spatially control formation of long-range (global) micropatterns in 2D and 3D respectively.[32] Since the

3D environments surrounding cells have been shown to affect their behavior, it is important for TE scaffolds to recreate these 3D structures.[33]

1.3.1 Conventional Fabrication Methods

To introduce porosity into scaffolds, local pores have been introduced by solvent casting particulate leaching, freeze drying, of gas foaming methods.[32, 34, 35] While these techniques have been refined to adjust pore size and alignment, the formation of these pores is still largely a random process, making it difficult to construct larger structures (eg. channels) with spatial precision.[13, 32] Additionally, the high porosity of these scaffolds often results in low and inhomogeneous mechanical strength.[13, 32]

The extracellular matrix is comprised of fibrous proteins and proteoglycans (50-500 nm diameter) that serve mechanical as well as bioactive functions.[9, 36] Fiber-forming processes such as (thermally induced) phase separation, molecular self-assembly, and electrospinning have been used to reproduce similar fibrous structures.[37] We focus on electrospinning as a versatile method for fabricating fibrous constructs in the nano-microfiber range.

Electrospinning is an old method of fiber production that uses electric charge to draw fibers from a polymer solution or melt.[38] Electrospinning is performed by pumping a polymer solution through a needle (spinneret) with a high applied voltage. As charge accumulates in the solution droplet, electrostatic repulsion overcomes the surface tension allowing formation of a Taylor cone, whereby the polymer enters flight toward a grounded or oppositely charged collector. If sufficient intermolecular forces exist to overcome Rayleigh instability, a solid stream of polymer will form. Otherwise, small polymer droplets will be deposited by electrospraying. As the solvent evaporates during flight, nonaxisymmetric whipping of the

polymer stream occurs due to Rayleigh instability.[38] This causes fiber to narrow to 0.01-10μm while drying during flight and then depositing on a collector.[39]

Electrospinning is a relatively inexpensive method that permits control of fiber diameter and alignment for a variety of natural and synthetic polymers.[39, 40] Additionally, electrospinning has grown in popularity for tissue engineering research because of the resemblance of electrospun fibers to the extracellular matrix.[41, 42] A challenge of using electrospinning for tissue engineering scaffolds is the limited cellular infiltration into the fibers due to tight fiber packing.[9, 43] Furthermore, modified approaches may be necessary to create 3D constructs from the typical 2D fiber deposition.[44-50]

1.3.2 Microfabrication

Miniaturization of the integrated circuit and optoelectronics industries introduced early micro- and nano-fabrication techniques such as photolithography and etching.[51, 52] These tools have since been used to develop devices such as microsensors, microactuators, microfluidics, and microelectronics, collectively known as microelectromechanical systems (MEMS). These methods are capable of producing extremely high resolution (250nm) but are largely limited to materials such as photoresists, silicon, and glass.[53]

The development of soft lithography reduced time and cost by eliminating the clean room in addition to enabling micropatterning of soft materials.[54] One soft lithography method, microcontact printing (Figure 2), enables the patterning of biological molecules while replica molding (Figure 3A) is useful for introducing topographical features into substrates such as grooves, channels, and posts.[53, 54] Other soft lithography processes include microtransfer molding, micromolding in capillaries, and solvent-assisted micromolding (Figure 3B-D). Soft

lithography traditionally uses poly(dimethylsiloxane) PDMS, a soft, gas permeable, and transparent material. These properties make PDMS substrates useful for supporting cellular applications and the development of organ-on-a-chip devices[53, 55, 56] Because of the small volume, large throughput, and high sensitivity of these devices, soft lithography continues to be developed as an efficient diagnostic tool for real-time diagnostics, DNA sequencing, biodefense, implantable drug delivery, and minimally-invasive imaging.[52, 57-59] Methods to fabricate TE scaffolds are being developed by stacking or rolling porous and degradable substrates patterned by soft lithography.[60-63]

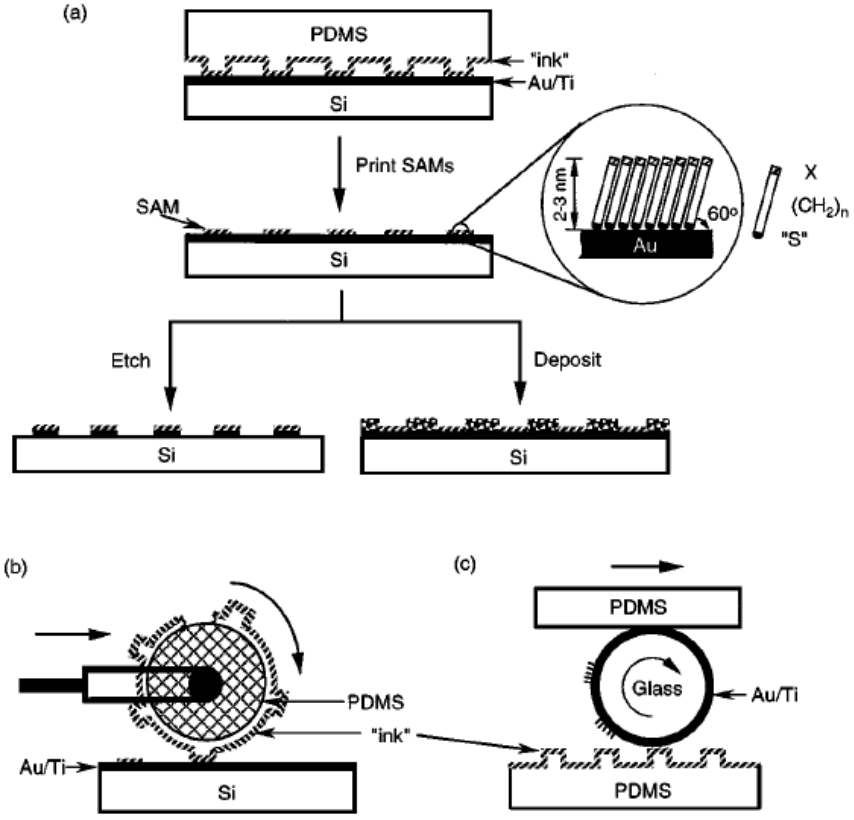

Figure 2. Soft Lithography Method of Microcontact Printing. Reproduced from [53]

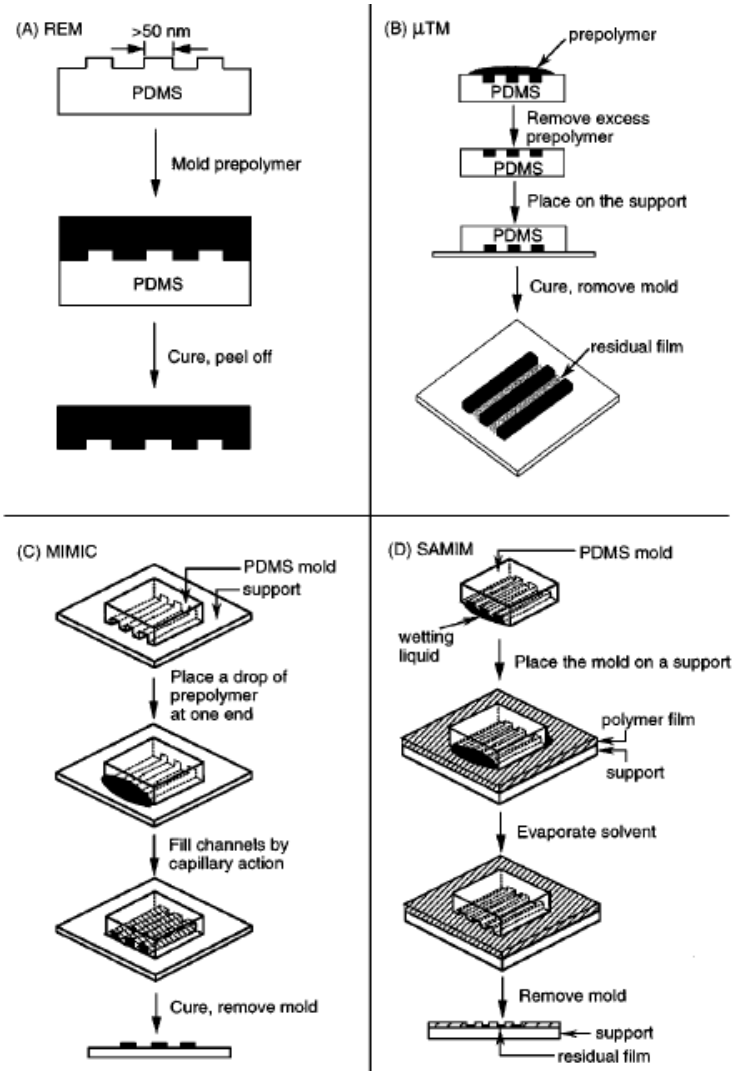

Figure 3. Soft Lithography Techniques (a) Replica molding, (b) microtransfer molding, (c) micromolding in capillaries, (d) solvent-assisted micromolding. Reproduced from [53]

1.3.3 Solid Freeform Fabrication

Solid freeform fabrication (SFF) includes a wide range of automated techniques that use computers to manufacture scaffolds in a layer-by-layer fashion. Advantages of SFF include precise control of material deposition as well as the ability to customize geometry for an individual patient based on data collected from anatomical scans.[13] SFF equipment varies in price from a few hundred dollars for hobbyist devices to tens of thousands for industrial

equipment. SFF methods can be categorized by different features such as type of material printed (polymer, metal, powder, photopolymer solution, cells, hydrogels) or mode of action (light, nozzle, printer).[13] We briefly describe these methods using the American Society for Testing and Materials (ASTM) terminology. In addition to directly structures as printed, they can also be used as a sacrificial mold with indirect processing.[13]

Powder bed fusion, or selective laser sintering (SLS)/ selective laser melting (SLM), uses thermal energy to selectively fuse defined regions in a bed of powder. This method offers resolution between 50μm and 500μm as determined by particle size and laser. This method has traditionally been used for processing metals (eg. titanium) but has recently been expanded to include hydroxyapatite, poly(caprolactone), poly(lactic acid), poly(hydroxybutyrate-co-hydroxyvalerate), and bioglass.[64-70] Because of the high modulus of most of these materials, SLS scaffolds are mostly used for bone and dental implants.

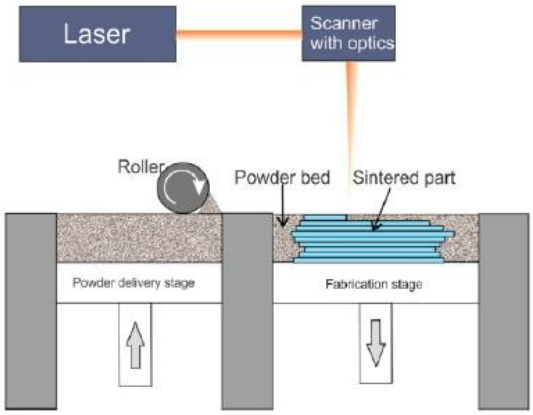

Figure 4. Powder bed fusion. Reproduced from [71]

Vat photopolymerization, or stereolithography (SLA), uses focused light to selectively cure a photopolymer with high resolution (1-30μm). Use of two photon polymerization or digital-mirror devices (DMD) can greatly improve resolution or fabrication speed respectively.[72-74] Applications within TE have used photocrosslinkable polymers (eg. poly(propylene fumarate)

(PPF), methacrylated PCL) and hydrogels (eg. gelatin-methacrylate, gelatin-methacrylamide, hyaluronic acid-methacrylate, and poly(ethylene glycol-diacrylate).[72, 73, 75] While these hydrogels can incorporate cells during the build process, the photopolymers and initiators may be cytotoxic to cells.[76-78]

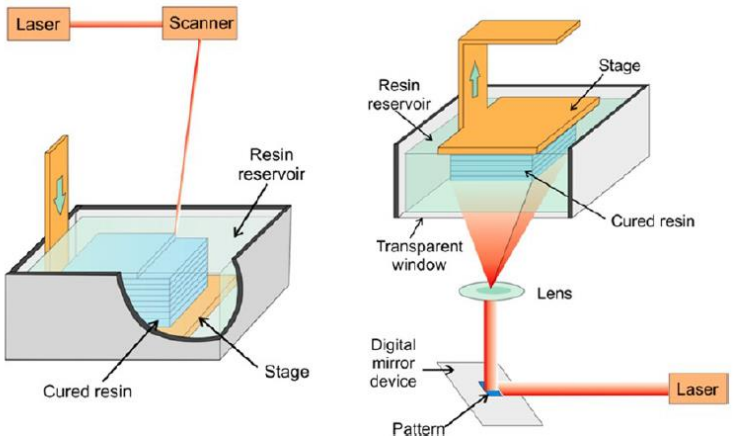

Figure 5. Vat polymerization. Reproduced from [71]

Material extrusion, or fused deposition modeling (FDM), mechanically extrudes a material through a nozzle and fuses it to the previous layer. While hobbyist equipment using this method is some of the least expensive, this method requires stock material in filament form. Commercially-available filament was traditionally limited to acrylonitrile-butadiene-styrene (ABS) although poly(lactic acid) (PLA) and poly(vinyl alcohol) (PVA) have recently become available. Although custom-made filament has been used to print poly(caprolactone) (PCL), hopper- and syringe-based extruders are gaining popularity for printing a wider range of materials.[79-82] Furthermore, the low resolution (xy:250µm, z:50µm) of traditional FDM is being improved in pressure assisted microsyringe which uses custom fabricated glass capillaries to obtain features of approximately 10-30µm.[63, 71]

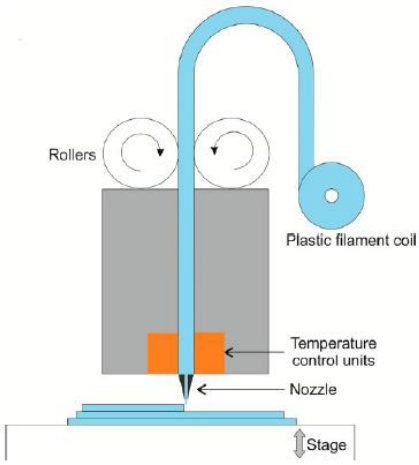

Figure 6. Material Extrusion. Reproduced from [71]

Material jetting (3D plotting) selectively deposits droplets of soft build materials. These droplets have traditionally been initiated by thermal or actuated inkjet printing (Figure 7 A/B). Printing of biological material (termed cytoscribing) dates back to 1988 where a Hewlett-Packard printer was used deposit collagen and fibronectin.[83] Extrusion and laser forward transfer (Figure 7 C/D) can also be considered variations of 3D plotting with characteristics of FDM and SLA respectively. The use of aqueous build materials permits printing of proteins and growth factors in addition to live cells in hydrogels or cell spheroids. 3D plotting of poly(ethylene glycol) diacrylate/alginate and agarose have been used to make heart valves and blood vessels respectively.[84, 85]

Challenges of these methods involve the effect of shear stresses (10m/s)[86] and heat for thermal inkjet on cell viability and function. By optimizing conditions, patterned fibroblasts as well as hippocampal and cortical neurons cells, have achieved over 90% viability while maintaining electrophysiological activity.[86, 87] The heat has also been used to transfect printed cells. Other limitations include a low resolution and clogging.[88]

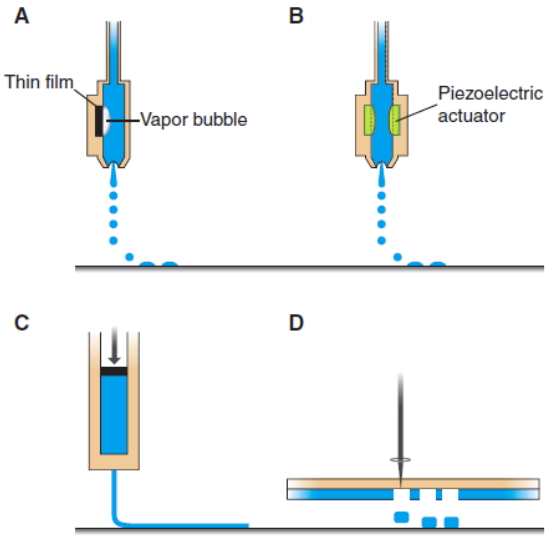

Figure 7. Material Jetting A) Thermal inkjet printing via microbubbles. (B) Inkjet printing by mechanical actuation. (C) Microextrusion. (D) Laser forward transfer. Reproduced from [31]

Binder jetting or 3D printing combines the powder bed of SLS with the material jetting technique to selectively bind powder materials with a liquid bonding agent. This method is typically used with ceramics such as hydroxyapatite for bone scaffolds.[89, 90] Scaffolds produced by this method suffer from low mechanical strength and a resolution around 300um.[90, 91]

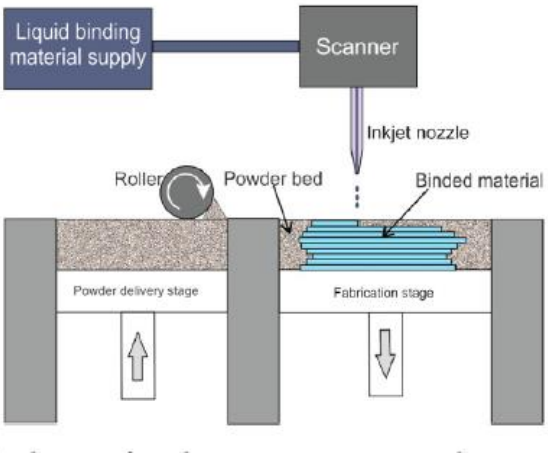

Figure 8. Binder Jetting. Reproduced from [71]

Sheet lamination, or selective deposition lamination (SDL)/laminated object manufacturing (LOM), uses a laser to cut a pattern in each layer of paper, plastic, or metal. These layers are adhered to the prior layer by bonding under a heated roller that glues or welds

the layers together.[71] This method can provide high resolution (xy:10µm, z:100µm) but has not seen much use in tissue engineering applications.[71]

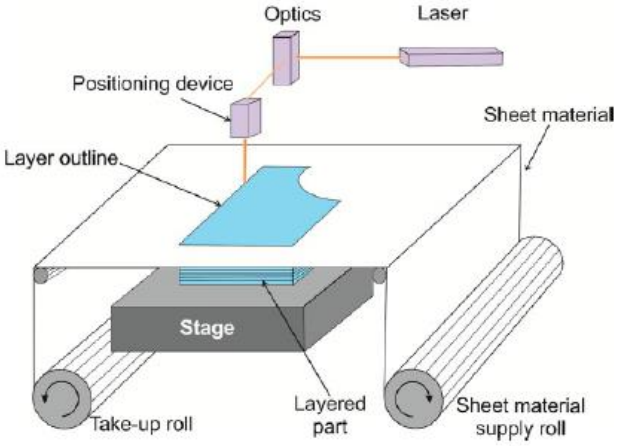

Figure 9. Sheet lamination. Reproduced from [71]

1.3.4 Combination Approaches

As technology converges, new methods borrow features of multiple modalities. For instance, electrohydrodynamic jet (also referred to as direct write melt electrospinning or near field electrospinning) demonstrates characteristics of both FDM and electrospinning.[92-94] Combination technologies may provide solutions to shortcomings of any one method. FDM-printed PCL was combined with 3D plotted hydrogels or electrospun PCL to improve strength and porosity respectively.[80, 95] Similarly, electrospinning was combined with 3D plotting or electrospraying of cells to create hybrid constructs with improved cellular integration.[43, 96]

2.0 SPECIFIC AIMS

The extracellular matrix is comprised of fibrous proteins and proteoglycans that facilitate cell attachment and permit diffusion of nutrients.[97] Additionally, large organs contain hierarchical 3D micropatterns.[97] It is difficult to fabricate TE scaffolds with both fibrous nanostructure and global micropatterns using existing techniques. For example, electrospinning is capable of fabricating nanofibrous scaffolds but cannot introduce global structures with defined spatial precision. In contrast, SFF methods is ideal for complex 3D design, but does not typically produce features that are fibrous or of the proper scale for cell attachment.[80]

The objective of this work was to develop a micropatterning technique (templated electrospinning) to introduce global structures with a specified shape and orientation into electrospun scaffolds. This step-wise process enables production of multi-layered structures with different materials and alignment. The fibrous nature of electrospun scaffolds is appropriate for mass transfer but is typically too dense to permit substantial cell migration.[9, 43] Thus, we hypothesized that cell migration into electrospun scaffolds could be facilitated and guided by incorporation of micropatterns. We tested this hypothesis by patterning scaffolds for peripheral nerves and microvascular networks. These structures were selected because of the micro-sized features and the increasing complexity from nerve to blood vessels which allowed us to sequentially improve our technique. Additionally, the ubiquitous nature of neurovascular structures throughout the body makes this relevant for most tissues. While others have combined

SFF with electrospinning to make composite structures[98, 99] or used sacrificial electrospun fibers,[100-106] to the best of our knowledge this might be the first report of defined sacrificial micropatterns in electrospun scaffolds.

This dissertation addressed the following specific aims:

1. **Introduce linear patterns into electrospun scaffolds to promote cellular infiltration into a biomimetic nerve guide.** Specifically, we:

- Introduced and maintained microchannel structures in fibrous nerve guides.
- Incorporated aligned fibers in microchannels to provide topographical guidance cues.
- Demonstrated Schwann cell infiltration into nerve guide microchannels

2. **Introduce bifurcating patterns into electrospun scaffolds to mimic branching structures of microvascular networks.** Specifically, we:

- Created custom vascular pattern with nontoxic water-soluble material
- Used templated electrospinning to transfer pattern into fibrous construct
- Demonstrated feasibility of endothelializing microvascular scaffolds

3. **Improve degradation, mechanical, and delamination properties by electrospinning poly(glycerol sebacate) (PGS).** Specifically, we:

- Electrospun PGS with minimal alterations
- Investigated mechanical properties and cytocompatibility of fibrous PGS
- Used electrospun PGS to create multi-laminate microvascular constructs

3.0 TEMPLATED ELECTROSPINNING WITH LINEAR PATTERNS TO PRODUCE BIOMIMETIC NERVE GUIDES

Chapter Aim

The aim of this chapter was to develop templated electrospinning techniques using linear patterns to mimic the architecture of native nerve. We hypothesized that reproducing the tubular structure of endoneurial tubes and fascicles with microchannels would confine axon paths to reduce misdirection. Additionally, aligned fibers have been shown to direct axons similar to the longitudinally-aligned Schwann cells of the Bands of Bungner. Since aligned fibers are difficult to present in 3D scaffolds, we maximized surface area of aligned fibers by lining the microchannels. These biomimetic nerve guides demonstrated increased Schwann cell infiltration compared to other designs.

Background

Peripheral nerve injuries accompany approximately 2.8% of trauma patients, or 100,000 people in the US and Europe annually.[107, 108] These injuries cause loss of sensation and muscle function, in addition to painful neuropathies in patients.[109] Due to an innate regenerative capacity of peripheral nerves, injuries yielding insignificant or no loss of axon continuity typically repair naturally.[110, 111] However, severe injuries causing complete nerve transection require surgical intervention. Small gaps are surgically anastamosed without tension while larger gaps are bridged by an implant to provide structural, mechanical, and biochemical support.

[112] Although autografts produce donor site morbidity and yield incomplete or inconsistent recovery, they are still preferred over alternative nerve guides and remain the clinical gold standard.[113] Consequently, prosthetic alternatives capable of matching or exceeding the performance of autografts are a highly active area of research.[113, 114]

Native nerve is organized into a hierarchical structure of parallel channels that are separated by three layers: endoneurium, perineurium, and epineurium (Figure 10). Axons ensheathed within endoneurial tubes extend from the cell body longitudinally toward their distal target. These tubes are bundled together within the perineurium to form fascicles. The whole nerve is enclosed by the epineurium.

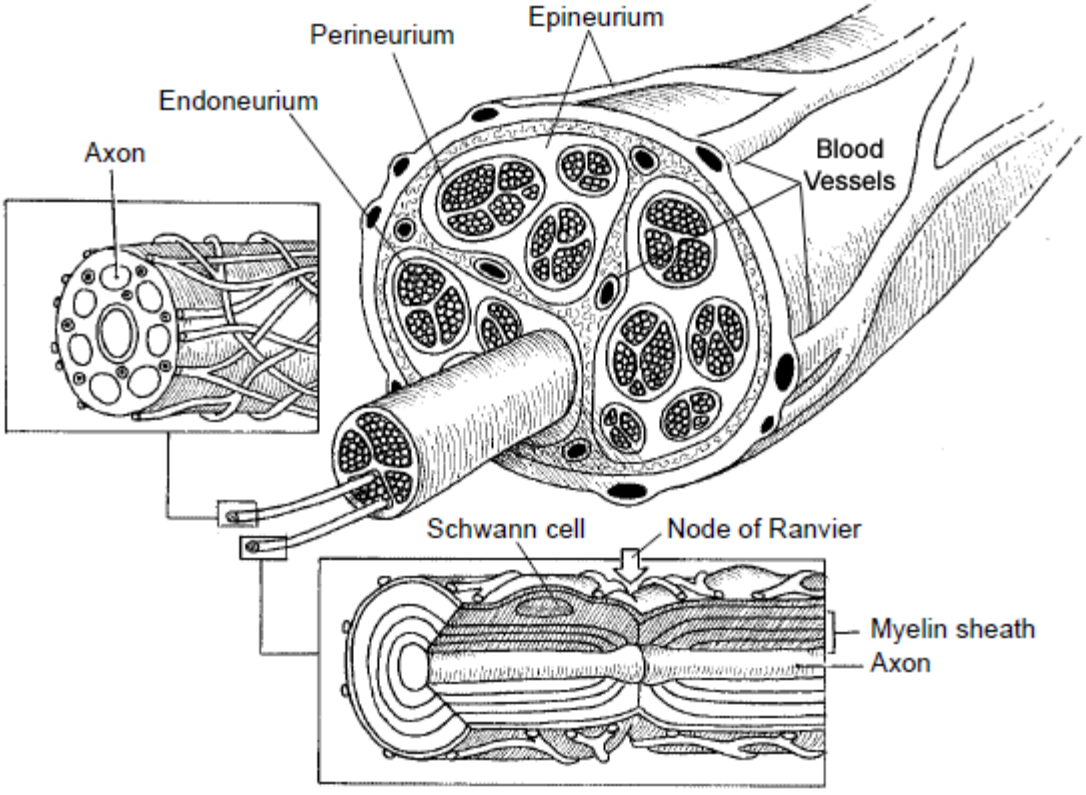

Figure 10. Structure of native nerve. Modified from [115]

Severed axons of peripheral nerves possess an innate ability to repair via Wallerian regeneration (Figure 11). During this process, Schwann cells (SC) are mobilized to phagocytose

cell debris. Schwann cells also proliferate and longitudinally align, forming the Bands of Bungner which can provide topographical cues to regenerating axons. However, axon extension is a slow process and requires proper guidance to re-establish the appropriate connections. Peripheral nerve guides can serve as the temporary scaffolds to support and direct axon extension.

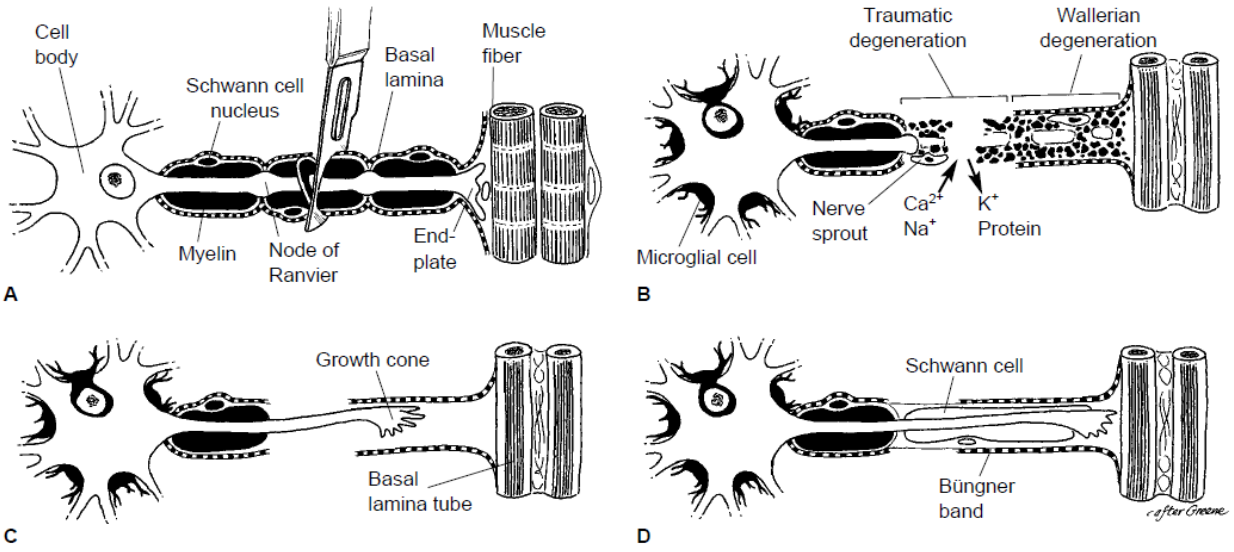

Figure 11. Process of Wallerian Regeneration. Reproduced from[115]

3.1 INCORPORATION OF PARALLEL CHANNELS WITHIN FIBROUS NERVE GUIDES

3.1.1 Introduction

Existing nerve guides

Clinically-available nerve grafts are limited to single-lumen conduits constructed of collagen, poly(glycolic acid), poly (D,L-lactide-co-ε-caprolactone), poly(vinyl alcohol), or decellularized extracellular matrix (ECM) and yield outcomes inferior to autografts.[112] Moderate experimental

success has been achieved by nerve autografts and muscle basal lamina.[116] We believe this may be due in part to the confinement of the nerve within the complex multi-channel structure of the basal lamina. Through numerous fabrication methods researchers have attempted to mimic these designs but fail to achieve the same success.[117]

To address this challenge, we designed the first multi-channel nerve guide composed entirely of electrospun fibers intended to mimic the fascicular architecture and extracellular matrix respectively. Our design satisfies 3 design criteria that have not been achieved by previous methods. 1) Our design incorporates a high density of channels which is uncommon in other templating approaches. 2) We have greater control of channel size and regularity compared to freeze drying methods. 3) Our design consists of interconnected spaces between fibers instead of the solid walls created by casting methods. Additionally, we can customize many aspects of the design such as fiber diameter, composition, and alignment, in addition to channel diameter and spacing. We anticipate this design being especially useful for nerve repair in the future by incorporating aligned fibers, which can guide axon growth.

3.1.2 Experimental Section

Electrospinning

A 14% polycaprolactone (PCL) (Mn=80,000, Sigma) solution was prepared by dissolving PCL pellets in 5:1 trifluoroethanol:water at room temperature under agitation overnight.[118] Random fibers were deposited on the aluminum face of a custom collector (Figure 13A) during horizontal stationary electrospinning (Figure 12A). The collector also had two fine tooth combs (18 teeth per cm) attached to the sides to align sutures in a regularly-spaced parallel pattern. Radially-aligned fibers were deposited around the guide via rotating electrospinning (Figure 12B) to

prevent unraveling. For both electrospinning methods, the collector was placed 25 cm from the needle and the polymer solution was pumped through a 21 gauge needle at a flow rate of 25µl·min^{-1}. Electrostatic potentials of 15 kV positive and 10 kV negative were attached to the needle and collector respectively.

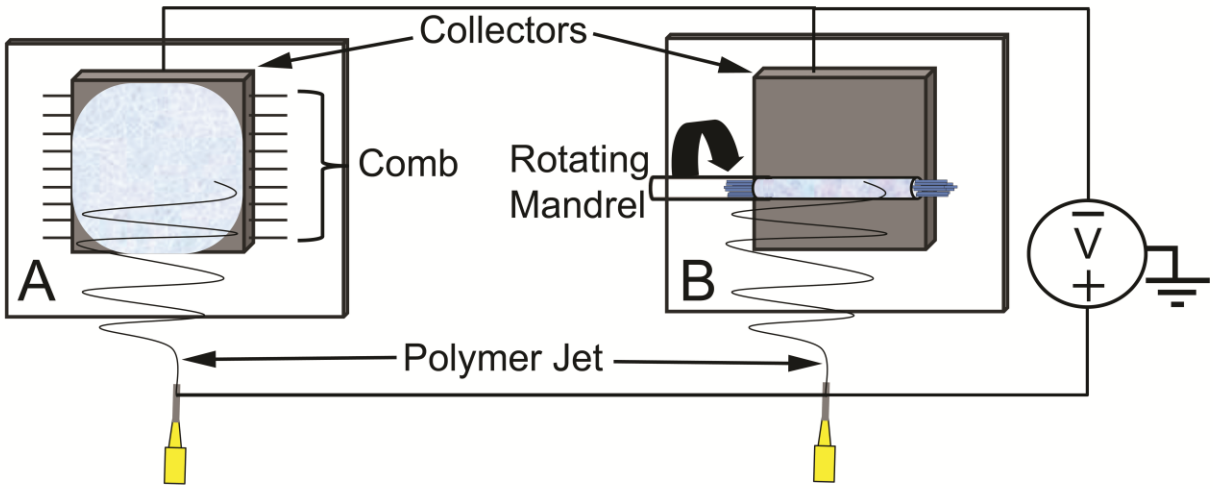

Figure 12. Diagram of electrospinning(A) A stationary electrospinning set-up is used to produce a random fiber mesh. A polymer solution is pumped from syringe at a constant rate. A positive voltage is attached to syringe needle; a negative voltage is attached to an aluminum collector plate. The positively-charged polymer dries to form a thin fiber during flight toward the negatively-charged collection plate. (B) Rotational electrospinning set-up is used to produce radially-aligned fibers. Same process as stationary electrospinning is used except the fibers are deposited on a mandrel rotating in front of the collector

Nerve Guide Preparation

A random mesh of PCL fibers were deposited on the aluminum face of a collector by stationary electrospinning a set volume, V_1 µL, of PCL solution (Figure 13A). Sutures were woven taut around the teeth on the collector to form N parallel strand templates atop the electrospun fibers (Figure 13B). Sutures were covered with a second layer of random PCL fibers by electrospinning a set volume, V_2 µL (Figure 13C). The entire construct was placed in a vacuum chamber overnight to remove residual solvent. The thickness of each layer is adjusted by varying volumes V_1 and V_2 and the number of channels equals N.

After drying, the sutures were cut at both ends to release the electrospun mat from the collector (Figure 13D). The multilayered electrospun mat was rolled up parallel to the sutures and secured with two collagen sutures (Figure 13E). Recent designs used parafilm to secure the template strands rather than tying with sutures. The outside was then sealed with a thin sheath of aligned PCL microfibers by electrospinning 50µL PCL while rotating the nerve guide at 60 rpm in front of the collector (Figure 12B). This outer sheath helps to prevent nerve guide from unraveling. The patterning sutures were removed, creating aligned channels in their void. The nerve guide preparation was completed by trimming the guide to the desired length by cutting each end (Figure 13F). This removes the peripheral regions of the electrospun mat with low fiber density. Prior to trimming the guide, it was soaked in deionized water (diH_2O) for 1 hour and frozen on dry ice. The integrity of the micro-channels was better maintained during sectioning if water was allowed to penetrate the nerve guide and frozen to mechanically support it during cutting. The nerve guides were stored in microcentrifuge tubes until use.

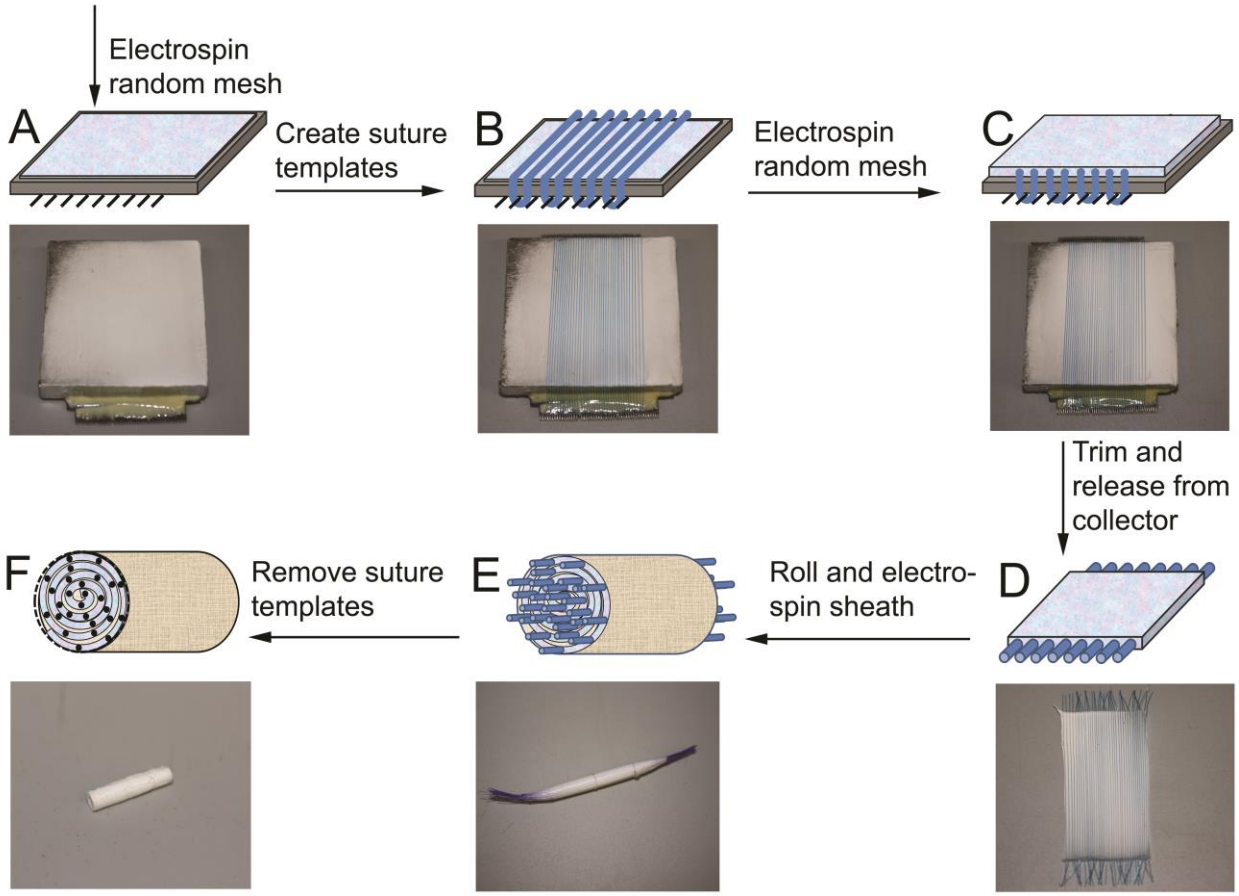

Figure 13. Fabrication scheme for suture-templated electrospinning nerve guide.Deposit a thin layer (V1) of random electrospun PCL fibers via stationary electrospinning setup. (B) Create channel template by stringing aligned sutures across first PCL layer and attaching to combs on sides of the collector. (C) Deposit second thin layer (V2) of random electrospun PCL fibers via stationary setup. (D) After drying excess solvent in vacuum, cut sutures on both ends and trim flat sheet to length. (E) Roll up nerve guide and secure. Electrospin aligned PCL sheath around outside of guide by rotating electrospinning set-up. The template strands of one end of the nerve guide are placed in a tube and secured by parafilm. This is rotated at 60rpm in front of collector plate as 50 µl of aligned fibers are deposited around the exposed region. (F) Sutures are manually removed. Electrospun nerve guide is soaked in water to allow penetration and guide is cut after freezing on dry ice.

Porosity

The porosity of the guide, including channels, was estimated used the geometric equations outlined in the paper by Yang.[119] Briefly, the porosity, P, is calculated from equation 1.

$$P = \left(1 - \frac{V_p}{V_t}\right) * 100 \quad (1)$$

V_p is the volume of the polymer and V_t is the total volume of the guide, obtained from the following equations.

$$V_p = \frac{m_t}{d_p}$$ (m_t-mass of total guide) (d_p-density of polymer) (2)

$$V_t = \pi r_t^2 * l$$ (r_t-radius of total guide) (l=length) (3)

The term V_p/V_t in equation 1 represents the volume occupied by the polymer. Thus, one minus this value provides the volume of the free space in the guide including gaps between fibers and the channels. The volume (V_c) and percent porosity (P_c) contributed from the channels is also obtained from equations 4 and 5.

$$V_c = \pi r_c^2 * l * n$$ (r_c-radius of a channel) (n=number of channels) (4)

$$P_c = \left(\frac{V_c}{V_t - V_p}\right) * 100$$ (5)

Scanning electron microscope (SEM)

SEM samples were prepared by cutting thin (approximately 1-2 mm) transverse slices of nerve guides with a scalpel and adhering to an aluminum stub using carbon tape. The samples were dehydrated in a desiccator overnight. The samples were coated with 3nm of gold with a Cressington Sputter Coater and grounded to the stub with aluminum paint. Samples were imaged with a Jeol JSM-6330F SEM.

Analysis of electrospinning parameters

Reproducibility and layer thickness. Three guides were produced using V_1/V_2= 75 µL and 35 templates of 100 µm diameter. It should be noted that this was spun on a collector 7cm long and 4cm wide, so not all of the deposited fibers were in the portion used for the guide. The qualitative structure of 1-2 mm hydrated sections were observed on an Olympus SZX10 stereo microscope and compared to others where the layer thicknesses were varied such that V_1/V_2=40,

V_1=40/V_2=100, and V_1/V_2=100. Additionally, porosities determined from the above equations were reported.

Channel diameter. A guide was fabricated using template diameters of 20, 70, 100 and 150µm. The number of templates and layer thicknesses were adjusted based on template size. Optical images of 1-2mm hydrated samples were again viewed an Olympus SZX10 stereo microscope. ImageJ was used to determine channel size via two orthogonal diameter measurements for 10 channels per transverse-section. Average channel diameter (+/-) standard deviation is reported.

Cell Culture

Rat Schwannoma cell line RT4-D6P2T (ATCC CRL-2768) was kindly provided by the Badylak lab. Cells were cultured with Dulbecco's Modified Eagle Medium (DMEM) (ATCC 30-2002) with 10% fetal bovine serum (FBS), 1% antibiotic/antimycotic (Cellgro 30-004-Cl) in incubators at 37ºC and 5% carbon dioxide.

Nerve guides were sliced to lengths of 1.2 cm, sterilized by ethylene oxide, and washed in sterile 1X PBS for 2 days on an orbital shaker, changing PBS after the first day. Nerve guides were then incubated with 10µg/mL laminin solution at 37ºC for 13 hours. Nerve guides were washed once in 1X phosphate buffer solution (PBS) prior to cell seeding.

Cells (passage #8) were trypsinized and resuspended at a concentrated 7,633 cells/µL. A 65µL solution of cell suspension was pipetted into each side of the guide for a total of $1x10^6$ cells per guide. This not absorbed by the guide was pipette into each end a second time. Nerve guides were placed in 12 well plates and 1mL media was added to each well. The plates were placed in a 37ºC incubator for 1 hour. Nerve guides were then placed on a shaker in the incubator for 1 hour before transferring to new 12-well plates to eliminate the large number of

cells adhered to culture plate. Guides were incubated while shaking until evaluation at 4 and 11 day time points for 4',6-diamidino-2-phenylindole (DAPI) (n=3) and 3-(4,5-dimethylthiazol-2-yl)-2,5-diphenyltetrazolium bromide (MTT) (n=3).

Schwann cell SEM preparation. Guides containing cells were placed in a fixation solution (2.5% glutaraldehyde in 1X PBS) overnight at 4^{o}C. Nerve guides were then dehydrated through serial dilution in 25, 30, 50, 70, 80, 90, 100 percent ethanol in water. This was followed by dehydration in 3:1, 1:1, and 1:3 (3 times) ethanol:hexamethyldisilazane (HDMS). Nerve guides were immersed for 15 minutes in each solution. The nerve guide was then left in 100 percent HDMS in fume hood overnight for complete drying. The nerve guide was cut at a 45 degree angle cross-section to reveal the interior of the guide. Samples were prepared on SEM stubs as previously described.

Live/Dead/DAPI. Live/dead solution was prepared by adding calcein AM (20µM) and ethidium homodimer (1µM) to DMEM without phenol red or FBS. Three nerve guides from each time point were washed three times with 1X PBS before incubating in1.5 mL live/dead solution for 3 hours. Guides were then cut in half, frozen in OCT, and sectioned on a microtome to produce transverse and longitudinal slices (8 µm thick). The cell nuclei were stained with DAPI mounting solution and viewed on a Nikon Eclipse Ti inverted microscope. Analysis focused on identifying cell infiltration (location of cells relative to channels) and proliferation (number of cells). Due to background staining associated with the guide fibers, no immunofluorescence was used. Image look-up table (LUT) minimum threshold and G-value were adjusted to improve the contrast so DAPI could be seen in relation to the structures in the guide.

MTT. Three nerve guides, three guides without cells, and calibration curve cells seeded at 1, 0.5, 0.25, and 0.125 million cells per tissue culture polystyrene (TCPS) well and acclimated for 3 hours in culture were used for the MTT assay. Each sample was washed three times with 1X PBS to remove residual media containing phenol red. MTT solution (0.5mg/mL media without FBS or phenol red) was added to each well for 3 hours at 37°C. Small sections from the ends and center of the guides were section for imaging. Images did not clearly show MTT crystals and are not shown. DMSO was added to the remaining pieces of the seeded nerve guides and to the other samples. Mechanical disruption was applied to the seeded guides to solublize MTT trapped in the fibers. After 30 minutes, the solutions were removed and added to 96 well plates in triplicate for absorbance reading at 540nm.

3.1.3 Results and Discussion

Multi-channel electrospun design mimics nerve micropattern

Rationale for multi-channel design. An array of parallel microchannels is present in healthy nerves and preservation of this endoneurial structure is an optimistic indicator in the prognosis of nerve injuries [111]. Therefore, the major goal of our design was to incorporate endoneurial-like structures in a nerve guide. Single lumen nerve guides aid regeneration by concentrating chemical signals and restricting infiltration of inflammatory cells.[112] However, single lumen conduits fail to present a multi-channel structure like that of a native nerve. Furthermore, collapse of a single lumen conduit drastically impairs nerve repair.[117]

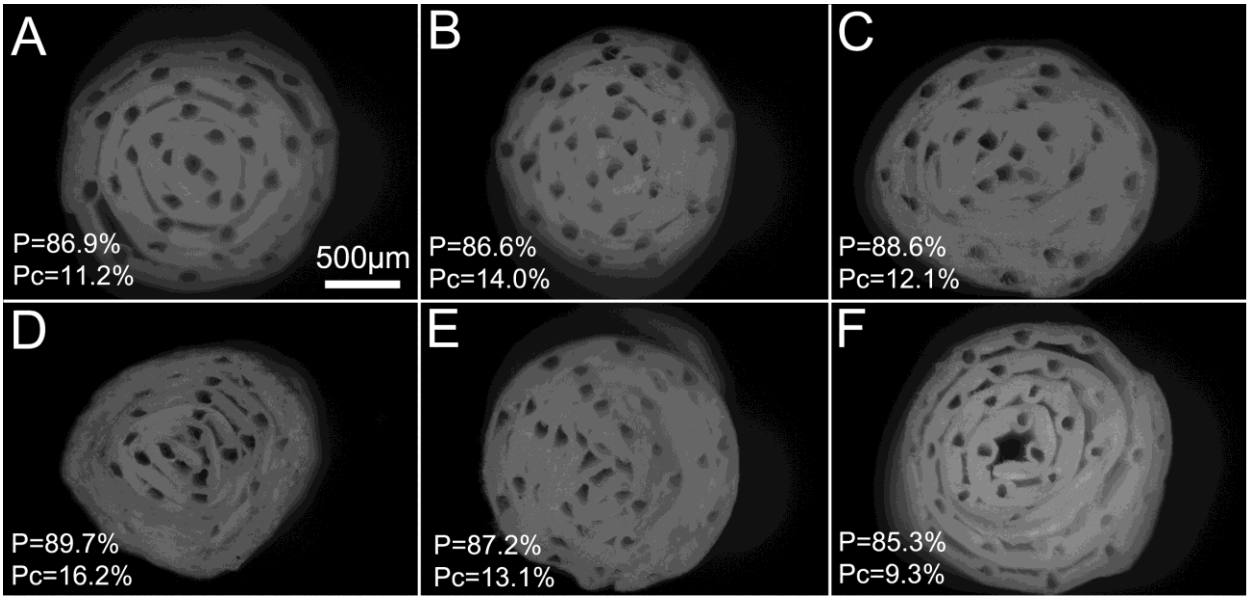

Figure 14. Optical images of transverse-sections of multi-channel guidesof difficult layer thickness and 35 templates. (100 μm diameter). Total porosity (P) and percent channel porosity (Pc) is reported for each guide. (A-C) V1/V2=75 μL, (D) V1/V2=40, (E) V1=40/V2=100, (F) V1/V2=100.

Existing multi-channel designs. Multi-channeled nerve guides have been fabricated by a variety of methods including freeze drying, injection molding, thermally-induced phase separation (TIPS), electrodeposition, and various combinations of these methods.[116, 117, 120-129] There are several key differences distinguishing our design from existing methods of producing multi-lumen guides. Our guide has electrospun fibers with an open porous structures to facilitate mass transport. Contrarily, mold casting, lithographic, and deposition techniques generate nerve guides with thick or continuous walls which are likely to limit mass transfer.[116, 117, 125, 128, 130, 131] Additionally, we report a high channel density, while many of these mold casting methods produce very few channels. Our fabrication scheme can create well-defined channels with a diameter as small as 33 μm. This can be contrasted with the other common methods such as freeze-drying, TIPS, and gas foaming which are porous but often lack control of channel size, orientation, and interconnectivity.[120-123] Other approaches capable of producing porous guides with defined channels are limited to 150 μm minimum diameter rods used to make the channels

and the difficulties associated with aligning and removing rod templates with large aspect ratios.[119, 126, 129] Finally, our layered fabrication scheme will allow us to make future modifications to incorporate aligned fibers within channels to provide nanometer-scale topographical guidance. Aligned electrospun fibers have demonstrated utility in directing nerve outgrowth as well as inducing morphology changes.[30, 132-136] The ability to perform this type of modification has not been demonstrated by other methods, making our approach unique.[137]

Rationale for electrospinning. Native nerve is surrounded by an extracellular matrix that is fibrous and porous.[138] The process of electrospinning has gained much attention in tissue engineering in recent years for its ability to controllably produce sub-micron to micron-sized fibers that mimic the fibrous nature of ECM.[42] However, since electrospinning is best-suited for production of two-dimensional meshes, incorporation into three-dimensional constructs appropriate for nerve regeneration has been difficult and limited.[139]

Current electrospinning methods. Existing methods of incorporating electrospun fibers into nerve guides radially- or axially-align fibers on the circumference of a hollow conduit or insert flat sheets into the lumen.[136, 140, 141] These methods do not utilize the entire cross-sectional area for adhesion and guidance or may not be appropriately oriented. Bundles of longitudinally-aligned electrospun fibers can also be inserted inside a cylindrical nerve guide to fill the lumen, but unlike channels, they do not confine nerve to particular paths.[141-144] Additionally, tight packing of these bundles may inhibit axon and Schwann cell migration. In contrast to existing electrospun nerve guides, our design creates a complex 3-dimensional construct with open channels to guide the nerve and Schwann cells between the fibrous substrate.

Fabrication

Our fabrication process successfully demonstrates proof of concept for a nerve guide constructed entirely of electrospun fibers. The two electrospun layers encapsulated the templates and exhibited sufficient interaction to prevent delamination. We believe that the insulating properties and smooth surface of the templates allow easy removal from the electrospun fibers without disrupting the channel architecture despite a large aspect ratio. Finally, the cylindrical shape was maintained by a circumferential sheath of fibers deposited around the outside.

Fibrous microstructure. A section of the 6-0 collagen nerve guide viewed by SEM (Figure 15A & B) demonstrates the structure of the electrospun fibers around the microchannels. This microfiber mesh creates an open network of paths for nutrient transport into and out of the channel. The fibers in Figure 15B show some artifact resulting from cutting. Thus, fiber morphology can be better evaluated from a flat sheet of the electrospun fibers (Figure 15E). This image shows smooth fibers of roughly uniform diameter. The unraveling of the coil as seen in Figure 15A was addressed in later guides by an electrospun sheath (Figure 15C) which fixes the guide in the circular shape. The circumferentially-oriented fibers of the sheath can be seen covering the layer of random fibers in Figure 15D.

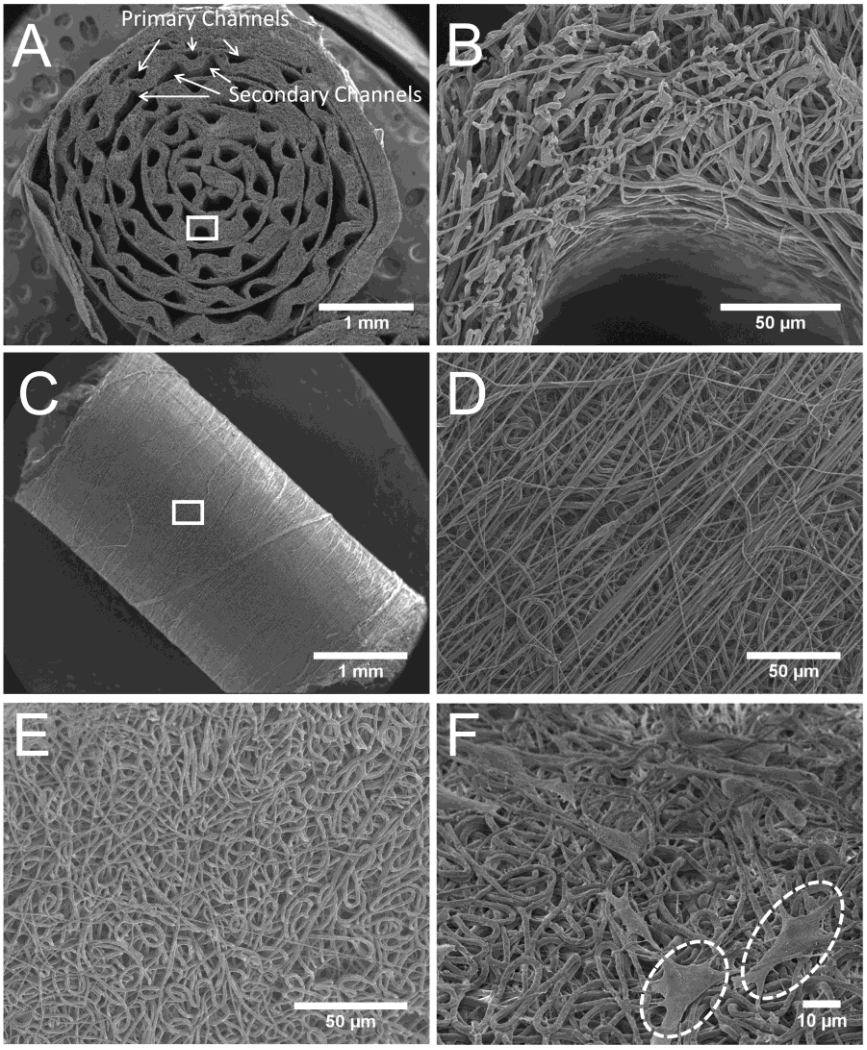

Figure 15. SEM images of microchannels and microchannels in the nerve guides.(A and B) Transverse-section of nerve guide with aligned channels at 25 and 650 X magnification. (C and D) Outside of rolled nerve guide sealed with an electrospun sheath (Shown at 25 and 500 X magnification). (E) Top view of randomly-oriented fiber mat before rolling to form guide. (F) Schwannoma cells on random fiber electrospun fibers inside nerve guide after in vitro culture. Two cells are highlighted with circles.

Primary and secondary channels. Multi-channel guides fabricated with a range of diameters are shown in Figure 16. Figure 16A shows a nerve guide with 25 channels approximately 176 µm in diameter fabricated with 4-0 synthetic sutures. Although not homogenous in shape or dimension, an equivalent number of secondary channels double the channel density. Secondary channels adjacent to each primary channel were formed by the space between the primary channels and the flat mesh. The size of these secondary channels is affected by the ratio of the two electrospun layers and the template diameter. Secondary

channels provide additional space for cell migration, but due to the inhomogeneity of these structures we focus on the primary channel. Figure 16B and C shows guides produced from 6-0 collagen and synthetic sutures respectively. Primary channels in these guides are more circular and the secondary channels more regular. One 10-0 guide was made for the purpose of demonstrating versatility of this method (Figure 16D). Only 10 channels were made since 10-0 sutures are very short and it requires many sutures to obtain the same number as larger sutures. Since the layer thickness was not adjusted for this design, the channels contribute very little open area for nerve growth and no secondary channels are present. As seen in the figure, 10-0 sutures do not act well as mandrels for rolling, resulting in loose rolling and the large central lumen observed in this figure. Due to the manual steps involved with this process we recognize that there may be a minimum diameter that is feasible with the current technique. Although, we do not think that this will hinder the success of our design, we hope to improve the precision with more automated techniques in the future.

Channel diameter. Suture templating resulted in channel diameters 13 to 28 μm larger than the sutures used to create the channels. We hypothesize that electrospun fibers are not attracted to the sutures and are not deposited tightly around them, accounting for the diameter differential. Although initial work began with collagen sutures, synthetic sutures or fishing line were later used due to easier removal.

Layer thickness. The thickness of each electrospun layer can have drastic effects on the structure and mechanics of the guide. The mentality behind our design is to minimize the layer thickness to facilitate transport through the walls and maximize the number of microchannels available while still providing sufficient mechanical strength. Figure 14D &E shows how thinner walls guides are less defined and more susceptible to deformation during cutting

compared to thicker guides in Figure 14F. Consequently, future work to increase open areas designated for cell adhesion will focus on increasing template spatial frequency, not decreasing wall thickness.

Porosity. Porosity was estimated using geometric calculations based on mass and volume of the final guide and the density of the PCL (1.145 g/cm^3). These volume calculations were supported by similar values obtained via a second set of calculations that used the V_1 and V_2, the 14% PCL polymer concentration, and the percent of the collector area used for making the guide. The total porosity and the percent contributed by the channels are reported in Figure 14. All guides in this sample set showed porosity above 85 percent. Additionally, void space between electrospun fibers contributed to the majority of porosity since the highest Pc was 16 percent. This supports the premise that our electrospun mats are highly porous and should be conducive to nutrient transport.

Reproducibility. As with any fabrication process, reproducibility is important. The current method contains two areas where variability can be introduced: electrospinning steps and manual steps. Achieving stable and consistent electrospinning conditions is essential to producing repeatable guides. Fiber diameter and morphology are known to be affected by electrospinning parameters which include acceleration voltages, polymer molecular weight, solution concentration, and humidity. One electrospinning complication that may arise is the formation of globs or nets of fibers depositing on the collector.[145] These do not form tightly around the template and cause defects in the design. A second variation that can greatly influence the outcome of templated guides is uneven distribution fibers on the collector. If uneven deposition occurs, some regions will be thick while others are thin and weak. To facilitate more uniform distribution, the collector may be slowly moved during electrospinning.

Rolling the flat sheet to form the cylindrical guide is the primary step in which manual variation can affect the outcome. As is evident in Figure 16A & D, a large central lumen is formed if the guide is not rolled tight enough. Contrarily, if the guide is too tight, compressive forces deform the channel shape when the template is removed. This is especially significant for guides with thin layers (Figure 14D). Additionally, template alignment is important for maintaining uniform spacing between channels.

Reproducibility can be achieved by maintaining consistent conditions between samples. These include electrospinning parameters (acceleration voltage, solvent and concentration of the polymer solution, distance, flow rate, humidity), thickness of fibrous mat, template size and spacing, and rolling tightness. Three guides produced by the same electrospinning and template conditions were imaged and shown in Figure 14A-C to demonstrate reproducibility of this method. The channel shape and overall quality of the guides becomes more vulnerable to cutting damage as the layer thickness decrease. This is evident in the bottom panel (Figure 14D-F) where channels become more defined as the layer thicknesses increase.

Fabrication time. The time required to fabricate guides using this technique include both electrospinning and templating times. Electrospinning time depends on the rate of spinning and the volume spun. This step can range from approximately 5-30 minutes accordingly. The templating step depends on the number of templates used. Template stringing time is approximately five per minute. This can vary depending on the size of the template and the skill of the person.

Versatile fabrication process

Synthetic nerve guides offer two advantages over autografts and allografts: availability and customizability. Our method of electrospinning with micro-templating demonstrates

customizability in many aspects of the design. Electrospinning is a versatile technique that allows tailoring of the fiber diameter and alignment by changing solution and process parameters [146]. Collagen and synthetic sutures of various sizes (6-0, 7-0, and 10-0) were used to demonstrate the ability to form channels with diameters ranging from 33-176μm (Fig 4). The available templates could theoretically be expanded to produce channels over the range of available template diameters: 10 μm with 11-0 to 800 μm with 6-0. However, as mentioned previously, we do not expect to be working in this range.

The number and spacing of sutures can also be altered to match the fascicle geometry of the nerve being replaced. Diameter and length of the guide can be increased by electrospinning wider meshes on larger collectors. Finally, this method is applicable with any electrospun polymer, where the stratified fabrication method permits different polymer to be used for each layer. Since electrospinning solutions can incorporate functional proteins or cells, we may be able to match mechanical properties or incorporate biochemical cues.[140, 147, 148]

Fiber diameter. Parameters for fiber and channel diameter have yet to be optimized for our nerve guide. The size of the fibers with respect to that of the cell can affect how the cell senses and interacts with the substrate.[42] The current electrospinning parameters produce a random mesh approximated by ImageJ measurements to be 2μm diameter fibers (Figure 15E). Control of diameter was not the focus of this work, but significant existing literature can be referenced to tightly control and measure diameter distribution over wide range. Endoneurium, perineurium, and epineurium of native nerve all contain bundles of longitudinally-aligned collagen fibrils ranging from 25-100nm in diameter.[149] However, prior work studying nerve and Schwann cell migration on longitudinally-aligned fibers demonstrates that some directional control may be lost with the use of very small fibers (293nm) and that larger fibers (759 and

1325 nm) yield quickest migration. Thus, while fiber diameter for the current design may affect the cell attachment and infiltration, future work involving incorporation of aligned fibers within channels will rely heavily on a diameter that is optimal for topographical guidance.

Channel diameter. From existing literature, it is unclear whether channel diameters near that of fascicles (200-400µm) or individual axons (2.5-22µm) are more conducive to axon regeneration.[150, 151] Prior work has not demonstrated statistically significant differences for axonal growth depending on channel size.[152] Although previous work with multi-channel guides showed that channels of small (12µm & 19µm) and (105 µm) medium diameter both supported rapid axon growth, small channels also restricted Schwann cell infiltration.[152] Consequently, our current method using medium-sized channels around 100µm may be appropriate.

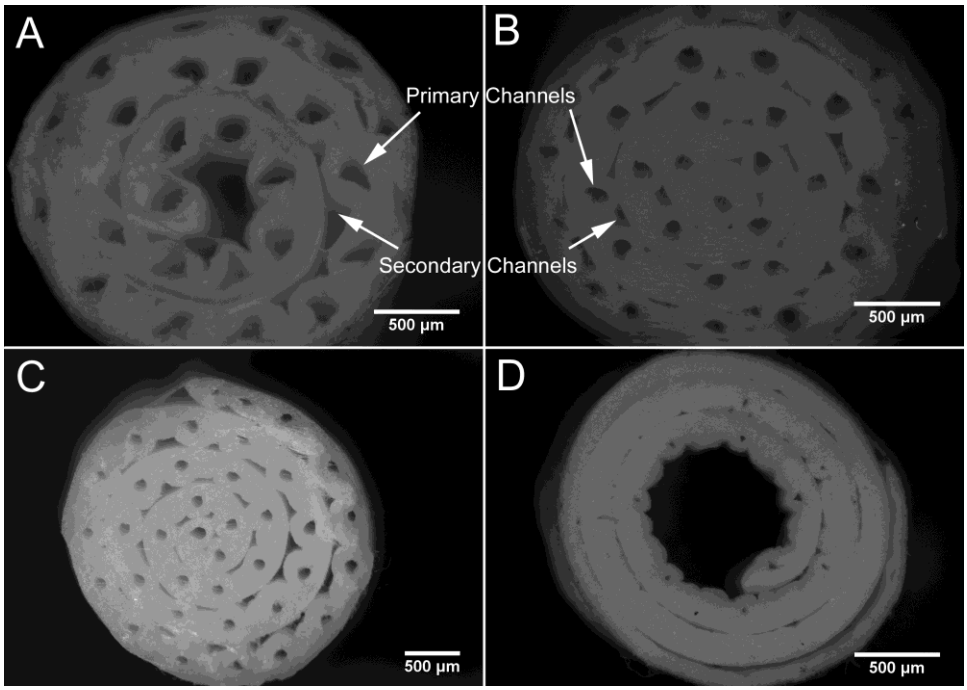

Figure 16. Optical images of multi-channel guides with varying channel diameters.The various guides are not optimized, but rather are used to demonstrate the different diameters achievable using the templating method. Nerve guide fabricated with: (A) 4-0 synthetic sutures (150µm) to produce channels 176 ± 39 µm in diameter; (B) 6-0 collagen sutures (100µm) to produce channels 117 ± 11 µm in diameter; (C) 6-0 synthetic sutures (70µm) to produce channels 98 ± 9 µm in diameter; and (D) 10-0 synthetic sutures (20µm) to produce channels 33 ± 6 µm in diameter. Scale bar = 500 µm.

Electrospun fibers permit Schwann cells to populate the guide

These guides were designed for application in peripheral nerve repair, so initial in vitro work was performed with Schwann cells. Schwann cells are critical to creating a permissive environment preceding nerve repair via phagocytosis of debris, deposition of basal lamina, and release of neurotrophic factors.[113] Although it is controversial whether Schwann cells precede axonal regeneration[153, 154]or follow axons into a lesion site[155, 156], Schwann cells are intricately involved in the regenerative process. For these reasons, tissue engineering approaches to nerve repair have incorporated Schwann cells from a variety of sources including autologous, allogeneic, cell lines, or stem cells.[113] Consequently it is important that Schwann cells respond appropriately to the environment created by our nerve guide.

We demonstrated the feasibility of our design using PCL since it can easily be electrospun. Since PCL is a component of FDA-approved nerve guides, Neurolac, and has been established as a suitable biomaterial from prior peripheral nerve research[112] in vitro biocompatibility tests were not repeated in this research. We aimed simply to demonstrate that Schwann cells infiltrate into the interior of the guide along the microchannels. While PCL exhibits slow degradation which may be suitable for the slow regeneration of nerves[157], we acknowledge that high hydrophobicity and lack of functional groups may preclude PCL from use in our final design.

Guides for all in vitro culture were coated with laminin prior to cell seeding. PCL alone does not contain any functional groups or bioactive domains for cellular recognition. However, in the body most foreign surfaces are quickly coated by natural protein adsorption. To mimic the adhesion sites present in vivo, nerve guides were coated in laminin, a protein known to improve Schwann cell adhesion, proliferation, and survival.[158]

SEM. Schwannoma cell adhesion and morphology on the fibrous electrospun substrate were observed after 8 days in culture. Images from SEM (Figure 15F) show the morphology of these cells on random electrospun fibers of the nerve guide interior. Cells on the random fibers appear to have rounded cell bodies sprawled out on top of the fibers. Cells adhere to random fibers via extension of several processes per cell but do not show any directional preference.

MTT. MTT results from seeded guides show absorbance readings close to that of one million cells. Actual MTT activity may be higher since the guide still contained areas of deep purple color that could not be freed despite mechanical disruption. This suggests that cells are not only alive but metabolically active. However, analysis of these results should consider that histology shows a high density of cells on the outside of the guide (Figure 18C & D) and that MTT cannot provide insight on location of metabolically active cells. Furthermore, thick layers of Schwann cells becoming overconfluent in aggregates may begin to change phenotype and also skew results.

Live/Dead/DAPI. Live/Dead solutions were added to guides at 4 and 11 days (Data not shown). A layer of live cells were identified around the outside of the guide and only a few dead cells were seen evenly distributed throughout the entirety of the guide. DAPI staining showed many more cells distributed throughout the central region of the guide. We believe that the majority of the cells are alive but lack staining by the calcein AM since it is hydrophobic and likely adsorbed by the large surface area of PCL fibers. The staining of dead cells throughout the guide suggests that the more hydrophilic nature of the ethidium homodimer permits it to diffuse more freely. Consequently, the Live/Dead staining was not useful for characterizing cell growth in our guides. Thus MTT was used for quantification while DAPI staining was used to qualitatively inspect distribution and number.

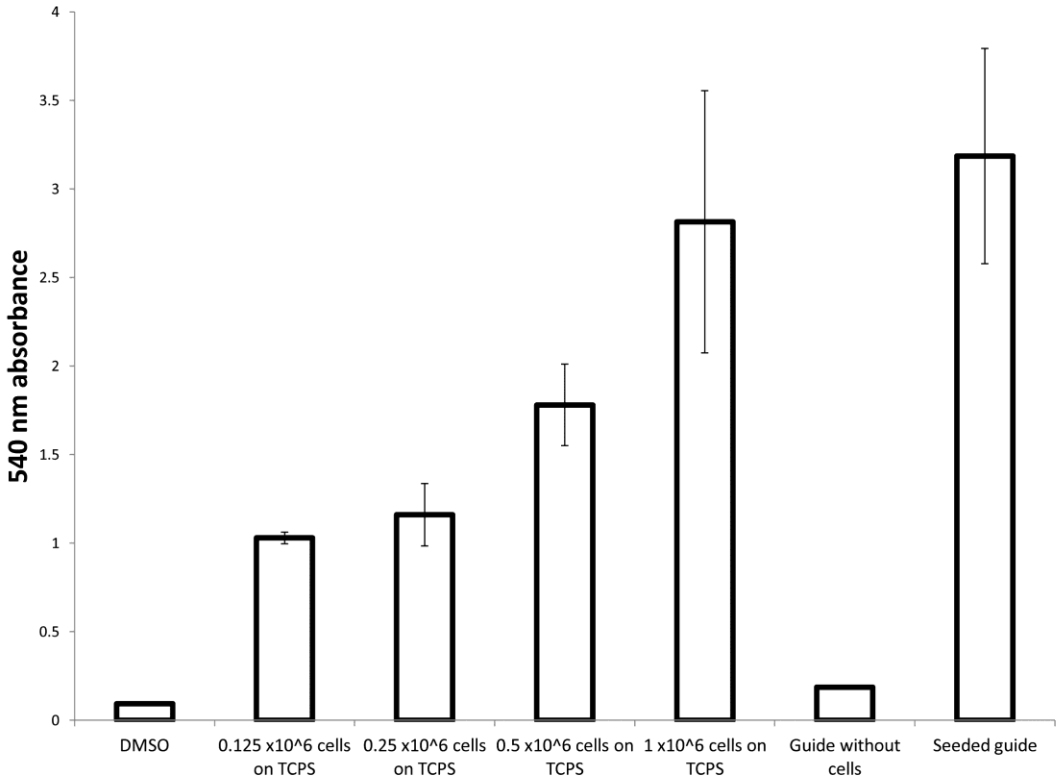

Figure 17. MTT absorbance at 540nm MTT was solubilized in DMSO following conversion by cellular metabolism. Absorbance readings were measured in triplicate for each sample (n=3).

DAPI staining from longitudinal images reveal that Schwannoma cells can populate the entire length of the nerve guide (Figure 18C). By inspection, an increase in cell density can be observed from day 4 to day 11. This suggests cell proliferation within the guide channels, including the mid-section which has the least access to fresh media. Schwannoma cell migration and proliferation throughout the entire guide is further supported by increased cell density throughout channels in the transverse-sections of the nerve guides at the ends (Figure 18 B & D). These reveal that Schwannoma cells primarily reside within the channel lumens and gaps between layers with less penetration into the fibrous walls. This distribution pattern of cells within channels is also seen in longitudinal sections in Figure 18C. The localization of cells

within the channel is consistent with literature reporting the scarcity of cell penetration into the interior of electrospun meshes.[159]

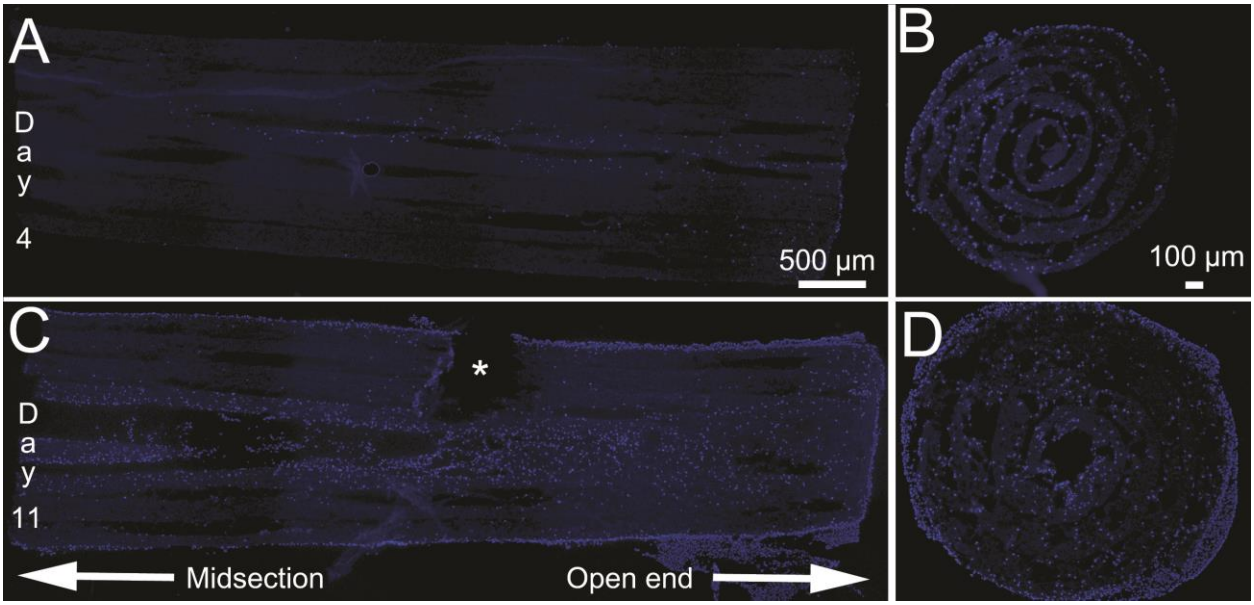

Figure 18. DAPI staining of Schwannoma cell nuclei in the multi-channel nerve guide.(A) Longitudinal section after 4 days in culture. (B) Transverse section at open end after 4 days in culture. (C) Longitudinal section after 11 days in culture. Asterisk indicates tear caused by sectioning. (D) Transverse section at open end after 11 days in culture. Note: Fluorescent look up table (LUT) was adjusted to make nerve guide visible.

We believe that the high surface area and porosity offered by electrospun structures enhances the cell penetration along the channels of the nerve guide. Additionally, open space offered by the channels provides regions of low growth resistance that serve to direct axons toward a single distal target. As supported by the in vitro cell culture, the diffusion permited by this fibrous mesh permits cell proliferation within even the central-most interior of the nerve guides (Figure 18). Additionally, the small size of voids between electrospun fibers restricts most cells from migrating into channel walls and minimizes influx of inflammatory cells from the surrounding tissue upon implantation. Electrospun fibers strike the balance between high interconnectivity that allows good mass transfer and small pathlength that confines Schwann cells and nerves within the channels.

Future work

This work is the first step in demonstrating a new design of synthetic nerve guides. Like any new technology, there are aspects awaiting further investigation. Two modifications that we believe are crucial involve transitioning to a more suitable biomaterial and automating the fabrication. Alternatives to PCL will be pursued in the future to increase hydrophilicity, introduce cell adhesion sites, and broaden degradation profile to match clinical needs. Ten-cycle compressive tests (not shown) demonstrate hysteresis after an initial plastic deformation. Thus to prevent channel collapse in future designs we will use an elastomer such as poly(glycerol sebacate) that increases elastic recovery.[160]

Variability introduced during the manual steps is a limitation that may be addressed using robotics in the future. Current methods involve templates that are extremely small and difficult to handle. Automating the process in the future should not only improve reproducibility, but also increase the channel density that can be achieved.

3.1.4 Summary

This work presents a new electrospun construct containing a high density of aligned microchannels mimicking the fascicles in nerve. We demonstrate a high number of channels of defined size and shape within a porous structure. We believe these features distinguish our design from existing ones. We also demonstrate the repeatability and versatility of this method and begin to characterize cellular response. We will continue to focus on translating this technology into clinically-useful products by testing the guides in a rat sciatic nerve model. Results from a pilot implantation demonstrate that the guide can anastamosed with 10-0 suture

and maintains its shape without unrolling. In the future, we will couple this design with stimulatory cues such as aligned fibers within the aligned channels and growth factors.

3.2 INCORPORATION OF LONGITUDINALLY ALIGNED FIBERS WITHIN CHANNELS OF FIBROUS NERVE GUIDE

3.2.1 Introduction

Topographical guidance cues

Literature reports that aligned fibers can provide direct paths to guide axon growth cone and Schwann cell migration.[132, 135, 161-165] Additionally, parallel fibers may be involved in the differentiation/maturation of neural stem cells and Schwann cells.[134, 166, 167] As summarized in the review by Spivey et al, "Clinical evidence suggests that nano- and microtopography incorporated into scaffolds does not merely improve peripheral nerve regeneration, but is in fact a prerequisite for meaningful restoration of nerve function."[168] Thus, topographical cues are especially important for enabling large gap regeneration. Despite promising results in 2-dimensional studies, incorporation of parallel fibers into 3-dimensional constructs has proven difficult by traditional electrospinning methods.[139]

Several types of nerve guides have been designed to incorporate aligned fibers, with recent results favoring highly open architectures. The simplest method to incorporate aligned fibers into a 3-D nerve guide is to fill the lumen of a conduit with a bundle of aligned fibers (Figure 19A).[30, 139, 169-175] This approach results in dense fiber packing, which impedes cell infiltration[113, 161] and reduces total axon number.[176] The second most common method is to line

the inner surface of a luminal conduit with aligned fibers (Figure 19B).[132, 136, 177-179] This approach benefits regeneration but does not maximize surface area for topographical guidance. To increase surface area, a third option places one to three aligned sheets in a conduit at low packing density (Figure 19C).[141, 180] Promising results from these designs also favored low fiber density since single-sheet designs regenerated more axons and out-performed three-sheet guides.[141]

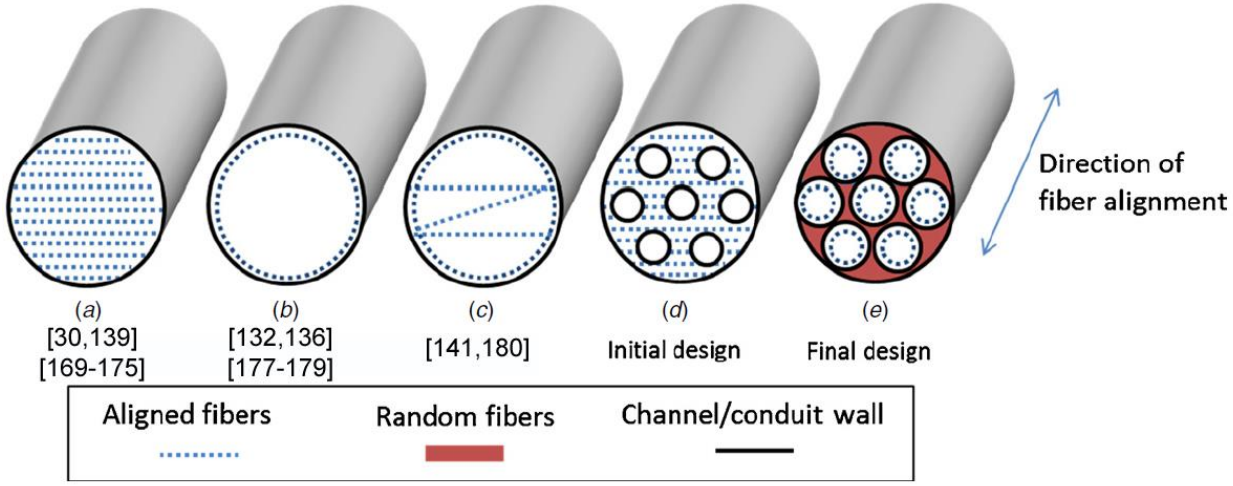

Figure 19. Incorporation of aligned fibers in existing (a-c) and proposed (d-e) nerve guides (a) High density of longitudinally-aligned fibers packed into lumen. (b) Longitudinally-aligned fibers line the lumen, but leave most of the cross-section open. (c) Stacked sheets of aligned fibers are placed in the lumen of the guide to provide greater topographical surface area. (d) Incorporation of microchannels into lumen of parallel fibers is difficult because low fiber entanglement allows fibers to slide, causing channel collapse. (e) Aligned fibers line multiple microchannels of nerve guide to provide high surface area of topographical cues.

Challenges to fabricating aligned fiber guide

Our goal was to: 1) incorporate high surface area of aligned fibers into a 2) highly-open nerve guide to mimic native nerve architecture. The initial approach to add channels to a fiber-filled lumen (Figure 19D) proved difficult since an entire guide of aligned fibers has low fiber entanglement, causing channels to fall apart. Thus, our criteria were amended to include: 3) sufficient structural integrity to avoid channel collapse. This was accomplished by fabricating channel-filled guides (Figure 19E) where aligned fibers line the lumens of microchannels, held in

place by random fiber mesh. We adapted our previous templated electrospinning technique to incorporate aligned fibers.[181] Slowly degrading polycaprolactone (PCL) fibers were aligned to provide sustained guidance while poly (lactic glycolic acid 50:50) PLGA fibers provide structural support until fibrin and extracellular matrix (ECM) are deposited.

3.2.2 Experimental Section

Materials

A nerve guide was constructed of electrospun polycaprolactone (PCL) and poly (lactic glycolic acid 50:50) PLGA fibers. A 14% PCL (Mn=80,000 Sigma-Aldrich Corp, St. Louis, MO) solution was prepared in 5:1 trifluoroethanol (TFE):H2O and 15% PLGA 5050-DLG-9A (Mn=168,000 Evonik Degussa Corporation, Birmingham, AL) was dissolved in 1,1,1,3,3,3-hexafluoro-2-propanol (HFIP). A custom parallel plate collector was used to collect fibers and string templates during fabrication (Figure 22(a)). It was constructed by placing two short pieces of aluminum orthogonal to parallel collector plates to maintain a specified distance during electrospinning and fabrication. Combs attached to the long sides of the parallel plate collector were used to keep templates in place as they were strung. The templates used for this design was 130μm diameter Trilene 2lb fishing line (Berkley, Spirit Lake, IA). This is much less expensive than sutures (as previously used) yet low friction for easy removal.

Electrospinning

Aligned PCL fibers were electrospun onto a parallel plate collector (Figure 20.1). Templates were strung parallel to the PCL fibers by weaving onto the combs (Figure 20.2). A second layer of aligned PCL fibers were electrospun on top of the templates (Figure 20.3). The

aligned fibers were then cut between templates with a scalpel to create openings (Figure 20.4). This caused the PCL fibers to form bundles around the template and created space for the PLGA layers to interact. Random PLGA fibers were electrospun to each both sides of the collector to hold the bundles of aligned fiber/channels in place (Figure 20.5). This was done by holding the parallel plate in front of a grounded razor. The templates were cut, and the composite rolled up (Figure 20.6). A thin sheath was deposited around the perimeter of the guide by electrospinning 15 µL PCL solution while rotating (60 rpm) the construct directly in front of a grounded razor blade (Figure 20.7). It was then placed in a vacuum oven at 45ºC for 24 hours to remove excess solvent. The templates were then removed and the guide trimmed to size (Figure 20.8).

(a)

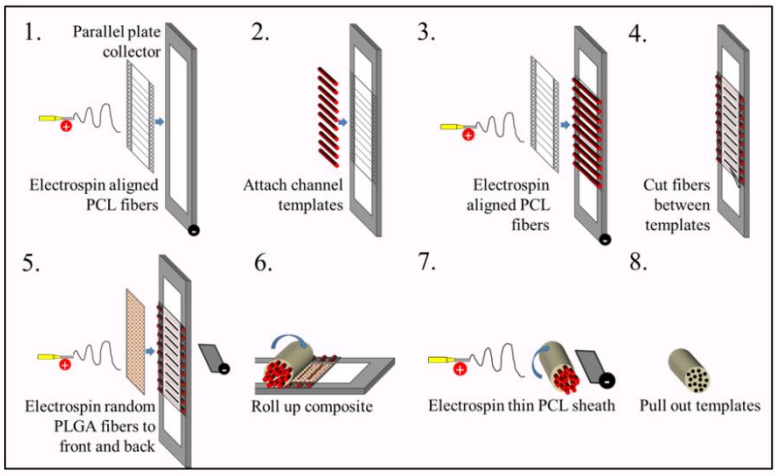

(b)

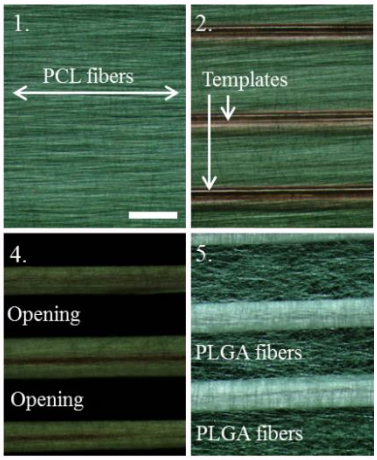

(c)

	Positive Potential (kV)	Negative Potential (kV)	Distance (cm)	Flow Rate (µL/min)
(1,3) Aligned PCL	10 on needle	10 on parallel plate	20	15
(5) Random PLGA	10 on needle	10 on razorblade	20	15
(7) PCL sheath	12 on needle	10 on razorblade	20	25

Figure 20. Schematic of nerve guide fabrication(a) with light microscope images of fibers and templates (b) and electrospinning parameters (c). 1) Aligned PCL fibers were deposited across gap of open collector by electrospinning. 2) Template was attached to collector parallel to PCL fibers. 3) Aligned PCL fibers were electrospun on top of template. 4) The PCL fibers were cut between templates with scalpel so PLGA layers in the next step could bind. 5) PLGA was electrospun to front and back to hold bundles of aligned fibers and templates together. 6) The composite was removed from the collector and rolled up. 7) A PCL sheath was electrospun around the outside to prevent unraveling. 8) After removing the solvent in a vacuum oven at 45ºC for 24 hours, the templates were pulled out and guide trimmed to size. (Scale bar:500µm).

Scanning Electron Microscope (SEM)

Samples were soaked in water and frozen on dry ice before cutting with a scalpel to 1-2mm transverse slices. The samples were then dehydrated in a desiccator overnight before sputter coating with 3.5nm gold with a Cressington Sputter coater. A Jeol JSM-6330F SEM was used to image the samples at 3kV acceleration voltage.

Image Analysis

Fast Fourier transform (FFT). Fiber alignment was quantified as described by Corey et al.[162] Briefly, FFT analysis was performed on greyscale images in ImageJ using the "FFT" function under "Process". The FFT output image was rotated 90^{o} to account for phase shift in transform to match SEM image. Radial summation of pixel intensity of FFT images was performed by selecting the FFT image with the circle tool and running the "*Radial profile"* plug-in (360^{o}, radial sums). Due to symmetry of FFT, 180^{o} was plotted (Figure 22C) with peak alignment centered on 0^{o}. The full-width half maximum (FWHM) was reported as a single index of fiber alignment. It is measured by the width of a function at half the height (peak-to-valley).

Fiber Diameter. Fiber diameter was quantified in ImageJ by drawing a horizontal line across the SEM image and measuring at least 30 fibers intersecting this line.

Channel analysis. Image analysis was performed on binary images of SEM cross-sections using Nikon NIS-Elements software. Three cross-sections with minimal cutting artifacts were selected for analysis. Channel area was measured by using the region of interest (ROI) tool to select channels by autodetect or by manually tracing. The ROI selection tool was also used to measure the area and perimeter for the whole construct. Assuming a circular shape, diameter and perimeter were calculated from the area for each channel. These values were used to determine the channel area percentage and surface area ratio by the equations shown below.

The first value reflects the open area of the guide available for cell infiltration. The surface area ratio represents how much more surface area of aligned fibers is provided by the multi-channel design than a single lumen design for a construct of equivalent length.

$$\text{Channel area percentage} = \frac{\text{sum of channel areas}}{\text{area of construct}} * 100 \qquad \text{Equation 1.}$$

$$\text{Surfacea area ratio} = \frac{\text{sum of channel perimeters}}{\text{perimeter of construct}} \qquad \text{Equation 2.}$$

Cell infiltration and attachment

Control guides. Cell infiltration into our experimental nerve guides was compared to control guides which contained longitudinally-aligned PCL fibers without channels. Aligned PCL was electrospun to open collectors as previously described in 200 µL intervals and rolled such that fiber alignment was parallel to the longitudinal axis. This was repeated until the diameter of the construct was equivalent to the experimental guides (approximately 1.75 mm). A sheath was electrospun around the outside using the same technique described for the experimental guides.

Cell seeding in fibrin. Rat Schwannoma cell line RT4-D6P2T (ATCC CRL-2768) were trypsinized and resuspended in 3 mg/mL fibrinogen (Sigma F8630) solution at 2 X 10^6 cells/mL. A 90 µL fibrinogen/cell solution was added to 10 µL thrombin (Sigma T4648) solution (2 mg/mL) and pipetted into the end of each segment of nerve guide (1.5-3.5mm length). The fibrin quickly gelled within 30 seconds and 2 mL Dulbecco's modified eagle medium (DMEM) (ATCC 30-2002) with 10% fetal bovine serum (FBS) and 1% antibiotic/antimycotic (Cellgro 30-004-Cl) was added to each guide in a 12-well plate. Cells were cultured for 24 hours in a 37ºC incubator at 5% carbon dioxide.

DAPI Staining. Guides were removed from media and fixed in 10% buffered formalin (Fisher Scientific SF100-4) for 15 minutes. They were then washed in deionized water before freezing in Tissue-Tek O.C.T compound (VWR 25608-930). Slides were prepared by cutting 50 µm longitudinal sections on a microtome and staining with DAPI mounting media (Vectorlabs H-1500). Images were captured on a Nikon Eclipse Ti inverted microscope.

SEM Imaging. Samples were fixed in 10% formalin for 15 minutes before washing in deionized water. They were then serially dehydrated by soaking in 100% ethanol, 3:1 ethanol: hexamethyldisilazine(HMDS), 1:1 ethanol:HMDS, 1:3 ethanol:HMDS, 100% HMDS for at least 15 minutes each. Samples were cut with a scalpel, placed on SEM stubs, and imaged with SEM as described above.

3.2.3 Results/Discussion

Biomimetic architecture

We designed nerve guides to mimic native nerve architecture and achieved a cross-sectional pattern for our electrospun nerve guide (Figure 21A&C) that is almost indistinguishable from decellularized nerve (Figure 21B&D) [images: courtesy Dr. Tatsuo Ushiki, M.D, PhD, Niigata University Graduate School of Medical and Dental Sciences]. Both contain a high number of channels surrounded with thin fibrous walls. It should be noted that channel diameter in our guide are approximately 30 fold larger than those in the decellularized nerve image. We chose 130 µm diameter based on existing literature suggesting that large channels are sufficient and likely preferable[152, 182] although the same technique could be translated to smaller channel sizes.

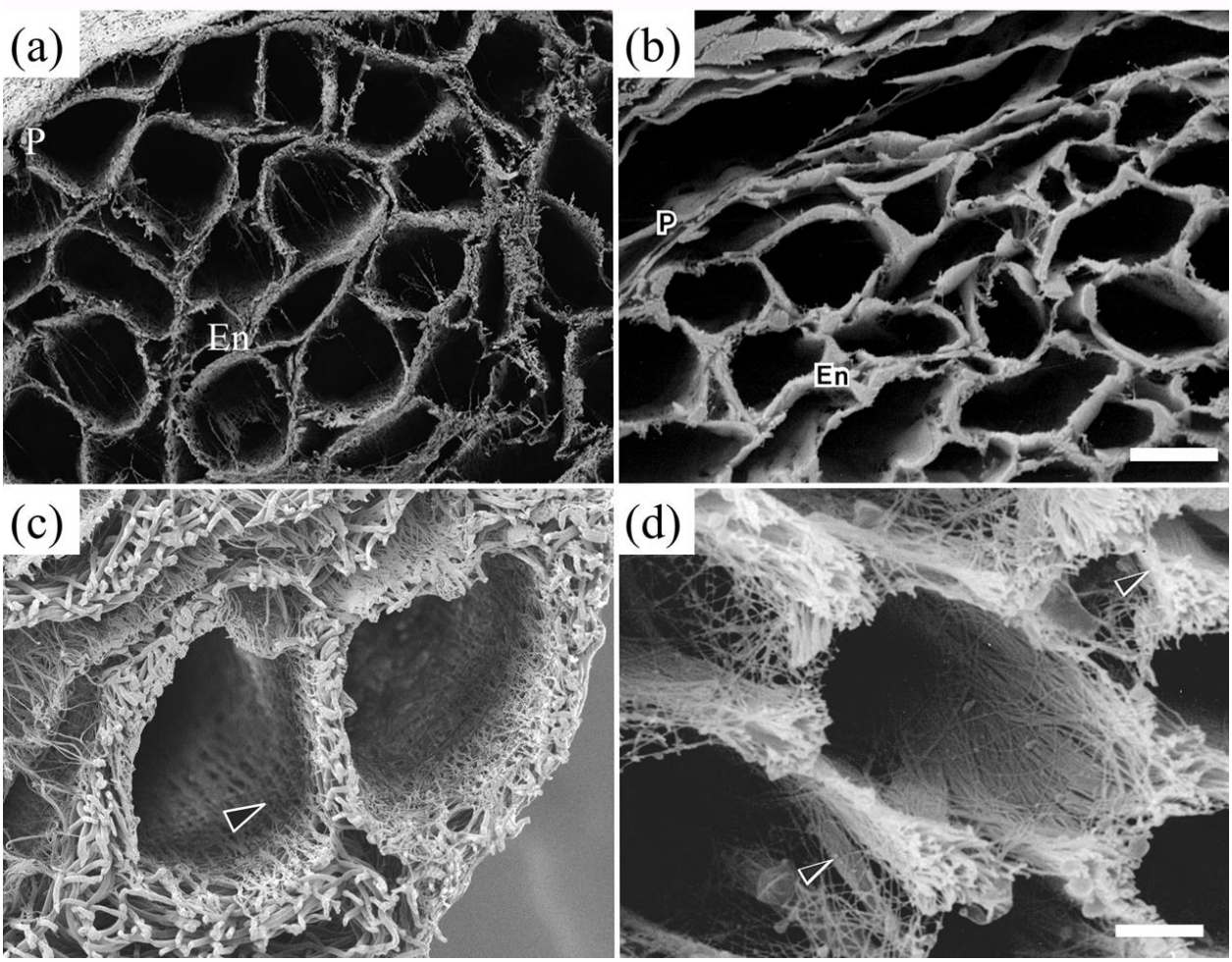

Figure 21. SEM images showing structural resemblance of(a,c) electrospun nerve guide to (b, d) decellularized nerve (images: courtesy Dr. Tatsuo Ushiki). *Adapted for reprint with kind permission from Springer Science and Business Media* [183]. Note the scale in electrospun images is larger than that of decellularized nerve. (a: 150µm, b: 5µm, c: 40 µm, d: 2 µm) P- perineurium. En-endoneurium. Arrowhead- c: aligned PCL fibers lining microchannel wall- d: longitudinally arranged collagen fibers.

Immobilization of aligned fibers for a stable structure

As described previously, a significant challenge of using aligned fibers for scaffolds is their tendency to fall apart due to low entanglement. We developed an innovative approach to secure the aligned fibers and maintain intact channels throughout the production process and in the final product. Fabrication is performed on custom-designed parallel plate collectors with three features that are key to this process. Firstly, the parallel plates offer a simple method to create aligned fibers without using rotation or transferring fibers from a mandrel. This is

supported by literature reports where parallel plates are used to electrospun aligned fibers of poly(lactic acid), polyamide-6, poly(ethylene oxide), PCL:collagen blends, or poly(vinyl alcohol).[184-188] Secondly, there is an aligned-to-random transition that occurs at the collector edges as discussed in the paper by Xie et al.[189] These random fibers help to hold the aligned PCL fibers in place until the fabrication is complete, after which they are cut off and discarded. Finally, the open collector permits electrospinning to both sides of the guide, resulting in better PLGA interaction and thinner walls than the flat plate method. The slits between aligned fibers were also crucial to allowing random PLGA fibers to bind and hold the bundles of parallel fibers/templates in place.

Aligned fibers are suitable for topographical guidance

The emphasis of this paper is the presentation of aligned fibers to cells to present topographical guidance in an open architecture to facilitate cell infiltration and neurite outgrowth. Thus fiber alignment is quantified to demonstrate directional preference. Fiber diameter is measured to ensure that it falls within the optimal range established in the literature.

Alignment. The aligned region of electrospun PCL can be distinguished from the random PCL fibers visually (Figure 22B&C). The FWHM values obtained by FFT of SEM images were used to quantitatively compare alignment fiber alignment. Fibers in the aligned region produced a FWHM value 1.6 times of random fibers. Although we did not establish criteria for minimal alignment, the FWHM value could be used in future designs to set a standard for alignment and ensure reproducibility.

Diameter. Average fiber diameter for the random and aligned regions of PCL were calculated to be 86 and 60 μm respectively. Prior literature suggests that neurite and Schwann cell migration are best directed by 5μm fibers compared those of larger diameters (30, 100, 200,

500) but also prefer 1.33 and 0.76 μm fibers over 0.29 μm fibers.[161, 190] Thus, fibers in the range of 0.76 μm to 5 μm should be appropriate for providing guidance cues. Additionally, the random PLGA fibers used for structural support were of larger diameter, resulting in larger pore sizes between fibers to permit greater cell infiltration.

High surface area for topographical guidance. By lining 58-72 microchannels with aligned fibers, the guides offer 5.6 times more surface area than single-lumen guides of equivalent length and diameter as estimated by equation 2. This guidance is expected to reduce aberrant growth and shorten time to recovery.

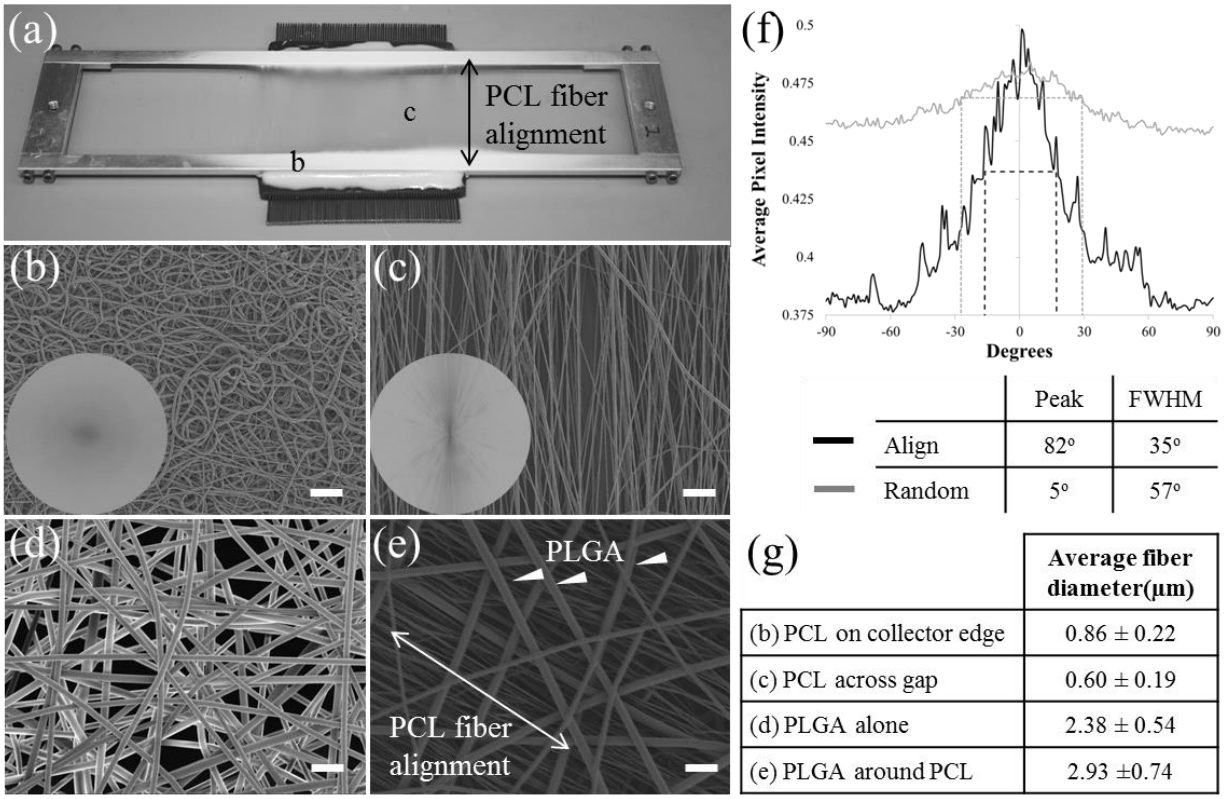

(g)

	Average fiber diameter(μm)
(b) PCL on collector edge	0.86 ± 0.22
(c) PCL across gap	0.60 ± 0.19
(d) PLGA alone	2.38 ± 0.54
(e) PLGA around PCL	2.93 ±0.74

Figure 22. Fiber collection on parallel plate collector.(a) Parallel plate collector maintained at fixed width by two perpendicular spacers. Dimensions of gap region were 4cm X 18cm. Note the edges of the long sides have been sharpened to a triangular edge for better fiber collection. Combs were attached to each side for template fixation. Electrospun PCL fibers were deposited randomly on the aluminum (b) and aligned across the gap (c). (b) SEM of random PCL fibers deposited on aluminum parallel plate of open collector [Insert: FFT of fiber SEM] (c) Aligned PCL fibers span gap between parallel plates. [Insert: FFT of fiber SEM], (d) SEM of random PLGA fibers, (e) SEM of random PLGA fibers [arrowheads] on top of aligned PCL fibers [arrow] (f) Graph of average pixel intensity in radial direction of FFT images adjusted to center around 0o,(g) Average fiber diameter of PCL and PLGA used in scaffold preparation. (Scale bar: b-e: 10 μm).

Open architecture for cell infiltration

Nerve guides constructed simply by filling conduits with aligned fibers may obstruct cellular infiltration. In contrast, our nerve guides offer 51% open space by reducing channel wall thickness and limiting aligned fibers to channel perimeters. The thickness of PCL and PLGA layers were adjusted to minimize wall thickness while maintaining strength to prevent channel collapse. In most channels, the wall is less than 20 microns. This will provide much more area for cell infiltration than our previous design (25% open)[181] and improve transport of nutrients and waste.

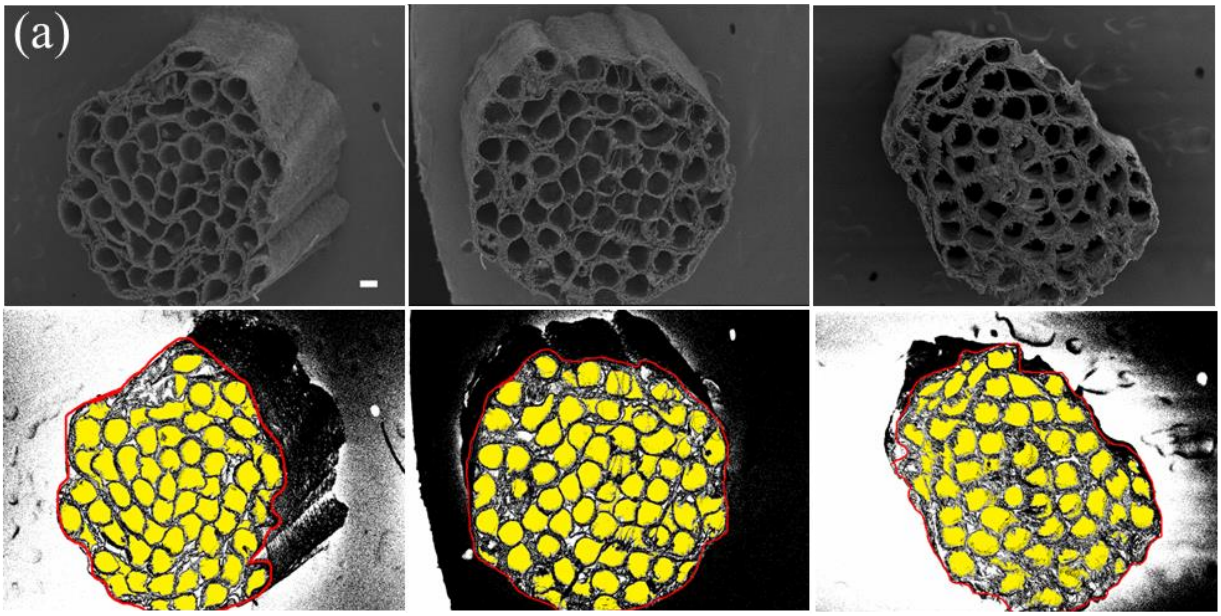

(b)

Number of channels	Channel diameter(μm)	Surface area ratio	Channel area percentage
65 ± 7	133.4 ± 24	5.67 ± 0.6	51 ± 5.6

Figure 23. Analysis of SEM images of 3 samples representative of nerve guide architecture.(a) A high number of microchannels can be observed. (b) Individual channel dimensions were measured to determine channel number, channel diameter, surface area ratio, and channel area percentage. (Channels highlighted in yellow, guide perimeter outlined in red) Table shows average values for 3 cross-sections ± standard deviation. (Scale bar: 100μm).

Schwannoma cell culture

In vitro experiments were performed to test our hypothesis that the open design of our experimental guide was more conducive to cell infiltration than control guides without channels. Additionally, aligned fibers would provide topographical cues to cells. Cells were seeded in both guides with fibrin gel to mimic the natural fibrin bridge that forms in guides during regeneration.

Closed architecture of control guides without channels

Control guides fabricated by methods described in Figure 19A contained longitudinally-aligned fibers but no channels. This method produced a closed cross-sectional structure with only a few open regions observed between layers (Figure 24A). The tight fiber packing can be observed clearly in Figure 24B&C, corresponding to cross-sectional and longitudinal sections of the control guides.

Fiber alignment promotes cell elongation

Cells in both guides exhibit elongated cell bodies when attached to the aligned PCL fibers (Figure 24D &F) while remaining more rounded on the random PLGA fibers (Figure 24E). This change in cell shape suggests that topographical cues are directing cell morphology. We anticipate that these cues will increase Schwann cell infiltration while also directing neurite outgrowth during regeneration.

Open architecture permits cell infiltration

The experimental guides show a moderate number of cells distributed evenly throughout the guide (Figure 24G). In contrast, the control guide shows only a few cells that are restricted to the gaps between layers (Figure 24H).

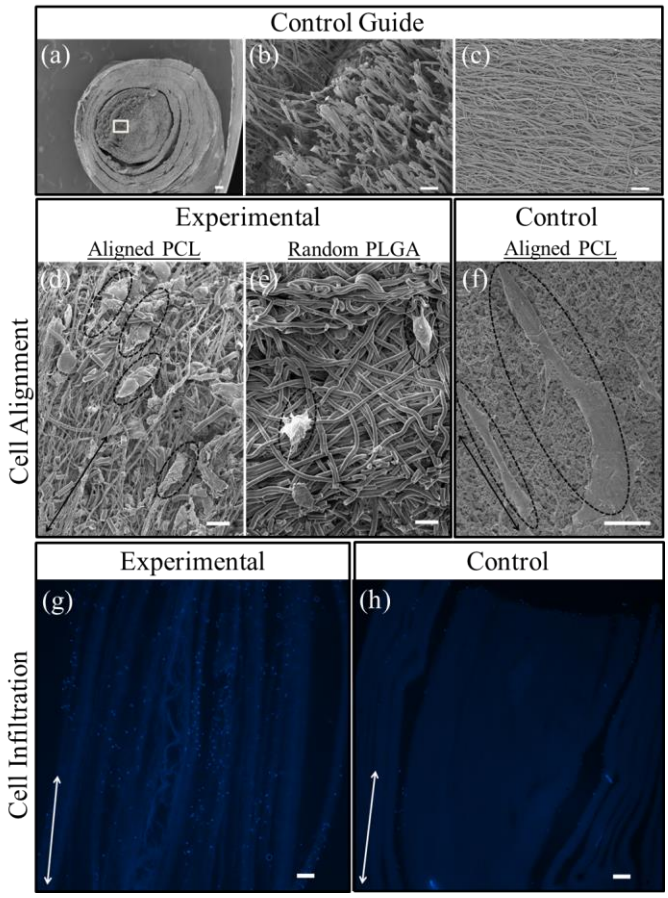

Figure 24. Results from Schwannoma cell culture on experimental and control nerve guides.(a-c) SEM of control nerve guide. (a) Cross-section of guide shows some openings between layers of aligned fibers. (b) Magnified cross-section from (a) showing aligned fibers with limited space for cell infiltration. (c) Longitudinal slice of guide showing fiber alignment along axis. (d) SEM showing Schwannoma cells elongated along PCL fibers in experimental guide. Some fragments of PLGA fibers are also present and may have broken during the dehydration/cutting steps. (e) SEM of Schwannoma cells on larger random PLGA fibers in experimental guide. (f) SEM of Schwannoma cells elongated on PCL fibers in control guide. Underlying fibers may be coated with fibrin. (g&h) Schwannoma cells seeded into nerve guides are characterized by DAPI staining. (g) Longitudinal section of experimental guide showing Schwannoma cells distributed throughout the guide. (h) Longitudinal section of the control guide showing few Schwannoma cells that are restricted to gaps between layers. Arrow indicates direction of fiber alignment and dashed circles identify cells. (Scale bar: a:100 μm, b-h: 10 μm).

Limitations and future work

Collector Limitations

Several collector modifications were identified that could contribute to greater alignment and uniformity in the future. For instance, the open collectors were machined from aluminum rods and contained edge defects. In the future, the edges could be polished to remove

imperfections and increase alignment. Additionally, the combs attached to the collector protrude slightly and interfere with the PLGA deposition near the ends of the guide. Thus, approximately 1cm of the guides were trimmed from each end and discarded to remove these inhomogeneous regions. With a collector gap of 4cm, this leaves 2cm remaining of useable guide. We anticipate that these wasted regions can be minimized by laser cutting collectors from metal stock. Finally, there may be a maximum limit to the gap size across which fibers can form, limiting the size of nerve guides that could be fabricated by this method.

Reproducibility of channel linings

The current fabrication method is labor intensive and varies by operator. Figure 25 depicts SEM cross-sections of individual channels showing the desired lumenal lining as well as collapsed lining, delaminated lining, and no lining. These defects likely result from manual removal of the template and could introduce variability. The number of channels per guide also varies some since secondary channels can be formed between layers as a result of rolling while other channels may collapse under sufficient forces. A benefit of using the multichannel approach is that with the unfortunate collapse of or occlusion of a few channels should not result in complete failure of the guide due to remaining channels. Soluble templates are currently being investigated to allow the ends to be cut off with the physical template still in place and also reduce the chance that aligned fibers are disrupted during template removal. The high porosity of the guide should facilitate the dissolution and removal of template materials. The overall reproducibility of this type of guide will need to be improved before clinical translation and could benefit from the precision and reliability of robotic manufacturing.

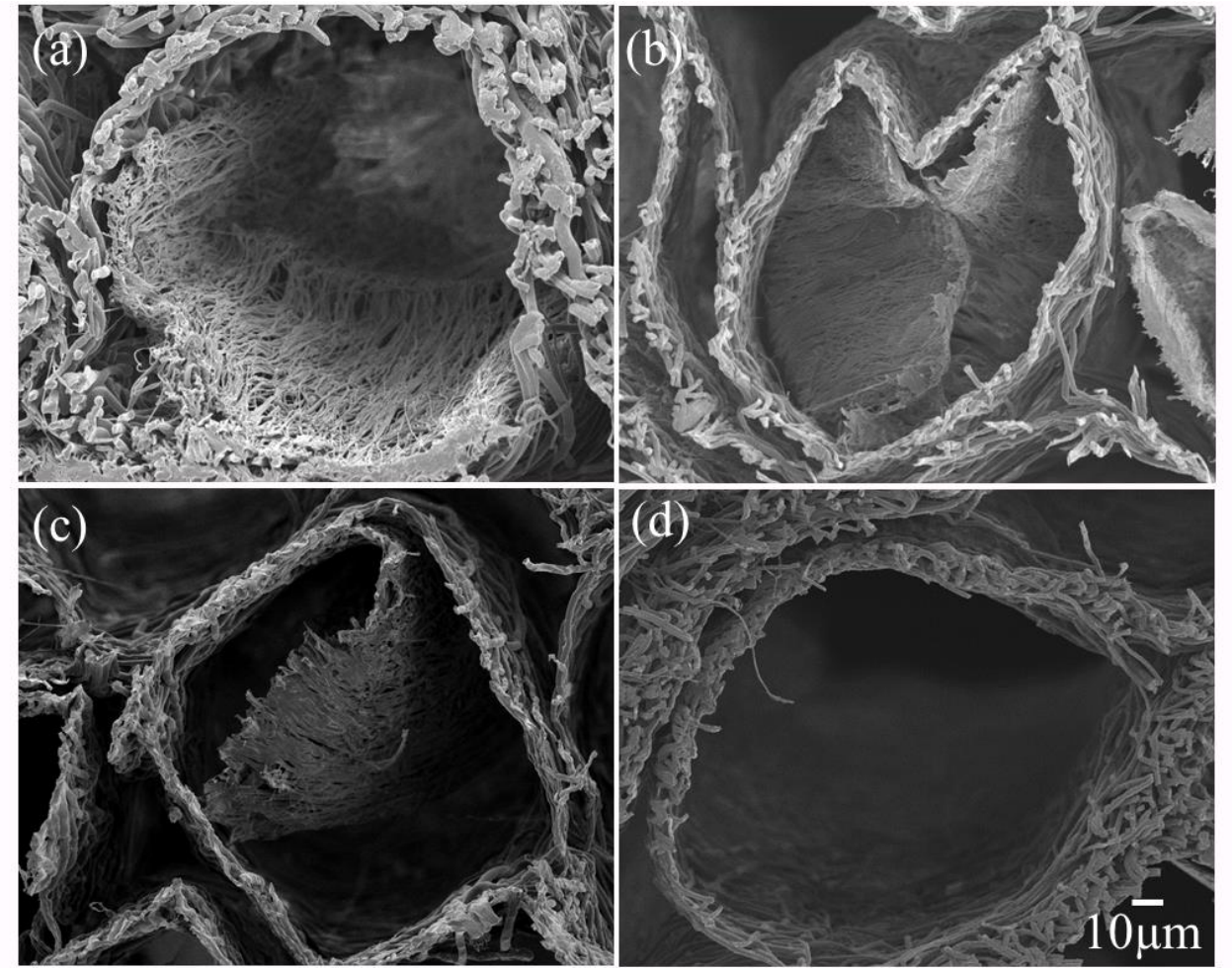

Figure 25. SEM of channels showing the microchannels lined with parallel fibers(a) lumenal lining, (b) collapsed lining (c) delaminated lining, or (d) no lining. (500X magnification)

3.2.4 Summary

We demonstrated a new technique to distribute aligned fibers within a 3D nerve guide that mimics the native architecture. The guide has thin walls and high channel number to maximize surface area without obstructing infiltrating cells. To fully test the benefits of our design will require in vivo testing. We anticipate this approach can be applied to other materials to match mechanical and degradation properties to improve nerve regeneration.

4.0 COMBINING FDM WITH TEMPLATED ELECTROSPINNING FOR MICROVASCULAR SCAFFOLDS

Chapter Aim

Prior work demonstrated constructive remodeling of acellular poly(glycerol sebacate)(PGS) vascular grafts in situ.[191, 192] We hypothesized that this regenerative process could be extrapolated to the microvasculature and used to perfuse TE scaffolds. The aim of this chapter was to pattern electrospun scaffolds with capillary-like branched templates that can be rapidly endothelialized. Electrospun poly(dioxanone) (PDO) was used as the scaffold material since electrospun PGS was being developed in parallel (Aim 3). An FDM printer was used to make branched templates with greater versatility and automation than the sutures in Aim 1. Additionally, nontoxic water-soluble poly(vinyl alcohol) (PVA) templating material enabled easy removal. Feasibility of endothelializing these of microvascular scaffolds was established in vitro.

Background

Sufficient vascularization is a 'major bottleneck' of solid organ tissue engineering and achieving it has even been called the 'holy grail of tissue engineering'.[2, 11] Transplanted cells often die from lack of oxygen and accumulation of waste. This is especially true for those with high metabolic activity such as neurons,[193] hepatocytes,[194] and cardiomyoctes.[5, 195]

There is extensive literature describing existing approaches to vascularize TE constructs.[1, 6, 196-201] Vascularization is critical for maintaining cell survival by providing effective nutrient delivery and waste removal beyond the 200 μm diffusion limit.[4, 5] Although angiogenic factors can induce sprouting of vessels into ischemic tissue, this slow (~ 0.1 mm per day) "extrinsic vascularization" (Figure 26) can take months to perfuse large organs, eliciting necrosis within the core.[1, 199] Even organs with a pre-formed internal vasculature can take up to 8 days to perfuse by inosculation (Figure 27).[202] Consequently, an intrinsic network (Figure 28) that can be sutured to host vessels is needed to provide immediate perfusion upon implantation.[199] Current sources of intrinsic vascular networks rely on harvesting vascularized pedicles from donor sites.

Summaries of current approaches are summarized below:

Porous or microfabricated scaffolds can facilitate cell ingrowth and vessel organization to hasten the slow extrinsic vascularization process. Methods for fabricating these scaffolds include photolithography, microcontact printing, micromolding, and laser direct writing.[1]

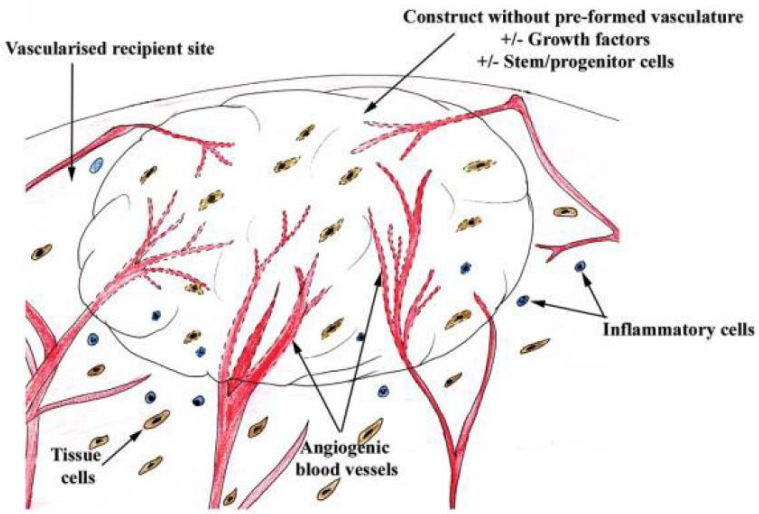

Figure 26. Extrinsic Vascularization. Reproduced from [199]

Coculture of endothelial cells with fibroblasts and other perivascular cells can form stable pre-formed vasculature in vitro. Coculture methods can also be combined with microfabrication methods such as the InVERT method.[203] However most coculture methods rely on inosculation since they are too weak to directly anastamose with host vessels. Additionally, low mechanical properties of immature cellular constructs hinder load-bearing applications.[96, 204, 205]

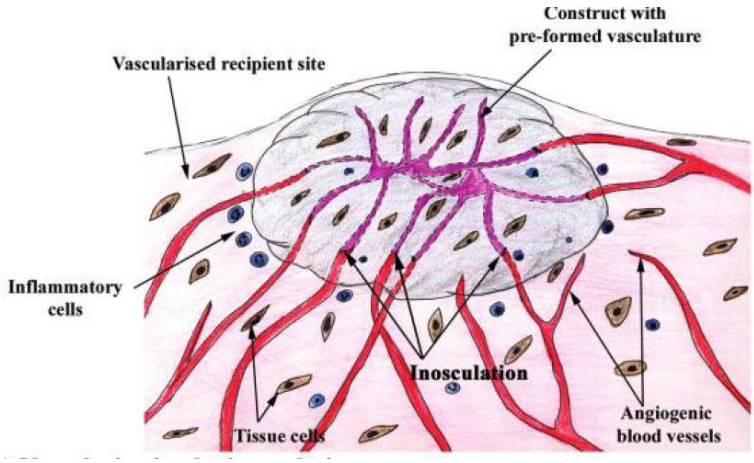

Figure 27. Inosculation. Reproduced from [199]

Prevascularization of a scaffold utilizes intrinsic sprouting from an arteriovenous loop (AV) implanted in a donor site. [206, 207] The presence of the vessel within the core of the construct permits rapid vascularization. Once established, this construct can be surgically removed and anastamosed at the target site.[208] While this is an effective method,[209] major drawbacks include the time and additional surgical site required to mature these in vivo.[1, 208]

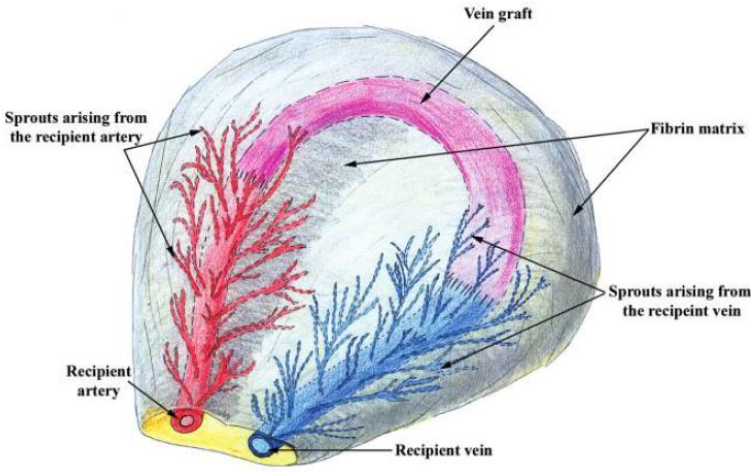

Figure 28. Intrinsic Vascularization. Reproduced from [199]

4.1 MICROVASCULAR SCAFFOLDS MADE BY COMBINED FUSED DEPOSITION MODELING AND ELECTROSPINNING

4.1.1 Introduction

Vascular networks within TE constructs have been developed through techniques including soft lithography,[60, 61, 210-219] cast hydrogels,[102, 220-227] coculture,[228-230] and solid freeform fabrication (SFF).[85, 231-240] Recent advances in these methods have made strides toward building 3D constructs, improving porosity, and incorporating different cell types.[61, 203, 220] However, shortcomings such as low mechanical strength (hydrogels),[204] limited diffusion through thick solid walls separating microvessels from parenchyma (soft lithography),[61] and nondegradability (poly(dimethylsiloxane) (PDMS)-based method) still hamper direct anastomosis and perfusion of TE constructs after implantation.

We address these issues by introducing a new technique that uses fused deposition modeling (FDM) as an indirect method to pattern vasculature networks within electrospun

scaffolds. The electrospun polydioxanone (PDO) scaffolds are strong and suturable, to allow direct anastomosis with host vessels. Additionally, electrospun fibers offer high porosity and surface area to permit diffusion and promote cell attachment, respectively.[241] Furthermore, PDO resorbs within 6 months.[242, 243] Feasibility of endothelializing these vascular networks is demonstrated by in vitro culture and perfusion.

4.1.2 Experimental Section

Micropatterned Template and Scaffold Fabrication

Fused deposition modeling. A FDM printer (AO-101, Lulzbot, Loveland, CO) was used to extrude capillary networks from 3 mm poly(vinyl alcohol) (PVA) filament (Ultimachine, South Pittsburg, TN) (Figure 29A-C). Printing was performed at 210°C nozzle temperature and 120°C bed temperature. Designs for the micropatterned template were written in G-code and optimized to maximize template uniformity and reproducibility. The printer was run using Pronterface open-source program.

Electrospinning. PDO (Sigma-Aldrich, St. Louis, MO) was dissolved in 1,1,1,3,3,3-hexafluoroisopropanol (HFIP, Oakwood Products Inc, West Columbia, SC) to prepare an 11% solution. This solution was pumped at 29 µL/min through a 22 gauge needle at 7 kV (+) and collected on an aluminum plate at 7 kV (-) and 20 cm away. The first layer of PDO fibers was deposited to an aluminum collector by vertically electrospinning 350 µL of the solution (Figure 29D-i). The printed PVA template was placed on the PDO fibers (Figure 29D-ii) before electrospinning a second layer of 350 µL PDO (Figure 29D-iii). The scaffold was removed from the aluminum collector and washed twice in deionized water with agitation for 24 h to remove PVA (Figure 29D-iv).

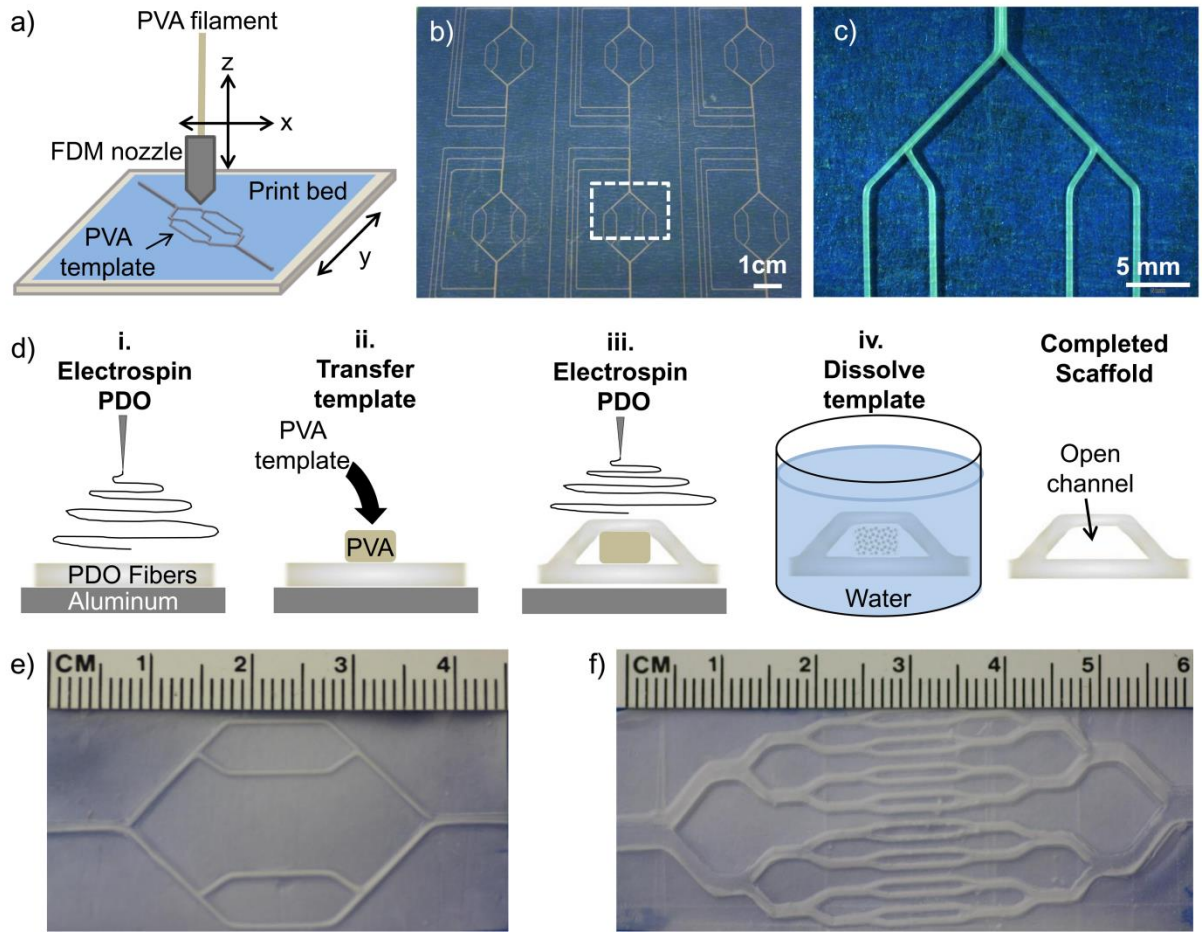

Figure 29. Fabrication of microvascular (MV) templates and electrospun MV scaffoldsFabrication of microvascular (MV) templates (a-c) and electrospun MV scaffolds (d-e) by FDM and electrospinning respectively. a) FDM extrudes a filament through a small (0.35mm) nozzle to fuse the material to the underlying layer. b) Automation of FDM process allows many templates to be quickly and uniformly produced. Supporting branches shown connecting the inlet and outlet are printed as part of the continuous path and trimmed before use. c) Optimization of the printing path and extrusion parameters permit fabrication of small diameter branched structures. d) Cross-sectional view of MV scaffold fabrication using templated electrospinning. e-f) Completed MV scaffolds with 2 (e) and 4 (f) bifurcations.

Scaffold Characterization

Scanning electron microscopy. The morphology of microchannels in electrospun PDO scaffolds was examined by scanning electron microscopy (SEM). Samples were fixed with 2.5% glutaraldehyde and dehydrated with graded ethanol and hexamethyldisilazane (HMDS). Dehydrated samples were sputter-coated with 3.5 nm gold and images were taken at 3 kV

acceleration voltage with a field emission SEM (JSM-6330F, Jeol, Tokyo, Japan). Average diameter of fibers was measured using ImageJ software (NIH, Bethesda, MD).

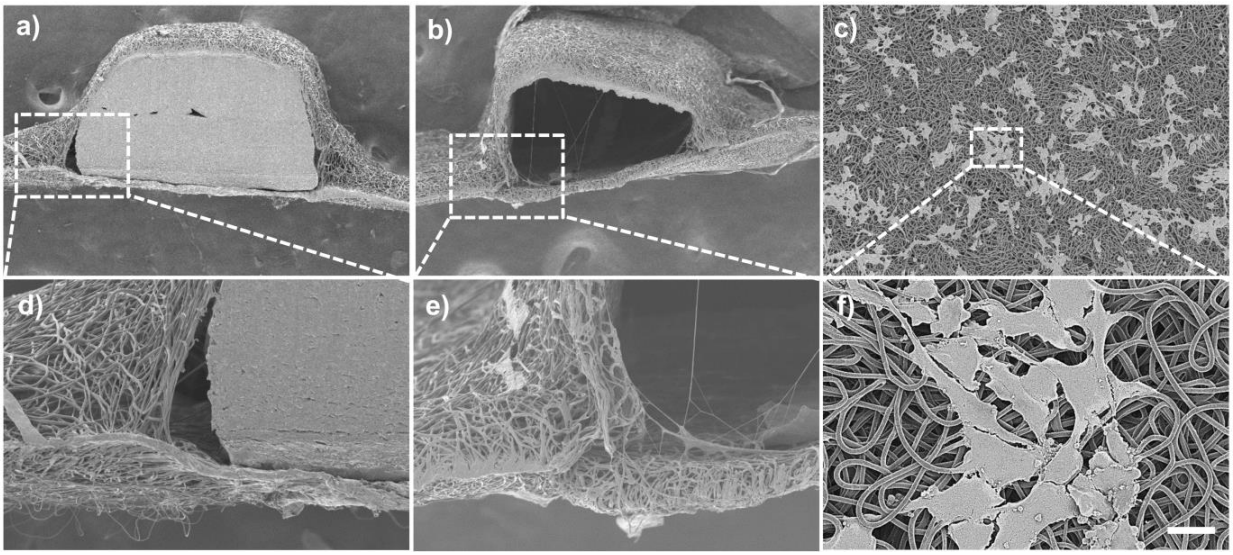

Figure 30. Scanning electron micrographs of electrospun PDO scaffoldswith PVA template in place (a/d) and after template is dissolved (b/e). HUVECs attached to fibrous PDO with a sprawled morphology (c/f). Scale bar: a-c (100 μm), d,e (40 μm), f (20 μm)

Mechanical Testing. Electrospun PDO sheets were punched using a dogbone-shaped die (28.75 x 4.75 mm outer dimensions, 8.25 x 1.5 mm narrow region). The thickness of hydrated samples was measured with a dial caliper (Mitutoyo). Uniaxial tensile tests were performed to failure at 25 mm/s using a 50 N load cell on a MTS Insight (Eden Prairie, MN). Suture retention strength was measured by methods described previously.[244] Briefly, a 6-0 suture was inserted 2 mm from the end of square sample and pulled until rupture. Suture retention strength was calculated as load/(suture diameter × sample thickness).

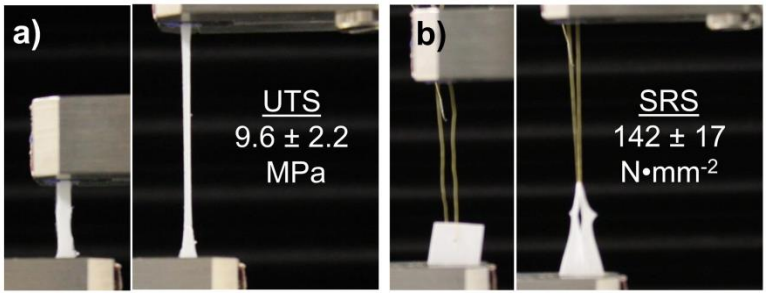

Figure 31. Mechanical properties of electrospun PDO sheetsMechanical properties of electrospun PDO sheets. a) Uniaxial tensile strength (UTS). b) Suture retention strength (SRS).

Cell Attachment in Static Culture

HUVECs (Lonza, Walkersville, MD) were cultured on fibronectin-coated (1 μg/cm^2; Chemicon International, Temecula, CA) plates using endothelial basal medium-2 (Lonza) supplemented with 10% fetal bovine serum (Hyclone, Logan, UT), 1% L-glutamine-penicillin-streptomycin (Mediatech, Manassas, VA), and endothelial growth medium-2 SingleQuot Kit (Lonza). Fibrous PDO sheets were cut to circular samples 12 mm in diameter and placed under metal rings (inner diameter 7.5 mm) in 24-well plates. They were sterilized with 70% ethanol, rinsed with PBS, and incubated with culture medium at 37 °C for 24 h. HUVECs (passage 4) were seeded at 1.0×10^6 cells/mL and cultured for 1 day under static conditions.

Bioreactor Culture

Exel PTFE safelet I.V. catheters (Fisher Scientific, Pittsburgh, PA) were inserted into the inlet and outlet channels and secured by PTFE sealant tape to provide connections for the bioreactor tubing. The fibrous PDO scaffold was transferred into a bioreactor chamber made with polycarbonate sheets (thickness 2.4 mm) and a silicone rubber (thickness 3.1 mm). HUVECs were seeded in the lumen of the scaffold at 1.0×10^6 cells/mL and allowed to attach uniformly to the scaffold lumen by rotating the chamber as 2 rpm for 4 h. After rotation, the bioreactor chamber was attached to the perfusion setup and the scaffolds were perfused with

fresh medium by using a peristaltic pump as a rate of 0.6 ml/min for 10 days. Medium was changed at every other day.

Fibrous PDO scaffolds were harvested on day 10 and washed with PBS. Both inlet and outlet channels were cut from scaffolds, embedded in Tissue-Tek optimal cutting temperature compound (Sakura Finetek Inc., Torrance, CA) and snap-frozen in liquid nitrogen. Cryosections were used for immunofluorescence staining to examine HUVEC lining and cell-cell junction.

Immunofluorescence staining

Cryosections 8-μm thick (for cross-sectional view) and other scaffolds regions (for top-down view) were fixed in 4% paraformaldehyde for 10 min at room temperature and rinsed twice with PBS. Tissue sites of each slide were blocked with 5% normal goat serum (Sigma) for 1 h at 37 °C, incubated with primary antibodies in 1% goat serum for 45 min at 37 °C, and incubated with secondary antibodies in 1% goat serum for 45 min at 37 °C. For HUVEC staining, rabbit polyclonal anti-human CD31 (1:100; Santa Cruz Biotechnology, Dallas, TX) and von Willibrand factor (vWF) (1:200; Abcam, Cambridge, MA) were used as primary antibodies and Alexa Fluor 594 goat anti-mouse IgG (1: 400; Invitrogen) and secondary antibody. For visualization of cell-to-cell junctions, rabbit polyclonal anti-human VE-cadherin (1:100; Santa Cruz) and Alexa Fluor 488 goat anti-rabbit IgG (1:200; Invitrogen) were used as primary and secondary antibodies. Nuclei were stained with 4',6-diamidino-2-phenylindole (DAPI; Invitrogen). Fluorescent images were viewed and captured with an inverted microscope (Eclipse Ti-E; Nikon Instruments, Melville, NY).

Perfusion

The bioreactor chamber was detached from the perfusion setup on day 10 and culture medium was aspirated from the lumen of microvascular channels of fibrous PDO scaffolds.

Fluorescein isothiocyanate (FITC)-labeled dextran (150 kDa, Sigma) solution was prepared in PBS (20 mg/mL) and injected into the lumen to visualize perfused microvascular channels through endothelial cell barrier. Fluorescent images were captured on an inverted microscope. The intensity of fluorescence in perfused microvascular channels was measured using the NIS-Elements software (Nikon). Acellular PDO scaffolds were used as a negative control.

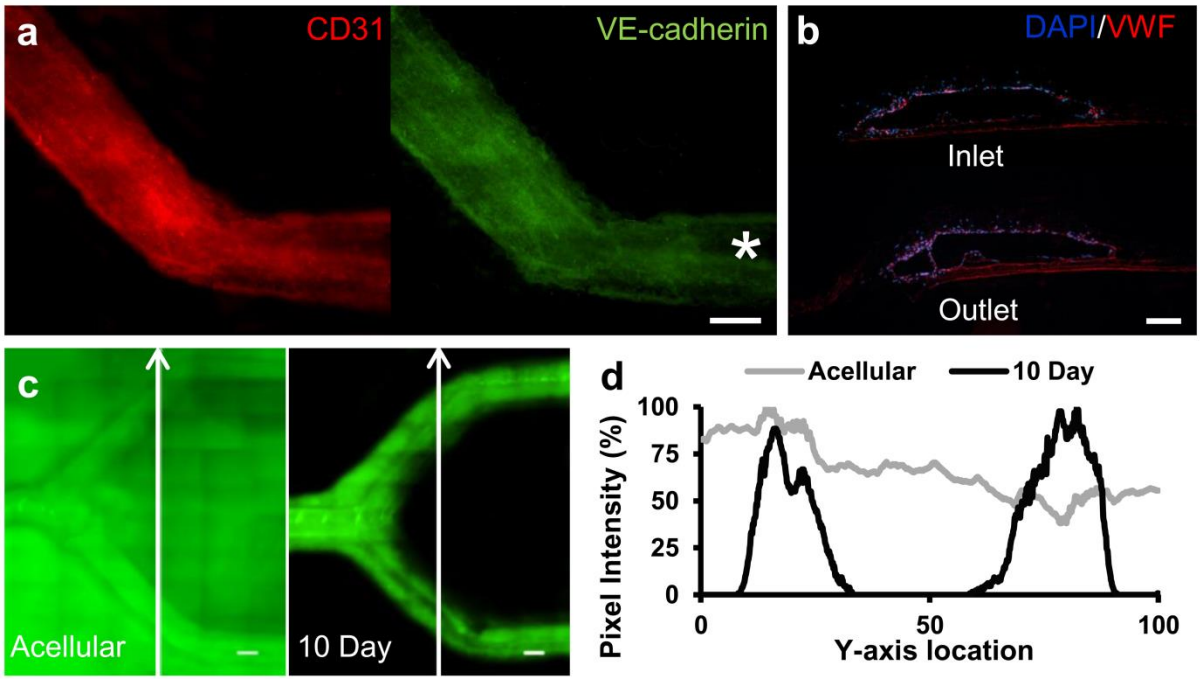

Figure 32. In vitro endothelialization of fibrous microvascular scaffolds.a) CD31/VE-cadherin staining of microvessel after 10 days culture (top-view). Asterisk indicates area of low cell density (Scale: 150 µm) b) DAPI/vWF staining of cross-sections of inlet/outlet sections after 10 days of culture (Scale: 100 µm) c) Perfusion of acellular and 10-day cultured scaffolds with FITC-labelled dextran. Channels after 10 days of culture demonstrate reduced permeability. The presence of FITC-labelled dextran beyond the channel walls indicates that channels are not yet water-tight. Pixel intensity along horizontal line is shown in graph (Scale: 1 mm)

4.1.3 Results and Discussion

Combining FDM with Templated Electrospinning

We present a micropatterning technique that combines FDM with the method of templated electrospinning (Figure 29).[245] FDM is an inexpensive SFF platform that offers high versatility for the manufacture of templates, allowing us to print branched patterns that mimic vascular

networks. While SFF and electrospinning have been used in various combinations for other applications,[80, 96, 98, 99, 246-249] the final composites contain material from both sources. In contrast, we used FDM only as an indirect fabrication method to create sacrificial templates used to pattern the electrospun meshes.

Since the FDM templates are non-linear patterns, they cannot be removed manually as previously described.[245] Instead, we fabricated templates out of PVA removed safely by dissolving in water. PVA is nontoxic, noncarcinogenic, generally regarded as safe by the USFDA and has been used in tissue adhesion barriers, nerve guides, and cartilage replacement.[250] FDM also offers a high-throughput (Figure 29B) alternative to the previous labor-intensive and time-consuming templating methods.[245] With FDM, template designs can be easily modified or scaled within the software.

The production of intricate single-layer templates differs significantly from the large 3D structures FDM is intended to produce. This presents several challenges to using FDM for our application. Those familiar with FDM recognize that the first layer is most likely to cause errors with adhesion to the print bed and layer thickness. By using a continuous path and optimized printing conditions (e.g., nozzle temperature, bed temperature, level bed, and dry filament), we demonstrate uniform dimensions and reproducible deposition (Figure 29C). Additionally, blue painter tape (3M ScotchBlue 2090) was applied to the bed to improve PVA adhesion. Another drawback of FDM is the high heat (210^{o}C) needed to extrude PVA. Since this heat also melts common degradable polyesters including PDO, the templates were transferred from the print bed rather than directly printed on the electrospun fibers.

Benefits of Microvascular Electrospun Scaffolds

Both the fibrous structure and the material properties of PDO contribute to the porous, suturable, and biodegradable nature of these scaffolds. Electrospun PDO produced well-defined microfibers with 1.5 μm average diameter (Figure 30F) with highly interconnected interstices to permit rapid diffusion of small molecules. Electrospun fibers also provide mechanical benefits compared to porous scaffolds produced by other methods such as solvent casting particulate leaching.[251] Mechanical testing demonstrates that fibrous PDO scaffolds are strong (9.6 MPa) with suture retention strength of 142 N/mm^2 (Figure 31). This is close to commonly-sutured electrospun poly(caprolactone) (PCL) (164 N/mm^2) and several times greater than poly(ether urethane urea) (PEUU)/ECM blends (35-59 N/mm^2) which were sutured for in vivo fixation.[244, 252] PDO is a FDA-approved material used for sutures that resorb within 6 months or faster for fibers with high surface area. [242, 243, 253] In vitro culture of HUVECs on electrospun PDO fibers also demonstrate good attachment as indicated by the sprawled morphology (Figure 30C&F).

Microvascular Endothelialization

Electrospun fibers are typically packed too tightly to permit rapid cell infiltration.[254] To facilitate endothelialization of our scaffolds, we introduced microvascular networks by templated electrospinning. Fibrous PDO layers deposit tightly around the PVA template (Figure 30A&D) and retain the channel shape even after PVA is dissolved (Figure 30B&E). This process transfers the microvascular pattern to the fibrous scaffold (Figure 29E). Figure 32 demonstrates that these channels permit cells to be seeded into predetermined regions of the scaffold. The fibrous nature permits fluid extravasation while seeding the cells through a filter-like process: fluid from the injected cell suspension exited through the fibers while trapping the cells against the channel walls.

After culturing for 10 days in a bioreactor, HUVECs attached and proliferated on the PDO fibers and formed a near-confluent layer. The cells formed adherens junctions along the channel as demonstrated by VE-cadherin and CD31 staining (top-view) (Figure 32A). The presence of HUVECs in the scaffold was further revealed by von Willibrand factor (vWF) staining of the channel cross-sections (Figure 32B). HUVEC staining within microvascular scaffolds revealed that despite being porous, the fibers prevent cells from immediate escape from the microchannels. Maturation of the HUVECs and confluence of EC layer were further evaluated by visualizing flow of FITC-labeled dextran solution perfused into the lumen (Figure 32C). The cultured microvessels show a drastic reduction in leakiness compared to the unseeded scaffold, representing barrier function of EC layer. Since some leaking still occurs, longer culture time may be necessary to allow HUVEC coverage of areas with low cell density (Figure 32A asterisk). Additionally, we expect to stabilize HUVECs to form water-tight vessels by coculturing with mural cells such as pericytes.[255]

We produced channels approximately 500 μm in diameter which is similar to small arteries and venules and will provide intrinsic vascularization to the most of the tissue.[256] By using a highly porous and degradable scaffold, we anticipate that further branching of the smallest vessels will be rapidly obtained by angiogenesis. Although FDM can achieve feature sizes of 250 μm, finer resolution is difficult to achieve since reducing nozzle diameter rapidly increases the extrusion pressure as described by the Hagen-Poiseuille equation.[63, 92] Thus, future work we will pursue other precise technologies such as pressure assisted microsyringe (PAM) and electrohydrodynamic (EHD) jet (direct melt electrospinning) which are capable of 10-30 μm feature size.[63, 92, 257] Additionally, we recognize the non-circular shape of the vessels that results from the square template cross-sections in combination with the fiber deposition pattern. As

template height increases, electrospun fibers encapsulate the template less tightly,[246] resulting in the sloped sides observed in Figure 32B. Due to this height effect, future iterations will use short and wide templates in conjunction with elastomeric fibers (e.g., poly(glycerol sebacate) (PGS)) to produce circular shapes once exposed to blood pressure, similar to balloon inflation.

4.1.4 Summary

In summary, we present a new technique that uses FDM with water-soluble PVA as an indirect fabrication method to pattern microvascular networks within fibrous 2D structures which we anticipate rolling[258] or layering[98] into 3D scaffolds. This approach overcomes several significant challenges of engineered microvasculature including limited perfusion capacity, low strength associated with hydrogel approaches, and nondegradability for PDMS-based approaches. We expect that the thin (<100 μm) fibrous channel walls will improve perfusion of parenchymal cells. The effectiveness of this device at perfusing the parenchyme will be tested by coculture experiments before in vivo validation.

5.0 ELECTROSPUN POLY(GLYCEROL SEBACATE) (PGS)

Chapter Aim

Pilot studies with implanted (PCL-PLGA) nerve guides suggest that a faster-degrading material that induces a milder inflammatory response would improve nerve regeneration. Additionally, we observed some delamination of PDO microvascular scaffolds. We hypothesized that the rapid degradation of poly(glycerol sebacate) (PGS) and the cohesive properties of oligo(glycerol sebacate) (OGS) could be used to address these limitations. Additionally, the mechanical modulus of PGS is suitable for matching that of nerve and blood vessel. The aim of this chapter was to create fibrous PGS by developing an electrospinning protocol that does not alter the PGS properties. PGS was electrospun by blending prepolymer (OGS) with poly(vinyl alcohol) (PVA) followed by thermal crosslinked. We report a method of electrospinning PGS that yields strong constructs with no observable changes to modulus or cytocompatibility.

5.1 ELECTROSPUN POLY(GLYCEROL SEBACATE) FOR IMPROVED MECHANICAL PROPERTIES

5.1.1 Introduction

Scaffold mechanical properties play an important role in the cellular microenvironment, influencing cell motility, organization, and differentiation.[17, 18] Traditional plastic biomaterials (poly(caprolactone) (PCL), poly(glycolic acid) (PGA), poly(lactic acid) (PLA));[259] as well as elastomeric biomaterials (poly(ether urethane urea) (PEUU), poly(3-hydroxybutyrate-co-4-hydroxybutyrate) (P3HB-co-P4HB), and poly(caprolactone-co-lactic acid) (PCL-co-LA));[260] have moduli in the MPa-GPa range, resulting in mechanical mismatch with soft tissue (kPa range). Poly(glycerol sebacate) (PGS) is a soft elastomer with a modulus between 25-1200 kPa depending on crosslinking density.[261] This has made PGS a unique and desirable material for soft tissue applications including vascular grafts,[192] cardiac patches,[262] nerve regeneration,[160] and retina repair.[263] Additionally, PGS degrades rapidly in vivo into the metabolites glycerol and sebacic acid, minimizing the duration of the host's inflammatory response.[261, 264]

The adoption of PGS scaffolds have been hampered by their need for gentle handling. The low tensile strength of scaffolds produced by solvent casting porogen leaching [265] precludes their use in load bearing environments or implants requiring suture anchoring. Porogen leached PGS can be composited with a stronger material to improve surgical handling,[192] but the additional material will influence the mechanical behavior and degradation of the scaffold.

Constructing fibrous scaffolds by electrospinning can improve the strength of PGS scaffolds[251] while introducing a fibrous topography resembling the structure of extracellular matrix.[241] However, electrospinning thermosets like PGS is challenging[266] for two reasons: (1)

The insolubility of crosslinked PGS in organic solvents necessitates the use of the noncrosslinked precursor, PGS prepolymer or oligo(glycerol sebacate) (OGS); and (2) OGS has a glass transition temperature (Tg) below room temperature causing the polymer to flow and fibers fuse into a nonporous sheet. This fusion is exacerbated by the heating needed for thermal crosslinking.

To overcome these challenges, we and others have developed a range of methods to electrospin PGS (Table 1). All of these techniques blend OGS with a carrier polymer that readily forms fibers to facilitate fiber formation. Unfortunately, if the carrier polymer is not removed or if OGS is not crosslinked, the mechanical properties differ substantially from those of unaltered PGS [264]. Our objective was to develop a simple and inexpensive method for electrospinning PGS scaffolds that retains the mechanical properties of crosslinked PGS without using toxic crosslinkers. Resultant scaffolds show improved suture retention and ultimate tensile strength compared to porogen leached scaffolds, suggesting an advantage in handling.

5.1.2 Experimental Section

Materials

Poly(vinyl alcohol) (PVA) was generously provided by Soarus LLC (Arlington Heights, IL) and 1,1,1,3,3,3-hexafluoroisopropanol (HFIP) was purchased from Oakwood Products Inc. (West Columbia, SC). PGS prepolymer (OGS) was synthesized in house as previously described.[264]

Production of fibrous PGS sheets

Fibrous PGS sheets were fabricated by 1) electrospinning OGS-PVA blends, 2) thermal crosslinking, and 3) purifying with water and ethanol as outlined in Figure 33.

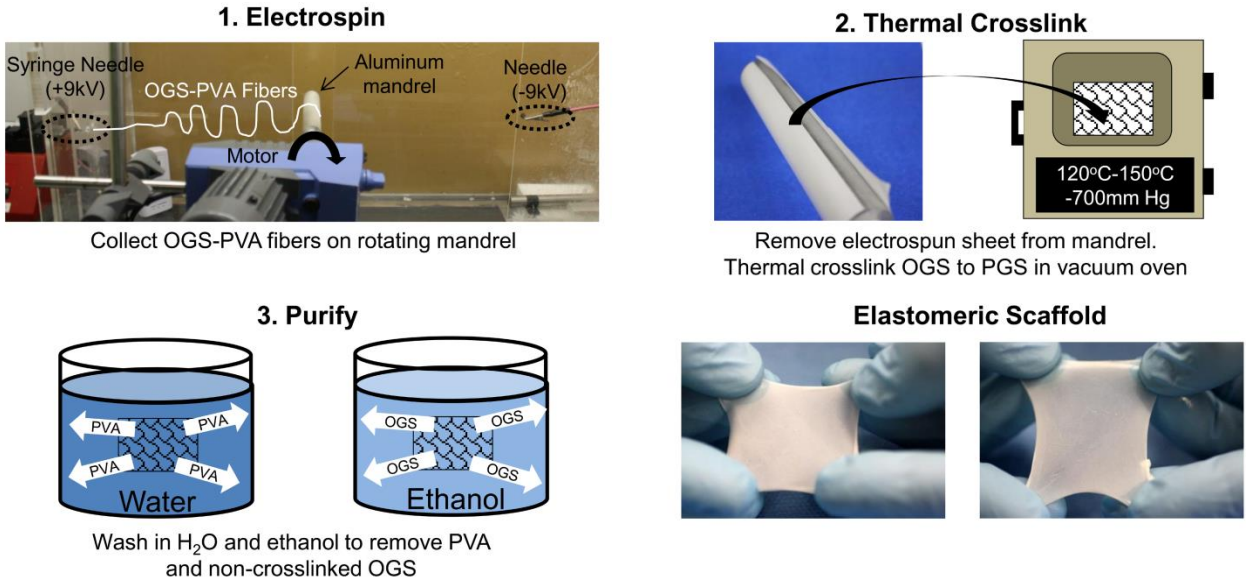

Figure 33. Fabrication of fibrous PGS sheets1. Electrospin OGS-PVA onto rotating (100 RPM) mandrel 30 cm from dispensing syringe needle at (+9kV), and 30 cm from negatively-charged needle (-9kV). 2. Crosslink the sheet with high temperate and vacuum. 3. Purify samples by washing in water for 24h to remove soluble PVA. Rinse in graded ethanol dilutions to remove non-crosslinked OGS.

A 16 w/v% solution was prepared by mixing OGS and PVA at 55:45 mass ratio and dissolving in HFIP overnight. This solution was pumped at 29 µL/min through a 22 gauge needle serving as the spinneret. Positive and negative 9 kV were applied to the spinneret and another needle positioned 60cm from the spinneret, respectively. Electrospun fibers were collected on a rotating aluminum mandrel (100RPM) placed between the needles at a 30 cm distance from the spinneret to (Figure 33-1). No voltage was placed on the mandrel.

Fibrous sheets were removed from the collector and crosslinked in a preheated vacuum oven under high temperature (120°C-150°C) and vacuum (-700mm Hg) (Figure 33-2). We investigated four crosslinking times at 120°C: 24, 48, 72, and 96h. Crosslinking at high temperature was also performed (120°C-24h followed by 150°C-24h).

Crosslinked fibrous sheets were purified by water and ethanol washes (Figure 33-3). PVA was removed by washing three times in ultrapure, deionized water (diH_2O) with gentle agitation for 24h. Non-crosslinked OGS was removed via serial ethanol washes (100%-1h, 70%-

1h, 50%-15min, 25%-15min, diH_2O-15min three times) with gentle agitation. Hydrated samples were used immediately or lyophilized for storage.

Characterization of electrospun PGS sheets

Fiber morphology was evaluated by scanning electron microscopy (SEM). Samples were prepared for SEM by adhering onto aluminum stubs with conductive carbon tape before sputter coating with gold-palladium to a 3.5nm thickness and viewing on a JSM-6330F SEM (JEOL, Tokyo, Japan). Fiber diameter was measured by image analysis with ImageJ (NIH, Bethesda, MD).

Purification was evaluated by mass loss. Dry samples were weighed on a microbalance before undergoing washing protocols. Sample thicknesses were also measured with dial calipers before and after purification. Fourier transform infrared attenuated total reflectance (ATR-FTIR) was measured on a Nicolet iS10 FTIR spectrometer (Thermo Scientific, Waltham, MA) after 1) electrospinning, 2) crosslinking, and 3) purification. Samples were compared to control films of pure PGS at the same crosslinking conditions. The thermal properties for the same groups were also measured by differential scanning calorimetry (DSC). Samples underwent two cycles of heating to 200^{o}C and cooling to -80^{o}C at 20^{o}C/min.

Mechanical properties

Mechanical properties of electrospun PGS blends were measured by uniaxial tensile testing. Samples were cut into dog bone shaped pieces using a customized punch with outer dimensions (28.75mm (L) * 4.75mm (W)) and a narrow region (8.25mm (L) * 1.5mm (W)). Sample thickness was measured by dial calipers. Samples were placed in an Insight MTS (Eden Prairie, MN) and then hydrated before straining to failure at 25 mm/min. Multi-cycle testing

from 10 to 100% strain for 100 cycles at 100 mm/min was performed to evaluate elastic recovery. Samples were kept hydrated during this process.

Suture retention strength (SRS) was measured by inserting a 4-0 suture 2mm from the edge of the long axis of 5mm x 20mm samples and strained to rupture. Suture retention strength was calculated as maximum load/(suture diameter x sample thickness) in N/mm^2.

Cell attachment and viability

Purified and unpurified samples of electrospun PGS sheets crosslinked at 120°C-48h and 120°C-24h, 150°C-24h were autoclaved at 121°C for 27min. Fiber morphology of autoclaved PGS sheets was observed via SEM (Figure 34).

Washed PGS sheets (1.2cm diameter) were placed under metal rings placed in 12-well plates and incubated in media (DMEM + 10% FBS +1% antibiotic) for 24h. 3T3 fibroblasts were seeded at 10,000 cells per well and cultured for 24h. Cell viability was assessed by Live/Dead assay (Molecular Probes, Eugene, OR) using fluorescent imaging. Replicates were fixed in 2.5% glutaraldehyde before dehydrating with a series of ethanol, followed by hexamethyldisilazane (HMDS, Alfa Aesar, Ward Hill, MA). Cell attachment was examined by SEM.

Cytocompatibility was performed according to the ISO 10993-5 standard for extract tests. Autoclaved disks were incubated in media at 20 g/mL overnight at 37°C. 3T3 fibroblasts were plated in a 96-well plate at 10,000 cells per well for 3h before incubating with the extract at 1 and 10mg/mL for 24h. Cells were incubated with serum-free medium with 2uM calcein AM and 4 uM ethidium homodimer for one half hour before capturing FITC and TRITC images at the center of each well (n=3 for each sample) with Nikon Eclipse Ti microscope. Live and dead cell numbers were quantified using "object count" in Nikon Elements software to threshold images

and exclude objects less than 10μm. Live percent was calculated as the number of live cells/total cells x 100. Since all wells contained some dead cells, the live percent was normalized to controls grown on tissue culture polystyrene (TCPS) with no extract.

Electrospun constructs

Tubular scaffolds were fabricated by electrospinning around various-sized mandrels coated with 1-2 w/v % hyaluronic acid and crosslinking and purifying as described above. Multi-laminate constructs were constructed by stacking fibrous sheets of electrospun OGS-PVA and placed between Teflon blocks while crosslinking to prevent curling. PGS arteriovenous (AV) shunt grafts were constructed by combining the tubular scaffolds with templated patterns as described in Aim 2.

Statistical analysis

ANOVA was performed in Minitab using the general linear model. Post-hoc comparisons with the control were performed using Bonferroni correction and 95% confidence interval.

5.1.3 Results and Discussion

Review of prior work

OGS is intrinsically difficult to electrospin.[266, 267] Existing literature pertaining to electrospun OGS uses a carrier polymer that is blended or electrospun by coaxial set-up (Table 1). Using PCL as a carrier polymer prohibits thermal crosslinking the PGS since PCL has a low melting point, resulting in uncrosslinked OGS-PCL blends in which PCL dominates the mechanical properties.[268] Additionally, noncrosslinked OGS may have a cytotoxic effect if not removed from the scaffold.[269] Gelatin has been used as a carrier but it requires crosslinking

agents such as glutaraldehyde, acrylate-ultraviolet (UV), or 1-Ethyl-3-(3-dimethylaminopropyl)-carbodiimide (EDC)-N-hydroxysuccinimide (NHS), which may adversely impact biocompatibility.[270-272] Coaxial electrospun OGS-PLLA tolerated thermal crosslinking and removal of the PLLA sheath by dissolution in dichloromethane (DCM).[267] However, DCM is toxic and a suspect carcinogen, requiring stringent and complete removal before biomedical applications. Our group has experienced similar challenges using a range of other carrier polymers (Table 1). PCL and PLGA carrier polymers melted during heating, poly(dioxanone) (PDO) and gelatin blends were severely weakened by heat, and poly(ethylene terephthalate) (PET) required purification using large quantities of toxic HFIP to remove the carrier polymer.

Table 1. Review of PGS electrospinning. Cells highlighted in blue meet our criteria of standard electrospinning, thermal crosslinking, and removal of carrier polymer. Cells highlighted in green match mechanical property with that of previously reported thermal-crosslinked PGS. *Mechanical testing performed at dry state.

Carrier Polymer	***i.* Electrospin Method**	***ii.* Crosslink method**	***iii.* Carrier removal**	***UTS (MPa)***	***Strain (%)***	***Modulus (MPa)***
PGS electrospinning in literature						
PLLA (2008) [267]	Core-sheath	Thermal	DCM	-	-	-
PLLA (2013) [273]	Core-sheath	Thermal	X	0.6-1.2	25	12
PCL (2013) [274]	Standard	X	X	3.5	-	7
PCL (2010) [268]	Standard	X	X	1.7-2.5	400-500	9-35
Gelatin (2009) [270]	Standard	Acrylate-UV	X	0.05	30-40	0.1 to 1
Gelatin (2011) [271]	Core-sheath	Glutaraldehyde	X	2*	61*	6*
Gelatin (2013) [275]	Standard	EDC-NHS	X	0.3-1	182-229	0.14-0.36
Development of PGS electrospinning within our laboratory						
PCL	Standard	X	X			
PLGA	Standard	Isocyanate	THF			
PDO	Standard	Thermal	X			
Gelatin	Standard	Thermal	X			
PET	Standard	Thermal	HFIP			
PVA	Standard	Thermal	H_2O	0.8-1.3	200-800	0.1-0.8
PGS						
PGS Film (Thermal-crosslinked)[261]				>0.5	>330	0.025–1.2

We ultimately selected PVA for the carrier polymer because (1) it does not melt during thermal crosslinking, and (2) it is highly water-soluble, enabling simple removal by dissolution

in water. Additionally, PVA itself is a nontoxic and noncarcinogenic biomaterial. It is approved by the FDA for applications in food chemistry and pharmaceuticals,[276] and is also being investigated for use in contact lenses, wound dressing, coatings for sutures and catheters, and other tissue engineered scaffolds.[276, 277] We acknowledge that some PVA appears to be incorporated into the final fibers. However, our results suggest that PVA does not significantly change the modulus or cytocompatibility compared to PGS alone.

Fiber morphology

Blending OGS with PVA enabled us to fabricate homogeneous round fibers of 2.8 ± 1.2μm diameter (Figure 34A) with fusion restricted to the contact points between fibers (Figure 34B). Although alignment was not the focus of this work, collection around a rotating mandrel resulted in elongated fibers oriented along the circumferential axis. We anticipate that fiber alignment can be further controlled by rotation rate, disk collectors, or auxiliary electrodes as previously described.[278] Randomly-deposited fibers were also electrospun onto a stationary plate (not shown), but were not characterized due to strong adhesion to the plate.

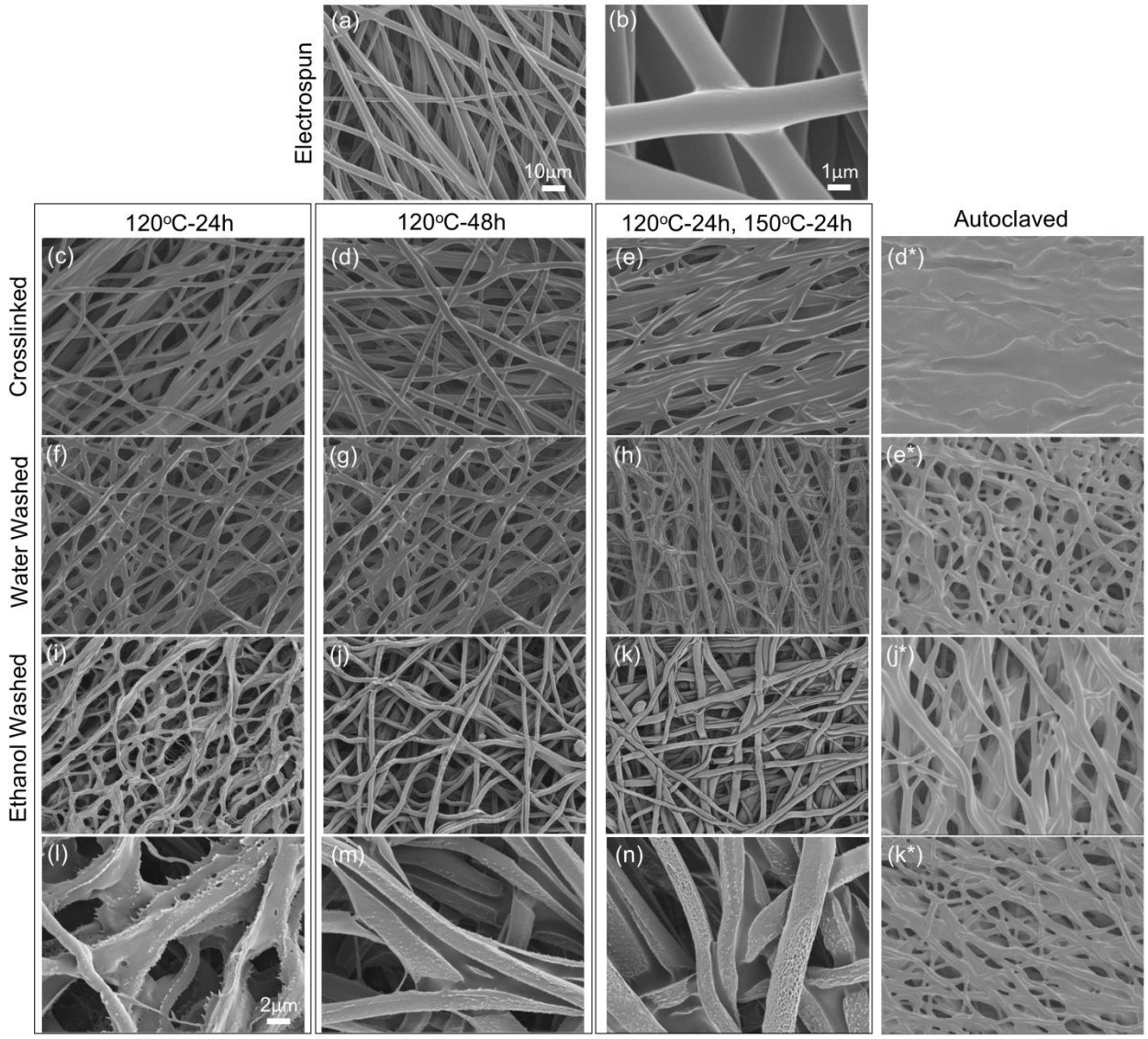

Figure 34. SEM of PGS-PVA fibers after electrospinning, crosslinking and purification.(a-b) Electrospun OGS-PVA fibers. (c-e) PGS-PVA after crosslinking at respective conditions. (f-h) PGS-PVA fibers after washing in water for 24h. (i-k) PGS-PVA after ethanol purification. (l-n) High magnification images of fiber structures from i-k respectively. (*) indicates respective sample after autoclaving. (Scale bar: 10µm for a, c-k and *; 2µm for l-n)

Maintaining the defined fibrous structure during thermal crosslinking was challenging since elevated temperatures cause OGS-PVA to soften and fuse. To improve fiber quality and minimize fiber fusion, we tested three different OGS-PVA mass ratios (60:40, 55:45, 50:50) and two different crosslinking conditions (instantaneous or gradual (4°C/h) heating) Results indicate that a ratio of 55:45 OGS:PVA is optimal for fiber quality (Figure A1), and that ramped heating

does not reduce fusion. The fibrous structure is retained after crosslinking but demonstrates increased fusion with more heat (Figure 34C-E).

We assessed the effects of water and ethanol purification on fiber morphology. Water washing appears to have little effect on fiber morphology (Figure 34F-H) while ethanol washes alter fiber shape and/or surface topography depending on crosslinking conditions (Figure 34I-K). Purified 120°C-24h fibers are irregularly-shaped and have small spines branching off the fiber surface (Figure 34L). Purified 120°C-48h fibers exhibit a semi-tubular shape with a hollow core (Figure 34M). PGS-PVA fibers crosslinked 120°C-24h, 150°C-24h are round but with a porous nanostructure and some recession near the fusion points (Figure 34N). We believe that the non-uniform fiber cross-section arises due to formation of OGS-rich and PVA-rich domains may result from OGS pooling near the bottom of fibers due to gravity; OGS flows at 120°C and 150°C, so it some OGS may pool at the bottom the OGS-PVA blended fiber prior to forming cross-linked PGS.

While the processing of thermosets is difficult, their resistance to heat and solvent is beneficial for sterilization. Many common degradable polyesters (PCL, PLGA, and PDO) have low melting points and cannot be autoclave sterilized. We demonstrate that purified PGS can be autoclaved without loss of the fibrous structure (Figure 34*). The presence of a significant amount of OGS in the unpurified low heat sample (Figure 34 D*) caused fusion between gaps when heated in the autoclave. In contrast, the purified sample (Figure 34 J*) containing only PGS retained its fibrous structure.

Purification Analysis

The remaining mass of all samples after water washing was greater than 55%, the percentage of OGS in the original solution (Figure 35A). This indicates that water washing is

not sufficient to remove all PVA. After ethanol washing, 120°C-24h and 120°C-48h were the only groups with less than 55% mass remaining (Figure 35A). Mass loss during the water wash likely represents PVA removal due to its high solubility in water. Mass loss during the ethanol wash likely includes OGS and PVA that was physically entangled within it, since both OGS and PVA are soluble in ethanol. These results suggest that the three most crosslinked groups (120°C -72h, 120°C-96h, 120°C -24h/150°C -24h) have some residual PVA in the final product. It is also possible that some residual PVA remains in the other groups since we predict substantial OGS mass loss in the ethanol wash (Figure A2).

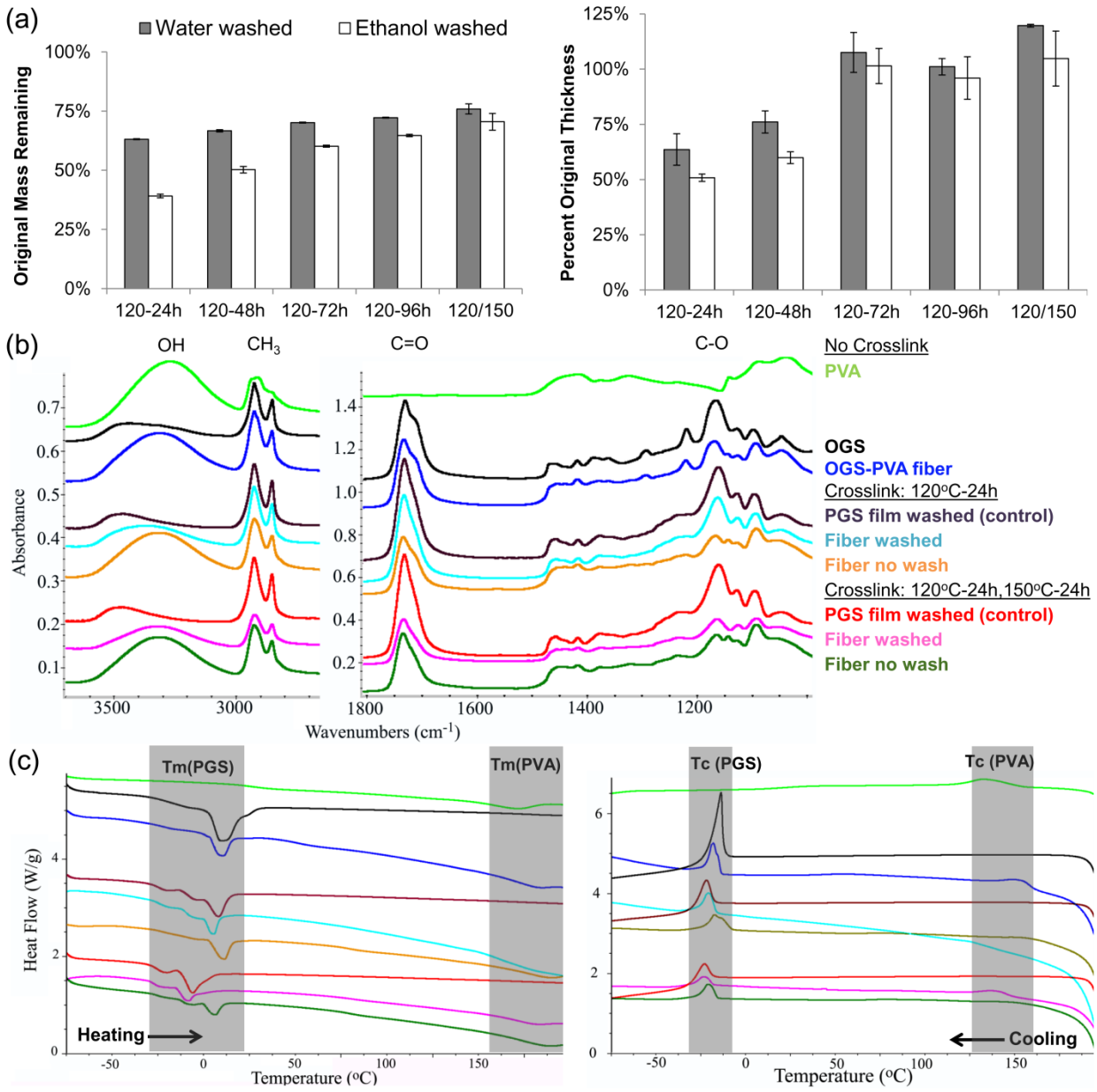

Figure 35. Purification analysis.(a) Percent of unwashed mass and thickness remaining after water and ethanol washes. (b) ATR-FTIR spectra of PVA, PGS and PGS-PVA during purification. (c) Heating and cooling curves from DSC measurements. Colors use the same legend as (b).

Quantification of residual PVA in the final product is difficult due to the chemical similarity to PGS. FTIR spectra of noncrosslinked OGS-PVA fibers show characteristics of both PVA (broad alcohol peak at 3300-3500 cm^{-1}) and OGS (alcohol peak at 3500 cm^{-1}, alkane at 2800-3000, carbonyl at 1750 and 1700, and carbon-oxygen bond at 1000-1300 cm^{-1}) (Figure

35B). FTIR spectra for PGS-PVA fibers and PGS films are similar except for the broad alcohol peak remaining in the fibrous sample. In the washed 120°C-24h fibers (cyan line) and less noticeably in the washed 120°C-24h, 150°C-24h group (pink line), the alcohol peak is shifted to higher wavenumber closer to that of the washed PGS film. Differential Scanning Calorimetry (DSC) was also performed to further elucidate the PVA content (Figure 35C). PVA has a melting point of 165°C that appears in both PGS-PVA samples regardless of purification. The PVA crystallization temperature of 135°C also appears in most PGS-PVA samples but is more subtle than the melting peaks. The most likely scenario for this residual PVA to occur is via physical entanglement within PGS fibers. Other possibilities involve PVA simply becoming insoluble as a result of thermal treatment[277] or chemically crosslinking with PGS by condensation reactions.

Successful removal of OGS during purification washes is also important. In the FTIR spectrum, the OGS peak around 1700cm^{-1} [279] significantly narrows after washing. DSC shows a melting point of 10°C for OGS that shifted down to around -10°C as crosslinked to PGS.[280] PGS-PVA fibers for both crosslinking groups demonstrated this crosslinking-dependent shift of the Tm(PGS). Additionally, the multi-peak Tm(PGS) profile of the purified samples closely matches that of the PGS film controls. The images of autoclaved fibers also provide insight into the OGS removal. The fibers in Figure 34D* are fused due to the significant OGS remaining, which is fluid enough to fill in pores during autoclaving. This effect disappears in Figure 34J* since the OGS is removed by the ethanol wash. Furthermore, autoclaved samples of both high heat crosslinked samples (Figure 34 E* and K*) shows little change, indicating that most of the OGS has been crosslinked to thermal-resistant PGS.

Mechanical properties

Uniaxial tensile testing was performed to evaluate the effect of three different crosslinking regimens on tensile properties (Figure 36). Samples were strained perpendicular and parallel to the electrospinning mandrel axis, although the orientation exhibited little effect on results. All samples demonstrated approximately 1 MPa of ultimate tensile strength (UTS) regardless of crosslinking. As crosslinking increased, the modulus increased from 100 to 800 kPa while the strain to failure (STF) decreased from 800% to 200% (Figure 36A). Elasticity was measured by performing 100-cycle multi-cycle testing. The highest crosslinking group exhibited some plastic deformation while both lower crosslinking groups showed full recovery after 100 cycles to 100% strain (Figure 36C). Similarly, the highest crosslinking group seemed more brittle, resulting in the lowest suture retention strength (SRS) (Figure 36D).

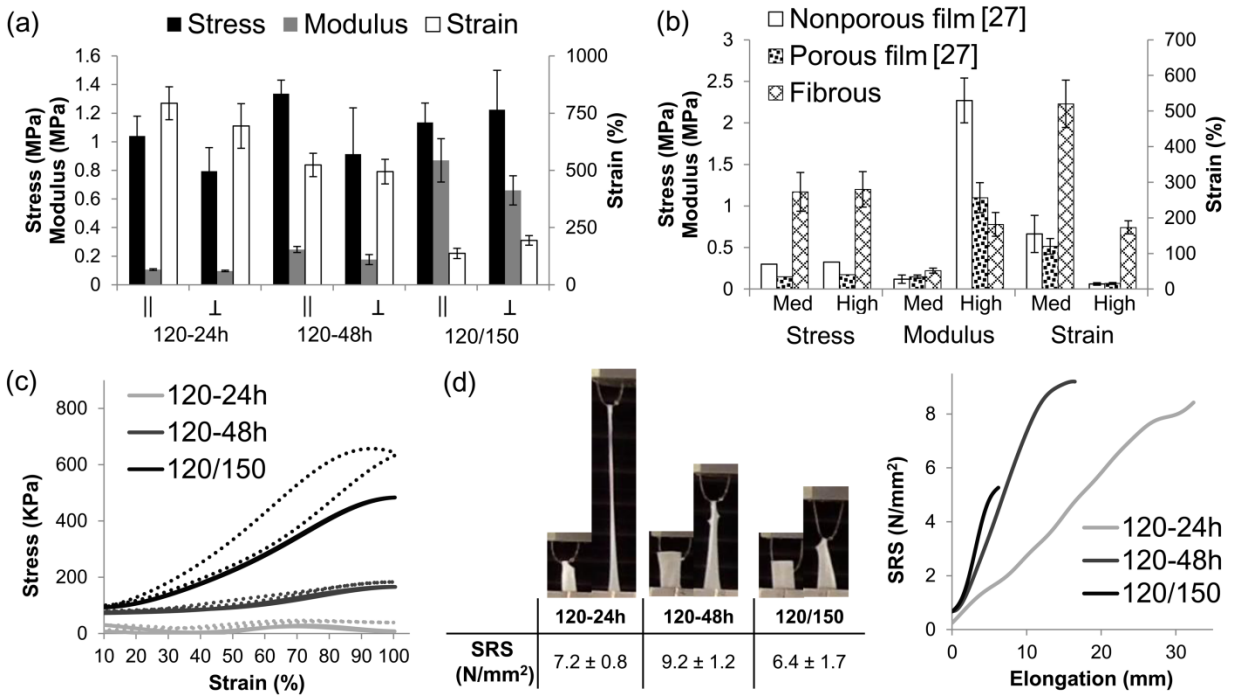

Figure 36. Mechanical testing(a) Tensile testing plot of samples strained parallel (||) or perpendicular (⊥) to fiber axis. (b) Comparison of fibrous PGS to previously reported mechanical properties for porous and non-porous films under similar conditions. Note: UTS values for nonporous and porous films was during testing of dry samples. "Med" crosslinking was 120oC for all samples. "High" crosslinking for porous and nonporous films was 150°C-48h but 120°C-24h, 150°C-24h for fibers. (c) Multi-cycle testing of high and low heat-crosslinked samples, strained to 10-100% for 100 cycles. (cycle 1:dotted lines, cycle 100: solid lines) (d) Suture retention strength.

PGS is a desirable material for soft tissue replacement because of modulus in the kPa range similar to those tissues. Despite the possible presence of residual PVA, our fibrous PGS sheets exhibited similar moduli to reported values for porous PGS (Figure 36B)[265] while demonstrating 3 times greater strength and 3 to 8 times larger strain-to-failure. As a biorubber, PGS can be elongated substantially and is elastic during cyclic testing. The increased elongation observed for electrospun PGS sheets is likely due to the ability of fibers to reorient during loading. Furthermore, we demonstrate that mechanical properties can still be tuned by adjusting the degree of crosslinking. Most importantly, we believe that this is the first report of suturable PGS scaffolds. The inability to hold suture was a significant shortcoming of SCPL PGS scaffolds and a leading motivation for this work. While the value for suture retention strength is less than PEUU blends (35-59 N/mm^2),[244] the large strain to failure for 120°C-24h and 120°C-48h samples (Figure 36D) allows the scaffold to be stretched while suturing in contrast to tearing as observed for PGS-gelatin samples (Figure A3).

This elastomeric response distinguishes our electrospun PGS scaffolds from those produced in other reports. Electrospun OGS or PGS blended with polyesters results in stiff materials due to the continued presence of the carrier. No mechanical data was reported for PGS fibers after PLLA removal in coaxially spun PGS-core PLLA-sheath fibers, but with PLLA still present elongation is one tenth that of PGS and the construct is 300 times stiffer.[273] Mechanical properties of PCL-OGS blends were closer to that of PCL alone than PGS elastomer.[268] PGS-gelatin blends closely match PGS properties when hydrated, but are more stiff by several orders of magnitude when dried and demonstrated rapid propagation of tear defects caused by suturing (Figure A3).

Cytocompatibility

We believe that the purified product has similar cytocompatibility to previously reported thermally-crosslinked PGS since no crosslinking agents were added. Additionally, since PGS was crosslinked, the scaffolds were washed in ethanol to remove residual monomers and unreacted OGS, believed to harm cells if not removed.[262, 269] Furthermore, the wash steps are performed in water and ethanol, avoiding harsh organic solvents. Live/Dead staining for cells in direct contact with the PGS sheets demonstrates the presence of live cells (Figure 37B). However, due to the red autofluorescence of the fibers, dead cells could not be clearly observed. Cytotoxicity of extracts from fibers was assessed using three crosslinking conditions and two concentrations for both purified and unpurified samples. Results were quantified by Live/Dead staining. None of the purified samples exhibited any significant difference in cytotoxicity from solvent casted PGS films, suggesting that residual PVA has a minimal effect. Only the non-purified 120^{o}C-24h group at 10mg/mL demonstrated significantly reduced cell viability compared to the control. As previously reported, the least crosslinked group has the most residual monomer and greatest effect on cell viability.[262, 269] However, this effect disappears if the fibers are washed with water and ethanol, suggesting that the purification steps are sufficient for removing this initial cytotoxicity. In agreement with previous observations, cells attach to PGS sheets[264] with morphology that changes from round to elongated as substrate stiffness is increased (Figure 37C).[281, 282] Further evaluation of cell response will be evaluated in vivo.

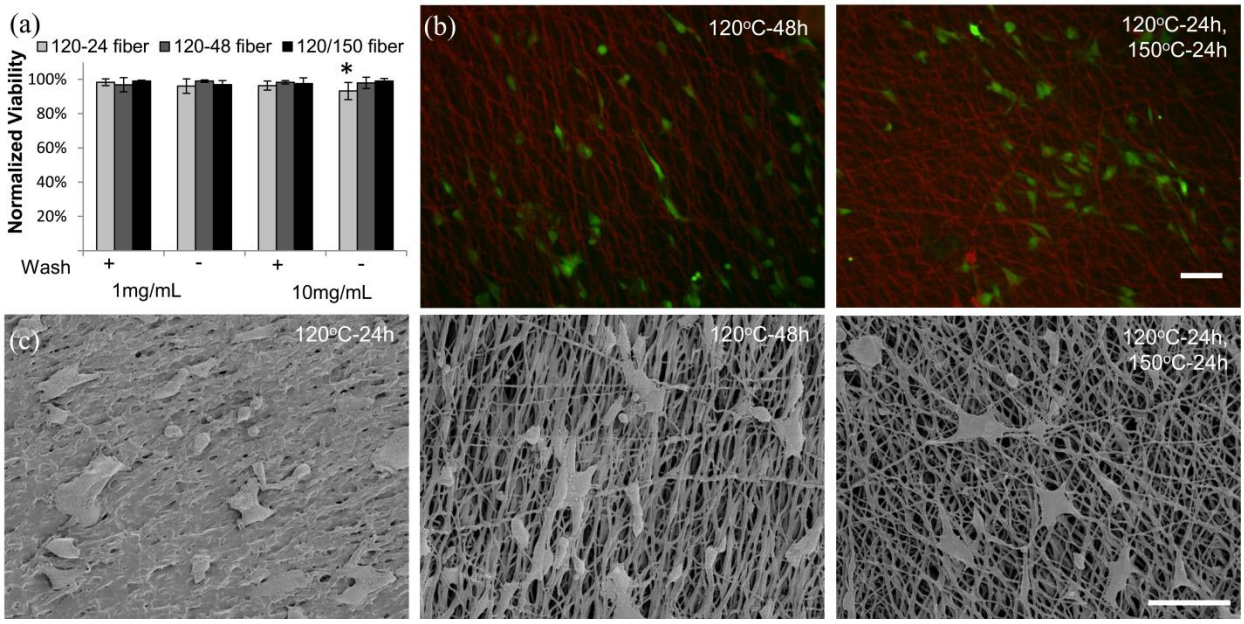

Figure 37. 3T3 fibroblast cytocompatibility with PGS-PVA fibers.(a) Normalized viability of 3T3 cells cultured with extract from PGS-PVA samples "+" and "-" indicate with or without purification in water and ethanol. (b) Live 3T3 cells (green) are visible attached to fibrous sheets of electrospun PGS-PVA. Scale: 100 µm. (c) SEM of 3T3 cells on PGS-PVA fibers. Note: all 3 groups have same cell density; 120-24ºC fiber compaction is artifact of HMDS dehydration that was not observed if lyophilized samples. Scale: 100 µm

Advantages of OGS-PVA electrospinning

Electrospun OGS-PVA offers advantages to both traditional SCPL PGS fabrication and other PGS electrospinning approaches. This work was motivated by the need for stronger PGS scaffolds. Tubular constructs fabricated by electrospinning OGS-PVA around small mandrels produce mechanically-robust scaffolds that permit easy suturing, stretching, and bending (Figure 38A). Additionally, SCPL is a labor-intensive method that requires a mold to hold the prepolymer in place until crosslinked and can be difficult to reproduce. SEM of electrospun scaffolds reveal a near-homogenous fibrous cross-section and uniform wall thickness (Figure 38B&C).

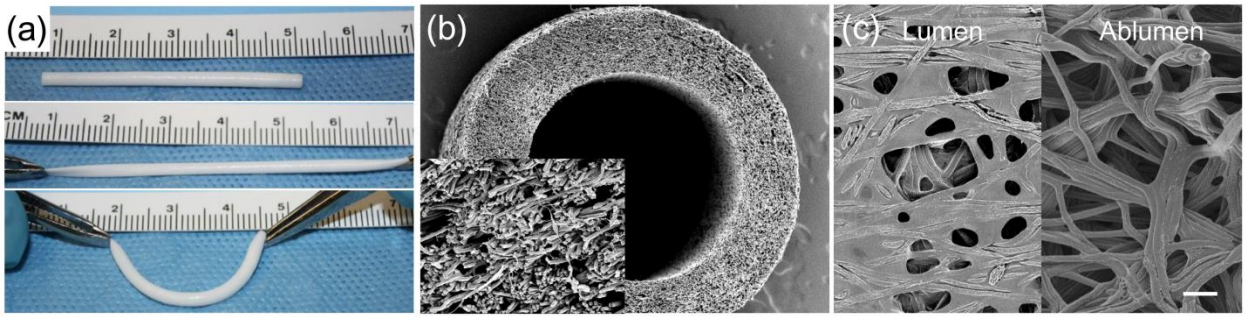

Figure 38. PGS-PVA fibrous conduits(a) 1.4 mm diameter tubular conduits demonstrate elastic properties and kink resistance during bending. (b) The fibrous morphology of these conduits can be observed in the cross-section (Scale: 200 µm, Insert: 20 µm). (c) The lumen and albumen are fibrous with some fusion of fibers on the luminal side, which was initially in contact with the mandrel used during fabrication. (Scale: 10 µm)

The cohesive property of OGS and the slight fiber fusion that occurs during thermal crosslinking make it useful for constructing multi-laminate constructs. This is achieved by stacking OGS-PVA sheets (Figure 39A) between Teflon blocks during thermal crosslinking. This offers a route to produce thick fibrous constructs (Figure 39B) that would otherwise take very long to electrospin. Furthermore, this bonding method presents a modular approach whereby different components can be fixed together by crosslinking. One example of this is shown in Figure 39 C&D where fibrous tubular PGS-PVA grafts are inserted into a PGS-PVA microvascular scaffold to provide a site for anastamosis with host vasculature.

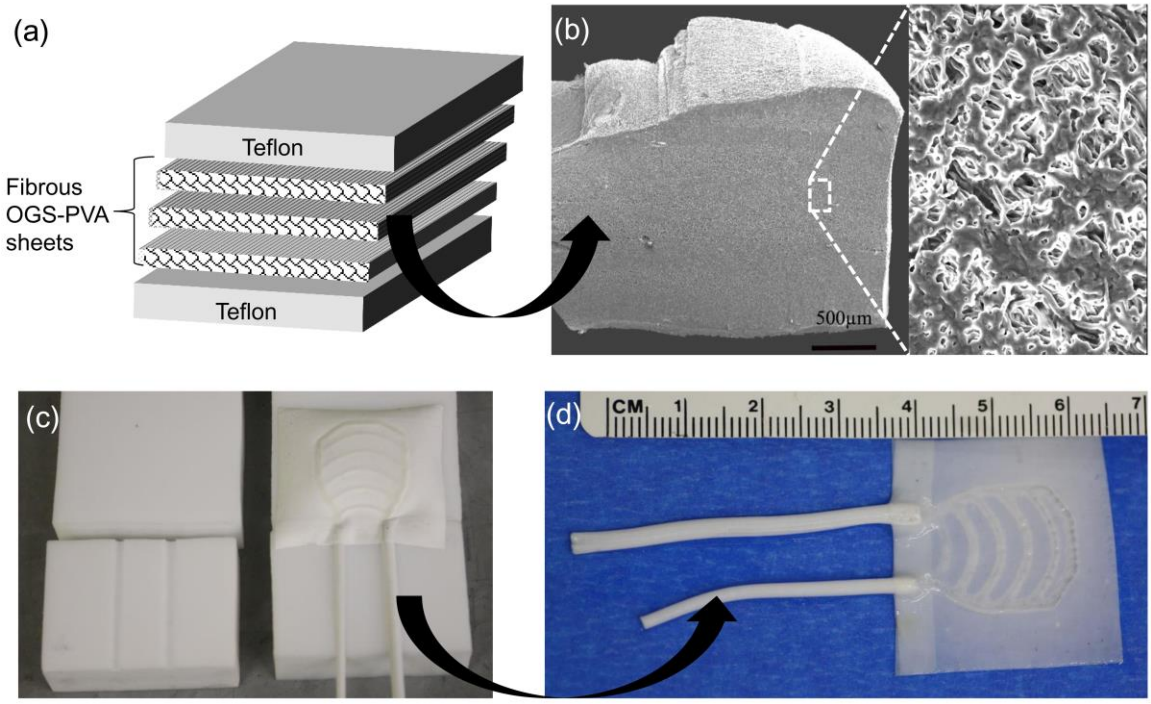

Figure 39. Multi-laminate PGS constructs. (a) Fibrous OGS-PVA sheets are stacked and placed between Teflon blocks to prevent curling during thermal crosslinking. (b) SEM of multi-laminate PGS construct (~2mm thick- y axis) and fibrous (insert). (c) Fabrication of PGS AV-shunt grafts by insertion of tubular OGS-PVA within microvascular scaffolds before thermal crosslinking. (d) PGS AV-shunt grafts after crosslinking and washing.

Furthermore, our method offers several key advantages to existing electrospinning approaches: 1) The elasticity and kPa modulus of thermally crosslinked PGS are retained. These mechanical properties are unique features of PGS that are believed to be critical in providing cells the mechanical stimuli to promote elastin formation. This elastic behavior requires the cross-linking of OGS to PGS as well as the removal of other polymers that alter mechanical response. 2) Potentially toxic components are minimized. Crosslinking achieved with heat minimizes residual toxicity compared with other methods. Noncrosslinked OGS and free monomers which may be harmful are removed via washes in ethanol, a benign solvent. The PVA removal in water is also nontoxic. 3) The technique is inexpensive. Disposable needles ($0.35) cost much less than custom coaxial needles ($790) used for core-shell electrospinning. Additionally, use of standard OGS avoids costly modifications (e.g. OGS-acrylate) which are

often costly to scale up. The PVA used as the carrier polymer for this experiment cost just $18/kg compared to $164/kg for gelatin (Sigma), $344/kg for PCL (Sigma), and $15,000/kg for PLLA (Sigma). This method also saves significant time since the electrospinning is stable and can be left alone with minimal oversight.

5.1.4 Summary

We demonstrate a simple method for electrospinning PGS using standard electrospinning techniques. This approach offers advantages to other fabrication methods, such as SCPL, by producing mechanically strong and fibrous scaffolds. Additionally, it reduces cost and safety concerns associated with other electrospinning approaches. This technique provides a new tool for processing several types of PGS scaffolds with more reliable handling for eventual implantation.

6.0 FINAL SUMMARY

While many common methods for producing TE scaffolds have actually been borrowed from other disciplines such as textiles (electrospinning), integrated circuits (micropatterning), and prototyping (SFF), the work presented here describes the development of a new TE-specific fabrication technique that focuses on creating the complex structure of native ECM. This method combines electrospinning and fused deposition modeling, which are both inexpensive technologies that are available to most labs. We anticipate that future improvements of templated electrospinning will benefit from the rapid advancements in both of these active areas of research.

6.1 BIOMIMETIC NERVE GUIDE-IMPACT AND FUTURE WORK

To the best of our knowledge, this is the first multi-channel nerve guide composed entirely of electrospun fibers. Our method offers spatial control of the microchannels that is not offered by many other approaches. Additionally, we efficiently present a high number of aligned fibers at low density to provide topographical guidance for axons and Schwann cells. Repair of peripheral nerve injuries using existing conduits has shown moderate success for short defects (<3cm). However, current literature and opinions suggest that topographical features such as these are essential to repair of larger nerve gaps.[168] Thus, we anticipate that our nerve guide may

create a norm for repair of large nerve gaps. To yield optimal outcomes, these guides will likely need to be combined with the appropriate cells and stimulatory molecules.

Preliminary tests with the PCL and PCL/PLGA nerve guides highlight the importance of material selection for peripheral nerve repair. The slow degradation and thick channel walls significantly limited the area for regeneration to occur. This was addressed in subsequent iterations by using much thinner walls and faster-degrading PLGA. However, the inflammatory response from this material resulted in fibrotic tissue formation that impaired regeneration. These results motivated the development of electrospun PGS which should rapidly degrade and match the mechanical properties of native nerve. We anticipate that PGS guides in combination with ECM proteins and growth factors can shift the response toward constructive remodeling. Yet, a concern for PGS nerve guides is that if these are used to repair large defects, the rapid degradation may cause collapse of the guide before it can be replaced with new ECM. Thus, a material gradient may be necessary to match the degradation rate with the remodeling process. Finally, we can foresee using similar multi-channel designs to develop scaffolds for other tissues with similar longitudinal channels such as skeletal muscle and bone.

6.2 MICROVASCULAR NETWORK

We demonstrated successful endothelialization of a unique microvascular network that is fibrous and strong. We believe that this approach makes our technique more applicable for in vivo scaffolds than other methods which are often weak and difficult to suture. The small A-V loop presented in this work will be used to study in situ endothelialization and optimize parameters such as heparinization and hemodynamics. Ultimately, these structures will be

incorporated into large organ scaffolds to provide rapid vascularization for parenchymal cells. Similarly, separate channels maybe used to spatially control seeding of parenchymal cells.

Significant challenges must still be overcome before adoption of this method for vascularization. One limitation is the difficulty connecting vessels between layers. While pseudo-3D constructs can be produced by rolling or stacking, the stratified nature of this method makes it difficult to make true 3D networks. A second challenge is creating microvessels over the full range of diameters, from millimeters to tens of microns. First, the template production should be capable of matching sizes in this entire range. Secondly, deposition of electrospun fibers has been shown to be affected by the height of insulators, resulting in "tent-like" fibers that do not tightly encapsulate the template.[246] If the template spacing is too narrow, these fibers can form bridges spanning templates, resulting in loss of resolution. A possible remedy to both of these challenges is to replace the random deposition of electrospun fibers with the precise positioning of fibers by direct-write melt electrospinning. Both the FDM and melt-electrospinning components could be attached to motorized stages for seamless and automated production. Further, reverse thermal gels may replace thermoplastics as the template material to avoid melting the scaffold while permitting incorporation of encapsulated cells.

6.3 FIBROUS POLY(GLYCEROL SEBACATE)

We produced fibrous PGS without chemical modification or changes to the crosslinking regimen. This should enable rapid and economical scale-up of electrospun PGS scaffolds. The electrospinning process should also lead to more reliable manufacturing as compared to salt-leaching methods. The most significant achievement from this work is the improved mechanical

strength, notably the suture retention. Scaffolds produced by salt-leaching tore easily, making them difficult to use in load-bearing applications without additional support material. Thus, electrospun PGS should permit better adoption of PGS scaffolds by both researchers and surgeons.

PGS offers several advantages over other available biomaterials. For instance, few materials have low a modulus suitable for soft tissue repair. The elastic property of PGS allows it to elongate with body movement, resulting in significant elastin synthesis in vivo. Additionally, the tendency of PGS prepolymer to flow and fuse has been previously considered a drawback of PGS. However, we were able to use this effect as an advantage to produce multi-laminate structures. While additive manufacturing for tissue engineering is becoming a crowded area of research, no one to our knowledge is developing laminated object manufacturing (LOM) for biological applications. We believe that the ability to easily produce sheets of fibrous PGS which can be laminated together to form larger constructs presents a promising opportunity for future exploration.

Several challenges still exist pertaining to the development of electrospun PGS. First, the electrospinning concentrations and ratios to obtain fibers fall within a narrow window. Polymer solutions outside this range results in electrospraying, total fiber fusion, or fiber dissociation. Thus, tailoring fiber diameter, composition, and morphology is challenging. Increasing porosity within electrospun scaffolds is another challenge that is familiar to most electrospinning techniques. Future work will involve incorporating additional PVA domains that may be removed to yield higher porosity. Finally, the rapid degradation of PGS may not be appropriate for some applications. A collection of poly(polyol sebacate)s have been reported in the literature and combining these may provide the ability to meet degradation requirements.[283]

6.4 FINAL CONCLUSIONS

The body contains amazing complexity that may be taken for granted until we aim to repair it. While creating entire organs de novo may be enticing, it can also be tempting to over-engineer solutions. Complex solutions are challenging to commercialize, ultimately failing to provide therapeutic benefit to patients. The methods described in this dissertation present a simple and versatile technique capable of introducing micropatterns within electrospun scaffolds. This technique was first demonstrated in the context of peripheral nerve guides, resulting in scaffold architecture this was almost indistinguishable from that of native nerve. Additionally, endothelialization of the microvascular network established proof-of-concept and laid the foundation to tackle the daunting challenge of vascularizing electrospun constructs. Finally, electrospun PGS not only addressed material shortcomings relating to templated electrospinning, but also significantly improved strength of PGS scaffolds, impacting a wide range of applications. We anticipate that these results will greatly impact their respective fields while this technology rapidly improves due to the popularity of both tissue engineering and 3D printing.

APPENDIX A

SECTION 5.0 SUPPLEMENTARY FIGURES

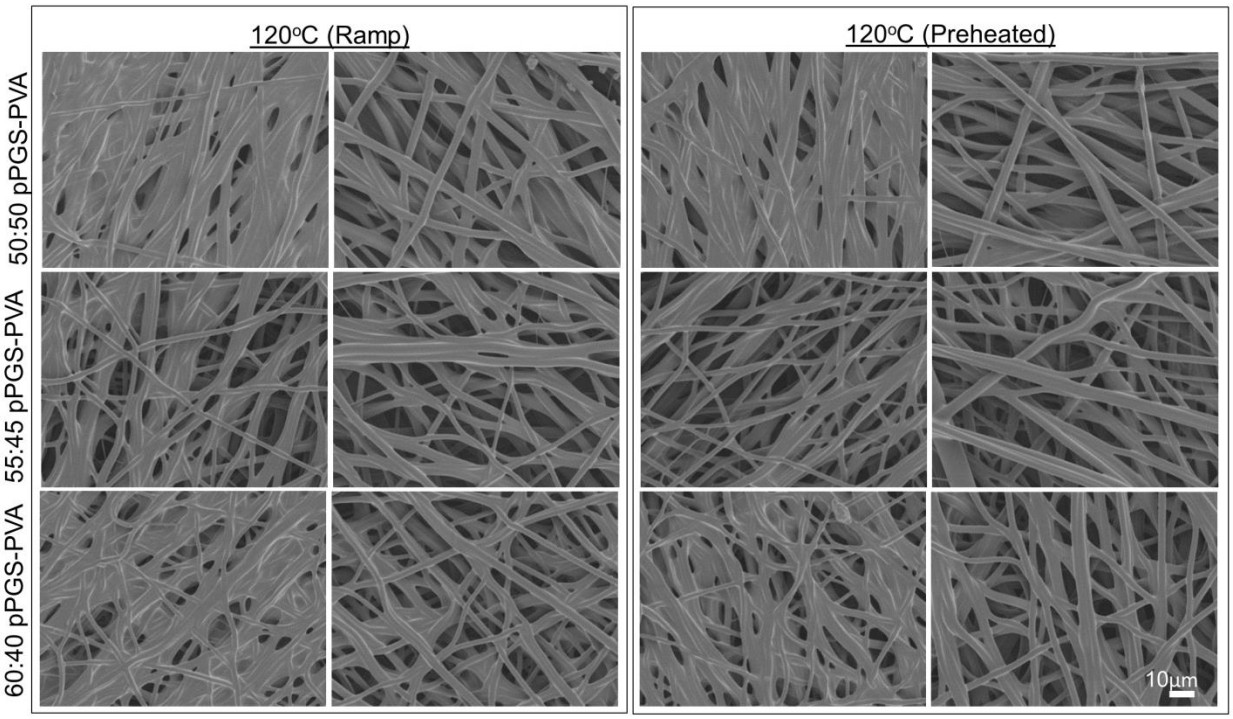

A1. Effect of heating rate and PGS-PVA ratio on fiber morphology. Both the mandrel-contacting and outer surfaces of the fibrous sheets are shown (left/right).

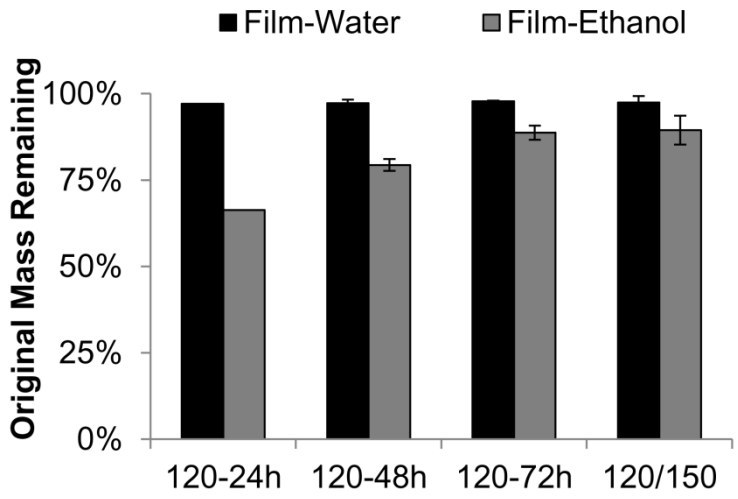

A2. Remaining mass of PGS films washed with water and ethanol. (No error bars for 120-24h since samples stuck together and were grouped in measurement)

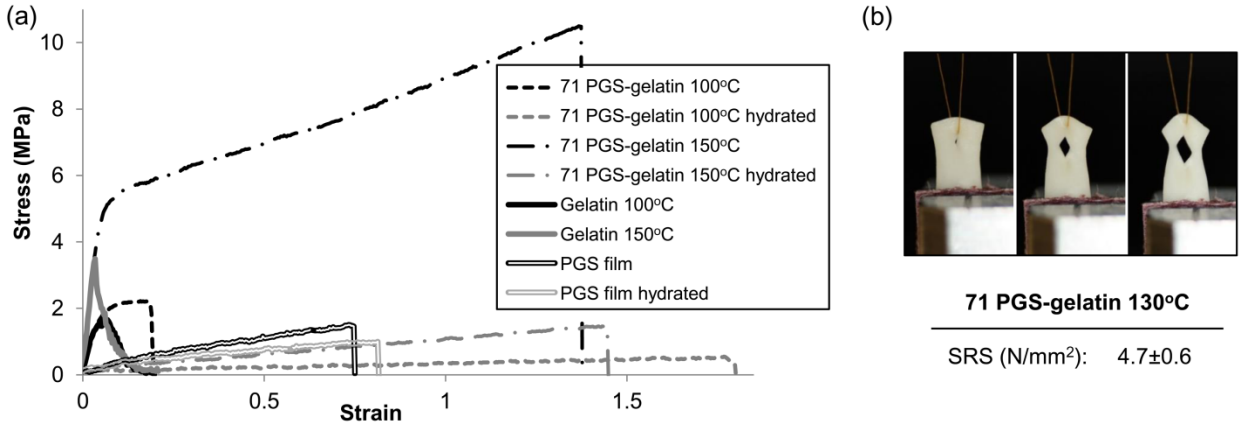

A3. Mechanical Testing of Fibrous Sheets of Electrospun PGS-gelatin blends (71% PGS- 29% Gelatin Type B) crosslinked at 100°C or 150°C for 24h. (a) Tensile testing of PGS-gelatin blends reveals large hydration-dependent changes in mechanical behavior. Hydrated samples are compared to electrospun gelatin (dry) and PGS films controls. Dry PGS-gelatin profiles exhibit stress-strain curves similar to that of gelatin at low strain and PGS at higher strain. Hydrated PGS-gelatin samples exhibit a low modulus similar to PGS and high strain to failure that exceeds PGS films. (b) Suture retention of PGS-gelatin blends shows rapid propagation of the tear defect caused by the suture.

BIBLIOGRAPHY

1. Baiguera, S.; Ribatti, D., Endothelialization approaches for viable engineered tissues. *Angiogenesis* **2013,** 16, (1), 1-14.

2. Badylak, S. F.; Taylor, D.; Uygun, K., Whole-organ tissue engineering: decellularization and recellularization of three-dimensional matrix scaffolds. *Annu Rev Biomed Eng* **2011,** 13, 27-53.

3. Place, E. S.; Evans, N. D.; Stevens, M. M., Complexity in biomaterials for tissue engineering. *Nat Mater* **2009,** 8, (6), 457-70.

4. Shieh, S. J.; Vacanti, J. P., State-of-the-art tissue engineering: from tissue engineering to organ building. *Surgery* **2005,** 137, (1), 1-7.

5. Uygun, B. E.; Yarmush, M. L.; Uygun, K., Application of whole-organ tissue engineering in hepatology. *Nat Rev Gastroenterol Hepatol* **2012,** 9, (12), 738-44.

6. Bae, H.; Puranik, A. S.; Gauvin, R.; Edalat, F.; Carrillo-Conde, B.; Peppas, N. A.; Khademhosseini, A., Building vascular networks. *Sci Transl Med* **2012,** 4, (160), 160ps23.

7. Freyman, T. M.; Yannas, I. V.; Gibson, L. J., Cellular materials as porous scaffolds for tissue engineering. *Progress in Materials Science* **2001,** 46, 273-282.

8. Bettinger, C. J.; Langer, R.; Borenstein, J. T., Engineering substrate topography at the micro- and nanoscale to control cell function. *Angew Chem Int Ed Engl* **2009,** 48, (30), 5406-15.

9. Dvir, T.; Timko, B. P.; Kohane, D. S.; Langer, R., Nanotechnological strategies for engineering complex tissues. *Nat Nanotechnol* **2010,** 6, (1), 13-22.

10. OPTN/SRTR 2012 Annual Data Report. *American Journal of Transplantation* **2013,** 14, (S1), 8-10.

11. Atala, A.; Kasper, F. K.; Mikos, A. G., Engineering complex tissues. *Sci Transl Med* **2012,** 4, (160), 160rv12.

12. Langer, R.; Vacanti, J. P., Tissue engineering. *Science* **1993,** 260, (5110), 920-6.

13. Billiet, T.; Vandenhaute, M.; Schelfhout, J.; Van Vlierberghe, S.; Dubruel, P., A review of trends and limitations in hydrogel-rapid prototyping for tissue engineering. *Biomaterials* **2013,** 33, (26), 6020-41.

14. Xu, T.; Zhao, W.; Zhu, J. M.; Albanna, M. Z.; Yoo, J. J.; Atala, A., Complex heterogeneous tissue constructs containing multiple cell types prepared by inkjet printing technology. *Biomaterials* **2012,** 34, (1), 130-9.

15. Melchels, F. P. W.; Domingos, M. A. N.; Klein, T. J.; Malda, J.; Bartolo, P. J.; Hutmacher, D. W., Additive manufacturing of tissues and organs. *Progress in Polymer Science* **2012,** 37, 1079-1104.

16. Wozniak, M. A.; Chen, C. S., Mechanotransduction in development: a growing role for contractility. *Nat Rev Mol Cell Biol* **2009,** 10, (1), 34-43.

17. Discher, D. E.; Janmey, P.; Wang, Y. L., Tissue cells feel and respond to the stiffness of their substrate. *Science* **2005,** 310, (5751), 1139-43.

18. Engler, A. J.; Sen, S.; Sweeney, H. L.; Discher, D. E., Matrix elasticity directs stem cell lineage specification. *Cell* **2006,** 126, (4), 677-89.

19. Hollister, S. J., Porous scaffold design for tissue engineering. *Nat Mater* **2005,** 4, (7), 518-24.

20. Crapo, P. M.; Gilbert, T. W.; Badylak, S. F., An overview of tissue and whole organ decellularization processes. *Biomaterials* **2011,** 32, (12), 3233-43.

21. Gilbert, T. W.; Freund, J. M.; Badylak, S. F., Quantification of DNA in biologic scaffold materials. *J Surg Res* **2009,** 152, (1), 135-9.

22. Tsuchiya, T.; Balestrini, J. L.; Mendez, J.; Calle, E. A.; Zhao, L.; Niklason, L. E., Influence of pH on Extracellular Matrix Preservation During Lung Decellularization. *Tissue Eng Part C Methods* **2014**.

23. Zhou, P.; Lessa, N.; Estrada, D. C.; Severson, E. B.; Lingala, S.; Zern, M. A.; Nolta, J. A.; Wu, J., Decellularized liver matrix as a carrier for the transplantation of human fetal and primary hepatocytes in mice. *Liver Transpl* **2011,** 17, (4), 418-27.

24. Ren, H.; Shi, X.; Tao, L.; Xiao, J.; Han, B.; Zhang, Y.; Yuan, X.; Ding, Y., Evaluation of two decellularization methods in the development of a whole-organ decellularized rat liver scaffold. *Liver Int* **2013,** 33, (3), 448-58.

25. Hiles, M.; Hodde, J., Tissue engineering a clinically useful extracellular matrix biomaterial. *Int Urogynecol J Pelvic Floor Dysfunct* **2006,** 17 Suppl 1, S39-43.

26. Baptista, P. M.; Siddiqui, M. M.; Lozier, G.; Rodriguez, S. R.; Atala, A.; Soker, S., The use of whole organ decellularization for the generation of a vascularized liver organoid. *Hepatology* **2011,** 53, (2), 604-17.

27. Ott, H. C.; Clippinger, B.; Conrad, C.; Schuetz, C.; Pomerantseva, I.; Ikonomou, L.; Kotton, D.; Vacanti, J. P., Regeneration and orthotopic transplantation of a bioartificial lung. *Nat Med* **2010,** 16, (8), 927-33.

28. Bozkurt, A.; Deumens, R.; Beckmann, C.; Olde Damink, L.; Schugner, F.; Heschel, I.; Sellhaus, B.; Weis, J.; Jahnen-Dechent, W.; Brook, G. A.; Pallua, N., In vitro cell alignment obtained with a Schwann cell enriched microstructured nerve guide with longitudinal guidance channels. *Biomaterials* **2009,** 30, (2), 169-79.

29. Bryers, J. D.; Giachelli, C. M.; Ratner, B. D., Engineering biomaterials to integrate and heal: the biocompatibility paradigm shifts. *Biotechnol Bioeng* **2012,** 109, (8), 1898-911.

30. Kim, Y. T.; Haftel, V. K.; Kumar, S.; Bellamkonda, R. V., The role of aligned polymer fiber-based constructs in the bridging of long peripheral nerve gaps. *Biomaterials* **2008,** 29, (21), 3117-27.

31. Derby, B., Printing and prototyping of tissues and scaffolds. *Science* **2012,** 338, (6109), 921-6.

32. Yarlagadda, P. K.; Chandrasekharan, M.; Shyan, J. Y., Recent advances and current developments in tissue scaffolding. *Biomed Mater Eng* **2005,** 15, (3), 159-77.

33. Fischbach, C.; Chen, R.; Matsumoto, T.; Schmelzle, T.; Brugge, J. S.; Polverini, P. J.; Mooney, D. J., Engineering tumors with 3D scaffolds. *Nat Methods* **2007,** 4, (10), 855-60.

34. Sachlos, E.; Czernuszka, J. T., Making tissue engineering scaffolds work. Review: the application of solid freeform fabrication technology to the production of tissue engineering scaffolds. *Eur Cell Mater* **2003,** 5, 29-39; discussion 39-40.

35. Dalton, P. D.; Woodfield, T.; Hutmacher, D. W., Snapshot: Polymer scaffolds for tissue engineering. *Biomaterials* **2009,** 30, (4), 701.

36. Chan, B. P.; Leong, K. W., Scaffolding in tissue engineering: general approaches and tissue-specific considerations. *Eur Spine J* **2008,** 17 Suppl 4, 467-79.

37. Luo, C. J.; Stoyanov, S. D.; Stride, E.; Pelan, E.; Edirisinghe, M., Electrospinning versus fibre production methods: from specifics to technological convergence. *Chem Soc Rev* **2012,** 41, (13), 4708-35.

38. Burger, C.; Hsiao, B.; Chu, B., Nanofibrous Materials and their Applications. *Annual Review of Material Research* **2006**, (36), 333-368.

39. Rutledge, G. C.; Fridrikh, S. V., Formation of fibers by electrospinning. *Advanced Drug Delivery Reviews* **2007,** 59, 1384-1391.

40. Subbiah, T.; Bhat, G. S.; Tock, R. W.; Parameswaran, S.; Ramkumar, S. S., Electrospinning of Nanofibers. *Journal of Applied Polymer Science* **2004,** 96, 557-569.

41. Huang, Z.-M.; Zhang, Y.-Z.; Kotaki, M.; Ramakrishna, S., A review on polymer nanofibers by electrospinning and their applications in nanocomposites. *Composites Science and Technology* **2003,** 63, 2223-2253.

42. Agarwal, S.; Wendorff, J. H.; Greiner, A., Use of electrospinning technique for biomedical applications. *Polymer* **2008,** 49, (26), 5603-5621.

43. Stankus, J. J.; Guan, J.; Fujimoto, K.; Wagner, W. R., Microintegrating smooth muscle cells into a biodegradable, elastomeric fiber matrix. *Biomaterials* **2006,** 27, (5), 735-44.

44. Ahirwal, D.; Hebraud, A.; Kadar, R.; Wilhelm, M.; Schlatter, G., From self-assembly of electrospun nanofibers to 3D cm thick hierarchical foams. *Soft Matter* **2013,** 9, 3164-3172.

45. Angarano, M.; Schulz, S.; Fabritius, M.; Vogt, R.; Steinberg, T.; Tomakidi, P.; Friedrich, C.; Mulhaupt, R., Layered Gradient Nonwovens of In Situ Crosslinked Electrospun Collagenous Nanofibers Used as Modular Scaffold Systems for Soft Tissue Regeneration. *Advanced Functional Materials* **2013,** 23, 3277-3285.

46. Badrossamay, M. R.; McIlwee, H. A.; Goss, J. A.; Parker, K. K., Nanofiber assembly by rotary jet-spinning. *Nano Lett* **2010,** 10, (6), 2257-61.

47. Blakeney, B. A.; Tambralli, A.; Anderson, J. M.; Andukuri, A.; Lim, D. J.; Dean, D. R.; Jun, H. W., Cell infiltration and growth in a low density, uncompressed three-dimensional electrospun nanofibrous scaffold. *Biomaterials* **2011,** 32, (6), 1583-90.

48. Cai, S.; Xu, H.; Jiang, Q.; Yang, Y., Novel 3D electrospun scaffolds with fibers oriented randomly and evenly in three dimensions to closely mimic the unique architectures of extracellular matrices in soft tissues: fabrication and mechanism study. *Langmuir* **2013,** 29, (7), 2311-8.

49. Shim, I. K.; Jung, M. R.; Kim, K. H.; Seol, Y. J.; Park, Y. J.; Park, W. H.; Lee, S. J., Novel three-dimensional scaffolds of poly(L-lactic acid) microfibers using electrospinning and mechanical expansion: Fabrication and bone regeneration. *J Biomed Mater Res B Appl Biomater* **2010,** 95, (1), 150-60.

50. Xue, J.; Feng, B.; Zheng, R.; Lu, Y.; Zhou, G.; Liu, W.; Cao, Y.; Zhang, Y.; Zhang, W. J., Engineering ear-shaped cartilage using electrospun fibrous membranes of gelatin/polycaprolactone. *Biomaterials* **2013,** 34, (11), 2624-31.

51. Tang, S. K. Y.; Whitesides, G. M., Basic microfluidic and soft lithographic techniques. In *Optofluidics: Fundamentals, Devices, and Applications*, Fainman, Y., Ed. 2009.

52. Kaazempur-Mofrad, M. R. In *A MEMS-Based Renal Replacement System*, Solid-state sensor, actuator and microsystems workshop, 2004; 2004.

53. Xia, Y.; Whitesides, G. M., Soft Lithography. *Annual review of material science* **1998,** 28, (153-184).

54. Qin, D.; Xia, Y.; Whitesides, G. M., Soft lithography for micro- and nanoscale patterning. *Nat Protoc* **2010,** 5, (3), 491-502.

55. Huh, D.; Hamilton, G. A.; Ingber, D. E., From 3D cell culture to organs-on-chips. *Trends Cell Biol* **2011,** 21, (12), 745-54.

56. Chang, R.; Nam, J.; Sun, W., Direct cell writing of 3D microorgan for in vitro pharmacokinetic model. *Tissue Eng Part C Methods* **2008,** 14, (2), 157-66.

57. Whitesides, G. M.; Ostuni, E.; Takayama, S.; Jiang, X.; Ingber, D. E., Soft lithography in biology and biochemistry. *Annu Rev Biomed Eng* **2001,** 3, 335-73.

58. Whitesides, G. M., The origins and the future of microfluidics. *Nature* **2006,** 442, (7101), 368-73.

59. Falconnet, D.; Csucs, G.; Grandin, H. M.; Textor, M., Surface engineering approaches to micropattern surfaces for cell-based assays. *Biomaterials* **2006,** 27, (16), 3044-63.

60. Fidkowski, C.; Kaazempur-Mofrad, M. R.; Borenstein, J.; Vacanti, J. P.; Langer, R.; Wang, Y., Endothelialized microvasculature based on a biodegradable elastomer. *Tissue Eng* **2005,** 11, (1-2), 302-9.

61. Wray, L. S.; Tsioris, K.; Gi, E. S.; Omenetto, F. G.; Kaplan, D. L., Microfabricated Porous Silk Scaffolds for Vascularizing Engineered Tissues. *Adv Funct Mater* **2013,** 23, (27), 3404-3412.

62. Wang, G. J.; Hsueh, C.-C.; Hsu, S.-H.; Hung, H.-S., Fabrication of PLGA microvessel scaffolds with circular microchannels using soft lithography. *Journal of Micromechanics and Microengineering* **2007,** 17.

63. Vozzi, G.; Flaim, C.; Ahluwalia, A.; Bhatia, S., Fabrication of PLGA scaffolds using soft lithography and microsyringe deposition. *Biomaterials* **2003,** 24, (14), 2533-40.

64. Partee, B.; Hollister, S. J.; Das, S., Selective Laser Sintering Process Optimization for Layered Manufacturing of CAPA 6501 Polycaprolactone Bone Engineering Scaffolds. *Journal of Manufacturing Science and Engineering* **2006,** 128, 531-540.

65. Shuai, C.; Gao, C.; Nie, Y.; Hu, H.; Zhou, Y.; Peng, S., Structure and properties of nano-hydroxypatite scaffolds for bone tissue engineering with a selective laser sintering system. *Nanotechnology* **2011,** 22, (28), 285703.

66. Yeong, W. Y.; Sudarmadji, N.; Yu, H. Y.; Chua, C. K.; Leong, K. F.; Venkatraman, S. S.; Boey, Y. C.; Tan, L. P., Porous polycaprolactone scaffold for cardiac tissue engineering fabricated by selective laser sintering. *Acta Biomater* **2010,** 6, (6), 2028-34.

67. Pereira, R. V.; Salmoria, G. V., Scaffolds of PDLLA/Bioglass 58S Produced by Selective Laser Sintering. *Materials Research* **2014**.

68. Kolan, K. C.; Leu, M. C.; Hilmas, G. E.; Brown, R. F.; Velez, M., Fabrication of 13-93 bioactive glass scaffolds for bone tissue engineering using indirect selective laser sintering. *Biofabrication* **2011,** 3, (2), 025004.

69. Duan, B.; Wang, M.; Zhou, W. Y.; Cheung, W. L.; Li, Z. Y.; Lu, W. W., Three-dimensional nanocomposite scaffolds fabricated via selective laser sintering for bone tissue engineering. *Acta Biomater* **2010,** 6, (12), 4495-505.

70. Pattanayak, D. K.; Fukuda, A.; Matsushita, T.; Takemoto, M.; Fujibayashi, S.; Sasaki, K.; Nishida, N.; Nakamura, T.; Kokubo, T., Bioactive Ti metal analogous to human cancellous bone: Fabrication by selective laser melting and chemical treatments. *Acta Biomater* **2011,** 7, (3), 1398-406.

71. Gross, B. C.; Erkal, J. L.; Lockwood, S. Y.; Chen, C.; Spence, D. M., Evaluation of 3D printing and its potential impact on biotechnology and the chemical sciences. *Anal Chem* **2013,** 86, (7), 3240-53.

72. Zhang, A. P.; Qu, X.; Soman, P.; Hribar, K. C.; Lee, J. W.; Chen, S.; He, S., Rapid fabrication of complex 3D extracellular microenvironments by dynamic optical projection stereolithography. *Adv Mater* **2012,** 24, (31), 4266-70.

73. Dean, D.; Jonathan, W.; Siblani, A.; Wang, M. O.; Kim, K.; Mikos, A. G.; Fisher, J. P., Continuous Digital Light Processing (cDLP): Highly Accurate Additive Manufacturing of Tissue Engineered Bone Scaffolds. *Virtual Phys Prototyp* **2012,** 7, (1), 13-24.

74. Ovsianikov, A.; Gruene, M.; Pflaum, M.; Koch, L.; Maiorana, F.; Wilhelmi, M.; Haverich, A.; Chichkov, B., Laser printing of cells into 3D scaffolds. *Biofabrication* **2010,** 2, (1), 014104.

75. Elomaa, L.; Teixeira, S.; Hakala, R.; Korhonen, H.; Grijpma, D. W.; Seppala, J. V., Preparation of poly(epsilon-caprolactone)-based tissue engineering scaffolds by stereolithography. *Acta Biomater* **2011,** 7, (11), 3850-6.

76. Williams, C. G.; Malik, A. N.; Kim, T. K.; Manson, P. N.; Elisseeff, J. H., Variable cytocompatibility of six cell lines with photoinitiators used for polymerizing hydrogels and cell encapsulation. *Biomaterials* **2005,** 26, (11), 1211-8.

77. Atsumi, T.; Fujisawa, S.; Tonosaki, K., (Meth)acrylate monomer-induced cytotoxicity and intracellular Ca(2+) mobilization in human salivary gland carcinoma cells and human gingival fibroblast cells related to monomer hydrophobicity. *Biomaterials* **2006,** 27, (34), 5794-800.

78. Yoshii, E., Cytotoxic effects of acrylates and methacrylates: relationships of monomer structures and cytotoxicity. *J Biomed Mater Res* **1997,** 37, (4), 517-24.

79. Zein, I.; Hutmacher, D. W.; Tan, K. C.; Teoh, S. H., Fused deposition modeling of novel scaffold architectures for tissue engineering applications. *Biomaterials* **2002,** 23, (4), 1169-85.

80. Kim, G. H.; Son, J. G.; Park, S. A.; Kim, W. D., Hybrid process for fabricating 3D hierarchical scaffolds combining rapid prototyping and electrospinning. *Macromolecular rapid communications* **2008**, 1577-1581.

81. Kim, J. Y.; Park, E. K.; Kim, S.-Y.; Shin, J.-W.; Cho, D.-W., Fabrication of a SFF-based three-dimensional scaffold using a precision deposition system in tissue engineering. *Journal of Micromechanics and Microengineering* **2008,** 18.

82. Kim, J. Y.; Jin, G. Z.; Park, I. S.; Kim, J. N.; Chun, S. Y.; Park, E. K.; Kim, S. Y.; Yoo, J.; Kim, S. H.; Rhie, J. W.; Cho, D. W., Evaluation of solid free-form fabrication-based scaffolds seeded with osteoblasts and human umbilical vein endothelial cells for use in vivo osteogenesis. *Tissue Eng Part A* **2010,** 16, (7), 2229-36.

83. Klebe, R. J., Cytoscribing: a method for micropositioning cells and the construction of two- and three-dimensional synthetic tissues. *Exp Cell Res* **1988,** 179, (2), 362-73.

84. Hockaday, L. A.; Kang, K. H.; Colangelo, N. W.; Cheung, P. Y.; Duan, B.; Malone, E.; Wu, J.; Girardi, L. N.; Bonassar, L. J.; Lipson, H.; Chu, C. C.; Butcher, J. T., Rapid 3D printing of anatomically accurate and mechanically heterogeneous aortic valve hydrogel scaffolds. *Biofabrication* **2012,** 4, (3), 035005.

85. Norotte, C.; Marga, F. S.; Niklason, L. E.; Forgacs, G., Scaffold-free vascular tissue engineering using bioprinting. *Biomaterials* **2009,** 30, (30), 5910-7.

86. Xu, T.; Gregory, C. A.; Molnar, P.; Cui, X.; Jalota, S.; Bhaduri, S. B.; Boland, T., Viability and electrophysiology of neural cell structures generated by the inkjet printing method. *Biomaterials* **2006,** 27, (19), 3580-8.

87. Saunders, R. E.; Gough, J. E.; Derby, B., Delivery of human fibroblast cells by piezoelectric drop-on-demand inkjet printing. *Biomaterials* **2008,** 29, (2), 193-203.

88. Moon, S.; Hasan, S. K.; Song, Y. S.; Xu, F.; Keles, H. O.; Manzur, F.; Mikkilineni, S.; Hong, J. W.; Nagatomi, J.; Haeggstrom, E.; Khademhosseini, A.; Demirci, U., Layer by layer three-dimensional tissue epitaxy by cell-laden hydrogel droplets. *Tissue Eng Part C Methods* **2009,** 16, (1), 157-66.

89. Leukers, B.; Gulkan, H.; Irsen, S. H.; Milz, S.; Tille, C.; Schieker, M.; Seitz, H., Hydroxyapatite scaffolds for bone tissue engineering made by 3D printing. *J Mater Sci Mater Med* **2005,** 16, (12), 1121-4.

90. Bose, S.; Vahabzadeh, S.; Bandyopadhyay, A., Bone Tissue engineering using 3D printing. *Materials Today* **2013,** 16, (12).

91. Vozzi, G.; Previti, A.; De Rossi, D.; Ahluwalia, A., Microsyringe-based deposition of two-dimensional and three-dimensional polymer scaffolds with a well-defined geometry for application to tissue engineering. *Tissue Eng* **2002,** 8, (6), 1089-98.

92. Wei, C.; Dong, J., Direct Fabrication of High-Resolution Three-Dimensional Polymeric Scaffolds Using Electrohydrodynamic Hot Jet Plotting. *Journal of Micromechanics and Microengineering* **2013,** 23.

93. Brown, T. D.; Dalton, P. D.; Hutmacher, D. W., Direct writing by way of melt electrospinning. *Adv Mater* **2011,** 23, (47), 5651-7.

94. Sun, D.; Chang, C.; Li, S.; Lin, L., Near-field electrospinning. *Nano Lett* **2006,** 6, (4), 839-42.

95. Schuurman, W.; Khristov, V.; Pot, M. W.; van Weeren, P. R.; Dhert, W. J.; Malda, J., Bioprinting of hybrid tissue constructs with tailorable mechanical properties. *Biofabrication* **2011,** 3, (2), 021001.

96. Xu, T.; Binder, K. W.; Albanna, M. Z.; Dice, D.; Zhao, W.; Yoo, J. J.; Atala, A., Hybrid printing of mechanically and biologically improved constructs for cartilage tissue engineering applications. *Biofabrication* **2013,** 5, (1), 015001.

97. Wang, X.; Ding, B.; Li, B., Biomimetic electrospun nanofibrous structures for tissue engineering. *Materials Today* **2013,** 16, (6).

98. Moroni, L.; Schotel, R.; Hamann, D.; de Wijn, J. R.; van Blitterswijk, C. A., 3D Fiber-Deposited Electrospun Integrated Scaffolds Enhance Cartilage Tissue Formation. *Advanced Functional Materials* **2008,** 18, 53-60.

99. Chen, R.; Morsi, Y.; Patel, S.; Ke, Q.-F.; Mo, X.-M., A novel approach via combination of electrospinning and FDM for tri-leaflet heart valve scaffold fabrication. *Frontiers of Chemistry in China* **2009,** 3, (4), 359-366.

100. Amoroso, N. J.; D'Amore, A.; Hong, Y.; Rivera, C. P.; Sacks, M. S.; Wagner, W. R., Microstructural manipulation of electrospun scaffolds for specific bending stiffness for heart valve tissue engineering. *Acta Biomater* **2012,** 8, (12), 4268-77.

101. Baker, B. M.; Gee, A. O.; Metter, R. B.; Nathan, A. S.; Marklein, R. A.; Burdick, J. A.; Mauck, R. L., The potential to improve cell infiltration in composite fiber-aligned electrospun scaffolds by the selective removal of sacrificial fibers. *Biomaterials* **2008,** 29, (15), 2348-58.

102. Bellan, L. M.; Pearsall, M.; Cropek, D. M.; Langer, R., A 3D interconnected microchannel network formed in gelatin by sacrificial shellac microfibers. *Adv Mater* **2012,** 24, (38), 5187-91.

103. Bellan, L. M.; Strychalski, E. A.; Craighead, H. G., Nanochannels fabricated in polydimethylsiloxane using sacrificial electrospun polyethylene oxide nanofibers. *Journal of Vacuum science technology B* **2008,** 26, 1728-1731.

104. Skotak, M.; Ragusa, J.; Gonzalez, D.; Subramanian, A., Improved cellular infiltration into nanofibrous electrospun cross-linked gelatin scaffolds templated with micrometer-sized polyethylene glycol fibers. *Biomed Mater* **2011,** 6, (5), 055012.

105. Gualandi, C.; Zucchelli, A.; Fernandez Osorio, M.; Belcari, J.; Focarete, M. L., Nanovascularization of polymer matrix: generation of nanochannels and nanotubes by sacrificial electrospun fibers. *Nano Lett* **2013,** 13, (11), 5385-90.

106. Ifkovits, J. L.; Wu, K.; Mauck, R. L.; Burdick, J. A., The influence of fibrous elastomer structure and porosity on matrix organization. *PLoS One* **2010,** 5, (12), e15717.

107. Noble, J.; Munro, C. A.; Prasad, V. S.; Midha, R., Analysis of upper and lower extremity peripheral nerve injuries in a population of patients with multiple injuries. *J Trauma* **1998,** 45, (1), 116-22.

108. Chiona, V.; Tonda-Turo, C.; Ciardelli, G., Artificial Scaffold for Peripheral Nerve Reconstruction. In *Essays on Peripheral Nerve Repair*, Geuna, S.; Tos, P.; Battiston, B., Eds. 2009; Vol. 87, pp 173-198.

109. Yan, H.; Zhang, F.; Chen, M.; Lineaweaver, W., Conduit Luminal Additives for Peripheral Nerve Repair. In *Essays on Peripheral Nerve Repair*, Geuna, S.; Tos, P.; Battiston, B., Eds. 2009; Vol. 87, pp 173-198.

110. Schlosshauer, B.; Dreesmann, L.; Schaller, H. E.; Sinis, N., Synthetic nerve guide implants in humans: a comprehensive survey. *Neurosurgery* **2006,** 59, (4), 740-7; discussion 747-8.

111. Campbell, W. W., Evaluation and management of peripheral nerve injury. *Clin Neurophysiol* **2008,** 119, (9), 1951-65.

112. Kehoe, S.; Zhang, X. F.; Boyd, D., FDA approved guidance conduits and wraps for peripheral nerve injury: A review of materials and efficacy. *Injury* **2011**.

113. Gu, X.; Ding, F.; Yang, Y.; Liu, J., Construction of tissue engineered nerve grafts and their application in peripheral nerve regeneration. *Prog Neurobiol* **2010**.

114. Schmidt, C. E.; Leach, J. B., Neural tissue engineering: strategies for repair and regeneration. *Annu Rev Biomed Eng* **2003,** 5, 293-347.

115. Lee, S. K.; Wolfe, S. W., Peripheral nerve injury and repair. *J Am Acad Orthop Surg* **2000,** 8, (4), 243-52.

116. Flynn, L.; Dalton, P. D.; Shoichet, M. S., Fiber templating of poly(2-hydroxyethyl methacrylate) for neural tissue engineering. *Biomaterials* **2003,** 24, (23), 4265-72.

117. Yao, L.; de Ruiter, G. C.; Wang, H.; Knight, A. M.; Spinner, R. J.; Yaszemski, M. J.; Windebank, A. J.; Pandit, A., Controlling dispersion of axonal regeneration using a multichannel collagen nerve conduit. *Biomaterials* **2010,** 31, (22), 5789-97.

118. Cao, H.; McHugh, K.; Chew, S. Y.; Anderson, J. M., The topographical effect of electrospun nanofibrous scaffolds on the in vivo and in vitro foreign body reaction. *J Biomed Mater Res A* **2009,** 93, (3), 1151-9.

119. Yang, Y.; De Laporte, L.; Rives, C. B.; Jang, J. H.; Lin, W. C.; Shull, K. R.; Shea, L. D., Neurotrophin releasing single and multiple lumen nerve conduits. *J Control Release* **2005,** 104, (3), 433-46.

120. Hu, X.; Huang, J.; Ye, Z.; Xia, L.; Li, M.; Lv, B.; Shen, X.; Luo, Z., A novel scaffold with longitudinally oriented microchannels promotes peripheral nerve regeneration. *Tissue Eng Part A* **2009,** 15, (11), 3297-308.

121. Bozkurt, A.; Brook, G. A.; Moellers, S.; Lassner, F.; Sellhaus, B.; Weis, J.; Woeltje, M.; Tank, J.; Beckmann, C.; Fuchs, P.; Damink, L. O.; Schugner, F.; Heschel, I.; Pallua, N., In vitro assessment of axonal growth using dorsal root ganglia explants in a novel three-dimensional collagen matrix. *Tissue Eng* **2007,** 13, (12), 2971-9.

122. Madaghiele, M.; Sannino, A.; Yannas, I. V.; Spector, M., Collagen-based matrices with axially oriented pores. *J Biomed Mater Res A* **2008,** 85, (3), 757-67.

123. Stokols, S.; Tuszynski, M. H., The fabrication and characterization of linearly oriented nerve guidance scaffolds for spinal cord injury. *Biomaterials* **2004,** 25, (27), 5839-46.

124. de Ruiter, G. C.; Spinner, R. J.; Malessy, M. J.; Moore, M. J.; Sorenson, E. J.; Currier, B. L.; Yaszemski, M. J.; Windebank, A. J., Accuracy of motor axon regeneration across autograft, single-lumen, and multichannel poly(lactic-co-glycolic acid) nerve tubes. *Neurosurgery* **2008,** 63, (1), 144-53; discussion 153-5.

125. Sundback, C.; Hadlock, T.; Cheney, M.; Vacanti, J., Manufacture of porous polymer nerve conduits by a novel low-pressure injection molding process. *Biomaterials* **2003,** 24, (5), 819-30.

126. Wang, A.; Ao, Q.; Cao, W.; Yu, M.; He, Q.; Kong, L.; Zhang, L.; Gong, Y.; Zhang, X., Porous chitosan tubular scaffolds with knitted outer wall and controllable inner structure for nerve tissue engineering. *J Biomed Mater Res A* **2006,** 79, (1), 36-46.

127. Ao, Q.; Wang, A.; Cao, W.; Zhang, L.; Kong, L.; He, Q.; Gong, Y.; Zhang, X., Manufacture of multimicrotubule chitosan nerve conduits with novel molds and characterization in vitro. *J Biomed Mater Res A* **2006,** 77, (1), 11-8.

128. George, P. M.; Saigal, R.; Lawlor, M. W.; Moore, M. J.; LaVan, D. A.; Marini, R. P.; Selig, M.; Makhni, M.; Burdick, J. A.; Langer, R.; Kohane, D. S., Three-dimensional conductive constructs for nerve regeneration. *J Biomed Mater Res A* **2009,** 91, (2), 519-27.

129. He, L.; Zhang, Y.; Zeng, C.; Ngiam, M.; Liao, S.; Quan, D.; Zeng, Y.; Lu, J.; Ramakrishna, S., Manufacture of PLGA multiple-channel conduits with precise hierarchical pore architectures and in vitro/vivo evaluation for spinal cord injury. *Tissue Eng Part C Methods* **2009,** 15, (2), 243-55.

130. Stokols, S.; Sakamoto, J.; Breckon, C.; Holt, T.; Weiss, J.; Tuszynski, M. H., Templated agarose scaffolds support linear axonal regeneration. *Tissue Eng* **2006,** 12, (10), 2777-87.

131. Wang, D. Y.; Huang, Y. Y., Fabricate coaxial stacked nerve conduits through soft lithography and molding processes. *J Biomed Mater Res A* **2008,** 85, (2), 434-8.

132. Madduri, S.; Papaloizos, M.; Gander, B., Trophically and topographically functionalized silk fibroin nerve conduits for guided peripheral nerve regeneration. *Biomaterials* **2010,** 31, (8), 2323-34.

133. Wang, C. Y.; Zhang, K. H.; Fan, C. Y.; Mo, X. M.; Ruan, H. J.; Li, F. F., Aligned natural-synthetic polyblend nanofibers for peripheral nerve regeneration. *Acta Biomater* **2010**.

134. Yang, F.; Murugan, R.; Wang, S.; Ramakrishna, S., Electrospinning of nano/micro scale poly(L-lactic acid) aligned fibers and their potential in neural tissue engineering. *Biomaterials* **2005,** 26, (15), 2603-10.

135. Yao, L.; O'Brien, N.; Windebank, A.; Pandit, A., Orienting neurite growth in electrospun fibrous neural conduits. *J Biomed Mater Res B Appl Biomater* **2009,** 90, (2), 483-91.

136. Chew, S. Y.; Mi, R.; Hoke, A.; Leong, K. W., Aligned Protein-Polymer Composite Fibers Enhance Nerve Regeneration: A Potential Tissue-Engineering Platform. *Adv Funct Mater* **2007,** 17, (8), 1288-1296.

137. Hadlock, T.; Sundback, C.; Hunter, D.; Cheney, M.; Vacanti, J. P., A polymer foam conduit seeded with Schwann cells promotes guided peripheral nerve regeneration. *Tissue Eng* **2000,** 6, (2), 119-27.

138. Zhang, Y.; Luo, H.; Zhang, Z.; Lu, Y.; Huang, X.; Yang, L.; Xu, J.; Yang, W.; Fan, X.; Du, B.; Gao, P.; Hu, G.; Jin, Y., A nerve graft constructed with xenogeneic acellular nerve matrix and autologous adipose-derived mesenchymal stem cells. *Biomaterials* **2010,** 31, (20), 5312-24.

139. Jha, B. S.; Colello, R. J.; Bowman, J. R.; Sell, S. A.; Lee, K. D.; Bigbee, J. W.; Bowlin, G. L.; Chow, W. N.; Mathern, B. E.; Simpson, D. G., Two pole air gap electrospinning: Fabrication of highly aligned, three-dimensional scaffolds for nerve reconstruction. *Acta Biomater* **2011,** 7, (1), 203-15.

140. Biazar, E.; Khorasani, M. T.; Montazeri, N.; Pourshamsian, K.; Daliri, M.; Rezaei, M.; Jabarvand, M.; Khoshzaban, A.; Heidari, S.; Jafarpour, M.; Roviemiab, Z., Types of neural guides and using nanotechnology for peripheral nerve reconstruction. *Int J Nanomedicine* **2010,** 5, 839-52.

141. Clements, I. P.; Kim, Y. T.; English, A. W.; Lu, X.; Chung, A.; Bellamkonda, R. V., Thin-film enhanced nerve guidance channels for peripheral nerve repair. *Biomaterials* **2009,** 30, (23-24), 3834-46.

142. Lietz, M.; Dreesmann, L.; Hoss, M.; Oberhoffner, S.; Schlosshauer, B., Neuro tissue engineering of glial nerve guides and the impact of different cell types. *Biomaterials* **2006,** 27, (8), 1425-36.

143. Mauck, R. L.; Baker, B. M.; Nerurkar, N. L.; Burdick, J. A.; Li, W. J.; Tuan, R. S.; Elliott, D. M., Engineering on the straight and narrow: the mechanics of nanofibrous assemblies for fiber-reinforced tissue regeneration. *Tissue Eng Part B Rev* **2009,** 15, (2), 171-93.

144. Yucel, D.; Kose, G. T.; Hasirci, V., Tissue Engineered, Guided Nerve Tube Consisting of Aligned Neural Stem Cells and Astrocytes. *Biomacromolecules* **2010**.

145. Leach, M. K.; Feng, Z. Q.; Tuck, S. J.; Corey, J. M., Electrospinning fundamentals: optimizing solution and apparatus parameters. *J Vis Exp* **2011**, (47).

146. Ghasemi-Mobarakeh, L.; Prabhakaran, M. P.; Morshed, M.; Nasr-Esfahani, M. H.; Ramakrishna, S., Electrospun poly(epsilon-caprolactone)/gelatin nanofibrous scaffolds for nerve tissue engineering. *Biomaterials* **2008,** 29, (34), 4532-9.

147. Jiang, H.; Hu, Y.; Zhao, P.; Li, Y.; Zhu, K., Modulation of protein release from biodegradable core-shell structured fibers prepared by coaxial electrospinning. *J Biomed Mater Res B Appl Biomater* **2006,** 79, (1), 50-7.

148. Townsend-Nicholson, A.; Jayasinghe, S. N., Cell electrospinning: a unique biotechnique for encapsulating living organisms for generating active biological microthreads/scaffolds. *Biomacromolecules* **2006,** 7, (12), 3364-9.

149. Gamble, H. J., Comparative Electron-Microscopic Observations on the Connective Tissues of a Peripheral Nerve and a Spinal Nerve Root in the Rat. *J Anat* **1964,** 98, 17-26.

150. Gustafson, K. J.; Pinault, G. C.; Neville, J. J.; Syed, I.; Davis, J. A., Jr.; Jean-Claude, J.; Triolo, R. J., Fascicular anatomy of human femoral nerve: implications for neural prostheses using nerve cuff electrodes. *J Rehabil Res Dev* **2009,** 46, (7), 973-84.

151. Terzis; Smith, D. H., *The peripheral nerve. Structure, function, reconstruction*. Raven Press: New York, 1990.

152. Scott, J. B.; Afshari, M.; Kotek, R.; Saul, J. M., The promotion of axon extension in vitro using polymer-templated fibrin scaffolds. *Biomaterials* **2011,** 32, (21), 4830-9.

153. Chen, Y. Y.; McDonald, D.; Cheng, C.; Magnowski, B.; Durand, J.; Zochodne, D. W., Axon and Schwann cell partnership during nerve regrowth. *J Neuropathol Exp Neurol* **2005,** 64, (7), 613-22.

154. Yannas, I. V., *Tissue and organ regeneration in adults*. 2001.

155. Kettenmann, H.; Ransom, B. R., *Neuroglia*. 2005.

156. Brushart, T. M., *Nerve Repair*. 2011.

157. Bolgen, N.; Menceloglu, Y. Z.; Acatay, K.; Vargel, I.; Piskin, E., In vitro and in vivo degradation of non-woven materials made of poly(epsilon-caprolactone) nanofibers prepared by electrospinning under different conditions. *J Biomater Sci Polym Ed* **2005,** 16, (12), 1537-55.

158. Chernousov, M. A.; Yu, W. M.; Chen, Z. L.; Carey, D. J.; Strickland, S., Regulation of Schwann cell function by the extracellular matrix. *Glia* **2008,** 56, (14), 1498-507.

159. Nisbet, D. R.; Forsythe, J. S.; Shen, W.; Finkelstein, D. I.; Horne, M. K., Review paper: a review of the cellular response on electrospun nanofibers for tissue engineering. *J Biomater Appl* **2009,** 24, (1), 7-29.

160. Sundback, C. A.; Shyu, J. Y.; Wang, Y.; Faquin, W. C.; Langer, R. S.; Vacanti, J. P.; Hadlock, T. A., Biocompatibility analysis of poly(glycerol sebacate) as a nerve guide material. *Biomaterials* **2005,** 26, (27), 5454-64.

161. Wang, H. B.; Mullins, M. E.; Cregg, J. M.; McCarthy, C. W.; Gilbert, R. J., Varying the diameter of aligned electrospun fibers alters neurite outgrowth and Schwann cell migration. *Acta Biomaterialia* **2010,** 6, (8), 2970-8.

162. Corey, J. M.; Lin, D. Y.; Mycek, K. B.; Chen, Q.; Samuel, S.; Feldman, E. L.; Martin, D. C., Aligned electrospun nanofibers specify the direction of dorsal root ganglia neurite growth. *J Biomed Mater Res A* **2007,** 83, (3), 636-45.

163. Neal, R. A.; Tholpady, S. S.; Foley, P. L.; Swami, N.; Ogle, R. C.; Botchwey, E. A., Alignment and composition of laminin-polycaprolactone nanofiber blends enhance peripheral nerve regeneration. *J Biomed Mater Res A* **2011**.

164. Gupta, D.; Venugopal, J.; Prabhakaran, M. P.; Dev, V. R.; Low, S.; Choon, A. T.; Ramakrishna, S., Aligned and random nanofibrous substrate for the in vitro culture of Schwann cells for neural tissue engineering. *Acta Biomater* **2009,** 5, (7), 2560-9.

165. Wang, H. B.; Mullins, M. E.; Cregg, J. M.; Hurtado, A.; Oudega, M.; Trombley, M. T.; Gilbert, R. J., Creation of highly aligned electrospun poly-L-lactic acid fibers for nerve regeneration applications. *J Neural Eng* **2009,** 6, (1), 016001.

166. Lim, S. H.; Liu, X. Y.; Song, H.; Yarema, K. J.; Mao, H. Q., The effect of nanofiber-guided cell alignment on the preferential differentiation of neural stem cells. *Biomaterials* **2010,** 31, (34), 9031-9.

167. Chew, S. Y.; Mi, R.; Hoke, A.; Leong, K. W., The effect of the alignment of electrospun fibrous scaffolds on Schwann cell maturation. *Biomaterials* **2008,** 29, (6), 653-61.

168. Spivey, E. C.; Khaing, Z. Z.; Shear, J. B.; Schmidt, C. E., The fundamental role of subcellular topography in peripheral nerve repair therapies. *Biomaterials* **2012,** 33, (17), 4264-76.

169. Toba, T.; Nakamura, T.; Shimizu, Y.; Matsumoto, K.; Ohnishi, K.; Fukuda, S.; Yoshitani, M.; Ueda, H.; Hori, Y.; Endo, K., Regeneration of canine peroneal nerve with the use of a polyglycolic acid-collagen tube filled with laminin-soaked collagen sponge: a comparative study of collagen sponge and collagen fibers as filling materials for nerve conduits. *J Biomed Mater Res* **2001,** 58, (6), 622-30.

170. Lundborg, G.; Dahlin, L.; Dohi, D.; Kanje, M.; Terada, N., A new type of "bioartificial" nerve graft for bridging extended defects in nerves. *J Hand Surg Br* **1997,** 22, (3), 299-303.

171. Ceballos, D.; Navarro, X.; Dubey, N.; Wendelschafer-Crabb, G.; Kennedy, W. R.; Tranquillo, R. T., Magnetically aligned collagen gel filling a collagen nerve guide improves peripheral nerve regeneration. *Exp Neurol* **1999,** 158, (2), 290-300.

172. Yoshii, S.; Ito, S.; Shima, M.; Taniguchi, A.; Akagi, M., Functional restoration of rabbit spinal cord using collagen-filament scaffold. *J Tissue Eng Regen Med* **2009,** 3, (1), 19-25.

173. Koh, H. S.; Yong, T.; Teo, W. E.; Chan, C. K.; Puhaindran, M. E.; Tan, T. C.; Lim, A.; Lim, B. H.; Ramakrishna, S., In vivo study of novel nanofibrous intra-luminal guidance channels to promote nerve regeneration. *J Neural Eng* **2010,** 7, (4), 046003.

174. Cai, J.; Peng, X.; Nelson, K. D.; Eberhart, R.; Smith, G. M., Permeable guidance channels containing microfilament scaffolds enhance axon growth and maturation. *J Biomed Mater Res A* **2005,** 75, (2), 374-86.

175. Stang, F.; Fansa, H.; Wolf, G.; Reppin, M.; Keilhoff, G., Structural parameters of collagen nerve grafts influence peripheral nerve regeneration. *Biomaterials* **2005,** 26, (16), 3083-91.

176. Yoshii, S.; Oka, M.; Shima, M.; Taniguchi, A.; Akagi, M., Bridging a 30-mm nerve defect using collagen filaments. *J Biomed Mater Res A* **2003,** 67, (2), 467-74.

177. Zhu, Y.; Wang, A.; Shen, W.; Patel, S.; Zhang, R.; Young, W. L.; Li, S., Nanofibrous Patches for Spinal Cord Regeneration. *Advanced Functional Materials* **2010,** 20, 1433-1440.

178. Zhu, Y.; Wang, A.; Patel, S.; Kurpinski, K.; Diao, E.; Bao, X.; Kwong, G.; Young, W.; Li, S., Engineering Bi-layer Nanofibrous Conduits for Peripheral Nerve Regeneration. *Tissue Engineering Part C: Methods* **2011**.

179. Subramanian, A.; Krishnan, U. M.; Sethuraman, S., Fabrication of uniaxially aligned 3D electrospun scaffolds for neural regeneration. *Biomed Mater* **2011,** 6, (2), 025004.

180. Hurtado, A.; Cregg, J. M.; Wang, H. B.; Wendell, D. F.; Oudega, M.; Gilbert, R. J.; McDonald, J. W., Robust CNS regeneration after complete spinal cord transection using aligned poly-L-lactic acid microfibers. *Biomaterials* **2012,** 32, (26), 6068-79.

181. Jeffries, E. M.; Wang, Y., Biomimetic micropatterned multi-channel nerve guides by templated electrospinning. *Biotechnol Bioeng* **2012,** 109, (6), 1571-82.

182. Moradzadeh, A.; Borschel, G. H.; Luciano, J. P.; Whitlock, E. L.; Hayashi, A.; Hunter, D. A.; Mackinnon, S. E., The impact of motor and sensory nerve architecture on nerve regeneration. *Exp Neurol* **2008,** 212, (2), 370-6.

183. Ushiki, T.; Ide, C., Three-dimensional organization of the collagen fibrils in the rat sciatic nerve as revealed by transmission- and scanning electron microscopy. *Cell Tissue Res* **1990,** 260, (1), 175-84.

184. Dersch, R.; Liu, T.; Schaper, A. K.; Greiner, A.; Wendorff, J. H., Electrospun nanofibers: internal structure and intrinsic orientation. *Journal of polymer science part A: Polymer Chemistry* **2002,** 41, 545-553.

185. Kakade, M. V.; Givens, S.; Gardner, K.; Lee, K. H.; Chase, D. B.; Rabolt, J. F., Electric field induced orientation of polymer chains in macroscopically aligned electrospun polymer nanofibers. *J Am Chem Soc* **2007,** 129, (10), 2777-82.

186. Secasanu, V. P.; Giardina, C. K.; Wang, Y., A novel electrospinning target to improve the yield of uniaxially aligned fibers. *Biotechnol Prog* **2009,** 25, (4), 1169-75.

187. Schnell, E.; Klinkhammer, K.; Balzer, S.; Brook, G.; Klee, D.; Dalton, P.; Mey, J., Guidance of glial cell migration and axonal growth on electrospun nanofibers of poly-epsilon-caprolactone and a collagen/poly-epsilon-caprolactone blend. *Biomaterials* **2007,** 28, (19), 3012-25.

188. Yang, D.; Lu, B.; Zhao, Y.; Jiang, X., Fabrication of aligned fibrous arrays by magnetic electrospinning. *Advanced Materials* **2007,** 19, 3702-3706.

189. Xie, J.; Li, X.; Lipner, J.; Manning, C. N.; Schwartz, A. G.; Thomopoulos, S.; Xia, Y., "Aligned-to-random" nanofiber scaffolds for mimicking the structure of the tendon-to-bone insertion site. *Nanoscale* **2010,** 2, (6), 923-6.

190. Wen, X.; Tresco, P. A., Effect of filament diameter and extracellular matrix molecule precoating on neurite outgrowth and Schwann cell behavior on multifilament entubulation bridging device in vitro. *J Biomed Mater Res A* **2006,** 76, (3), 626-37.

191. Allen, R. A.; Wu, W.; Yao, M.; Dutta, D.; Duan, X.; Bachman, T. N.; Champion, H. C.; Stolz, D. B.; Robertson, A. M.; Kim, K.; Isenberg, J. S.; Wang, Y., Nerve regeneration and elastin formation within poly(glycerol sebacate)-based synthetic arterial grafts one-year post-implantation in a rat model. *Biomaterials* **2013,** 35, (1), 165-73.

192. Wu, W.; Allen, R. A.; Wang, Y., Fast-degrading elastomer enables rapid remodeling of a cell-free synthetic graft into a neoartery. *Nat Med* **2012,** 18, (7), 1148-53.

193. Huchzermeyer, C.; Berndt, N.; Holzhutter, H. G.; Kann, O., Oxygen consumption rates during three different neuronal activity states in the hippocampal CA3 network. *J Cereb Blood Flow Metab* **2013,** 33, (2), 263-71.

194. Rotem, A.; Toner, M.; Tompkins, R. G.; Yarmush, M. L., Oxygen uptake rates in cultured rat hepatocytes. *Biotechnol Bioeng* **1992,** 40, (10), 1286-91.

195. Yamada, T.; Yang, J. J.; Ricchiuti, N. V.; Seraydarian, M. W., Oxygen consumption of mammalian myocardial cells in culture: measurements in beating cells attached to the substrate of the culture dish. *Anal Biochem* **1985,** 145, (2), 302-7.

196. Jain, R. K.; Au, P.; Tam, J.; Duda, D. G.; Fukumura, D., Engineering vascularized tissue. *Nat Biotechnol* **2005,** 23, (7), 821-3.

197. Kaully, T.; Kaufman-Francis, K.; Lesman, A.; Levenberg, S., Vascularization--the conduit to viable engineered tissues. *Tissue Eng Part B Rev* **2009,** 15, (2), 159-69.

198. Lovett, M.; Lee, K.; Edwards, A.; Kaplan, D. L., Vascularization strategies for tissue engineering. *Tissue Eng Part B Rev* **2009,** 15, (3), 353-70.

199. Lokmic, Z.; Mitchell, G. M., Engineering the microcirculation. *Tissue Eng Part B Rev* **2008,** 14, (1), 87-103.

200. Novosel, E.; Kleinhans, C.; Kluger, P., Vascularization is the key challenge in tissue engineering. *Advanced Drug Delivery Reviews* **2011,** 63, 300-311.

201. Rouwkema, J.; Rivron, N. C.; van Blitterswijk, C. A., Vascularization in tissue engineering. *Trends Biotechnol* **2008,** 26, (8), 434-41.

202. Black, M. J.; Chait, L.; O'Brien, B. M.; Sykes, P. J.; Sharzer, L. A., How soon may the axial vessels of a surviving free flap be safely ligated: a study in pigs. *Brittish Journal of Plastic Surgery* **1978,** 31, (4), 295-299.

203. Stevens, K. R.; Ungrin, M. D.; Schwartz, R. E.; Ng, S.; Carvalho, B.; Christine, K. S.; Chaturvedi, R. R.; Li, C. Y.; Zandstra, P. W.; Chen, C. S.; Bhatia, S. N., InVERT molding for scalable control of tissue microarchitecture. *Nat Commun* **2013,** 4, 1847.

204. Tirella, A.; Orsini, A.; Vozzi, G.; Ahluwalia, A., A phase diagram for microfabrication of geometrically controlled hydrogel scaffolds. *Biofabrication* **2009,** 1, (4), 045002.

205. Billiet, T.; Gevaert, E.; De Schryver, T.; Cornelissen, M.; Dubruel, P., The 3D printing of gelatin methacrylamide cell-laden tissue-engineered constructs with high cell viability. *Biomaterials* **2013,** 35, (1), 49-62.

206. Polykandriotis, E.; Arkudas, A.; Beier, J. P.; Hess, A.; Greil, P.; Papadopoulos, T.; Kopp, J.; Bach, A. D.; Horch, R. E.; Kneser, U., Intrinsic axial vascularization of an osteoconductive bone matrix by means of an arteriovenous vascular bundle. *Plast Reconstr Surg* **2007,** 120, (4), 855-68.

207. Findlay, M. W.; Dolderer, J. H.; Trost, N.; Craft, R. O.; Cao, Y.; Cooper-White, J.; Stevens, G.; Morrison, W. A., Tissue-engineered breast reconstruction: bridging the gap toward large-volume tissue engineering in humans. *Plast Reconstr Surg* **2011,** 128, (6), 1206-15.

208. Zdolsek, J. M.; Morrison, W. A.; Dingle, A. M.; Palmer, J. A.; Penington, A. J.; Mitchell, G. M., An "off the shelf" vascular allograft supports angiogenic growth in three-dimensional tissue engineering. *J Vasc Surg* **2011,** 53, (2), 435-44.

209. Polykandriotis, E.; Arkudas, A.; Horch, R. E.; Sturzl, M.; Kneser, U., Autonomously vascularized cellular constructs in tissue engineering: opening a new perspective for biomedical science. *J Cell Mol Med* **2007,** 11, (1), 6-20.

210. Naik, N.; Kumar, V.; Chaikof, E. L.; Allen, M. G., MEMS-assisted spatially homogeneous endothelialization of a high length-to-depth aspect ratio microvascular network. *Conf Proc IEEE Eng Med Biol Soc* **2011,** 2011, 290-3.

211. Choi, N. W.; Cabodi, M.; Held, B.; Gleghorn, J. P.; Bonassar, L. J.; Stroock, A. D., Microfluidic scaffolds for tissue engineering. *Nat Mater* **2007,** 6, (11), 908-15.

212. Esch, M. B.; Post, D. J.; Shuler, M. L.; Stokol, T., Characterization of in vitro endothelial linings grown within microfluidic channels. *Tissue Eng Part A* **2011,** 17, (23-24), 2965-71.

213. He, J.; Wang, Y.; Liu, Y.; Li, D.; Jin, Z., Layer-by-layer micromolding of natural biopolymer scaffolds with intrinsic microfluidic networks. *Biofabrication* **2013,** 5, (2), 025002.

214. Huang, Z.; Li, X.; Martins-Green, M.; Liu, Y., Microfabrication of cylindrical microfluidic channel networks for microvascular research. *Biomed Microdevices* **2012,** 14, (5), 873-83.

215. Mata, A.; Kim, E. J.; Boehm, C. A.; Fleischman, A. J.; Muschler, G. F.; Roy, S., A three-dimensional scaffold with precise micro-architecture and surface micro-textures. *Biomaterials* **2009,** 30, (27), 4610-7.

216. Moya, M. L.; Hsu, Y. H.; Lee, A. P.; Hughes, C. C.; George, S. C., In vitro perfused human capillary networks. *Tissue Eng Part C Methods* **2013,** 19, (9), 730-7.

217. Ye, X.; Lu, L.; Kolewe, M. E.; Park, H.; Larson, B. L.; Kim, E. S.; Freed, L. E., A biodegradable microvessel scaffold as a framework to enable vascular support of engineered tissues. *Biomaterials* **2013,** 34, (38), 10007-15.

218. Morgan, J. P.; Delnero, P. F.; Zheng, Y.; Verbridge, S. S.; Chen, J.; Craven, M.; Choi, N. W.; Diaz-Santana, A.; Kermani, P.; Hempstead, B.; Lopez, J. A.; Corso, T. N.; Fischbach, C.; Stroock, A. D., Formation of microvascular networks in vitro. *Nat Protoc* **2013,** 8, (9), 1820-36.

219. Zheng, Y.; Chen, J.; Craven, M.; Choi, N. W.; Totorica, S.; Diaz-Santana, A.; Kermani, P.; Hempstead, B.; Fischbach-Teschl, C.; Lopez, J. A.; Stroock, A. D., In vitro microvessels for the study of angiogenesis and thrombosis. *Proc Natl Acad Sci U S A* **2013,** 109, (24), 9342-7.

220. Miller, J. S.; Stevens, K. R.; Yang, M. T.; Baker, B. M.; Nguyen, D. H.; Cohen, D. M.; Toro, E.; Chen, A. A.; Galie, P. A.; Yu, X.; Chaturvedi, R.; Bhatia, S. N.; Chen, C. S., Rapid casting of patterned vascular networks for perfusable engineered three-dimensional tissues. *Nat Mater* **2012,** 11, (9), 768-74.

221. Gillette, B. M.; Jensen, J. A.; Tang, B.; Yang, G. J.; Bazargan-Lari, A.; Zhong, M.; Sia, S. K., In situ collagen assembly for integrating microfabricated three-dimensional cell-seeded matrices. *Nat Mater* **2008,** 7, (8), 636-40.

222. Golden, A. P.; Tien, J., Fabrication of microfluidic hydrogels using molded gelatin as a sacrificial element. *Lab Chip* **2007,** 7, (6), 720-5.

223. Hammer, J.; Han, L. H.; Tong, X.; Yang, F., A facile method to fabricate hydrogels with microchannel-like porosity for tissue engineering. *Tissue Eng Part C Methods* **2014,** 20, (2), 169-76.

224. Park, J. H.; Chung, B. G.; Lee, W. G.; Kim, J.; Brigham, M. D.; Shim, J.; Lee, S.; Hwang, C. M.; Durmus, N. G.; Demirci, U.; Khademhosseini, A., Microporous cell-laden hydrogels for engineered tissue constructs. *Biotechnol Bioeng* **2010,** 106, (1), 138-48.

225. Seto, Y.; Inaba, R.; Okuyama, T.; Sassa, F.; Suzuki, H.; Fukuda, J., Engineering of capillary-like structures in tissue constructs by electrochemical detachment of cells. *Biomaterials* **2010,** 31, (8), 2209-15.

226. Sun, J.; Wang, Y.; Qian, Z.; Hu, C., An approach to architecture 3D scaffold with interconnective microchannel networks inducing angiogenesis for tissue engineering. *J Mater Sci Mater Med* **2011,** 22, (11), 2565-71.

227. Wang, X.-Y.; Jin, Z.-H.; Gan, B.-W.; Lv, S.-W.; Xie, M.; Huang, W.-H., Engineering interconnected 3D vascular networks in hydrogels using molded sodium alginate lattice as the sacrificial template. *Lab Chip* **2014**.

228. Chen, Y. C.; Lin, R. Z.; Qi, H.; Yang, Y.; Bae, H.; Melero-Martin, J. M.; Khademhosseini, A., Functional Human Vascular Network Generated in Photocrosslinkable Gelatin Methacrylate Hydrogels. *Adv Funct Mater* **2012,** 22, (10), 2027-2039.

229. Marino, D.; Luginbuhl, J.; Scola, S.; Meuli, M.; Reichmann, E., Bioengineering dermo-epidermal skin grafts with blood and lymphatic capillaries. *Sci Transl Med* **2014,** 6, (221), 221ra14.

230. Kim, S.; Lee, H.; Chung, M.; Jeon, N. L., Engineering of functional, perfusable 3D microvascular networks on a chip. *Lab Chip* **2013,** 13, (8), 1489-500.

231. Gauvin, R.; Chen, Y. C.; Lee, J. W.; Soman, P.; Zorlutuna, P.; Nichol, J. W.; Bae, H.; Chen, S.; Khademhosseini, A., Microfabrication of complex porous tissue engineering scaffolds using 3D projection stereolithography. *Biomaterials* **2012,** 33, (15), 3824-34.

232. Nahmias, Y.; Schwartz, R. E.; Verfaillie, C. M.; Odde, D. J., Laser-guided direct writing for three-dimensional tissue engineering. *Biotechnol Bioeng* **2005,** 92, (2), 129-36.

233. Tsang, V. L.; Chen, A. A.; Cho, L. M.; Jadin, K. D.; Sah, R. L.; DeLong, S.; West, J. L.; Bhatia, S. N., Fabrication of 3D hepatic tissues by additive photopatterning of cellular hydrogels. *FASEB J* **2007,** 21, (3), 790-801.

234. Blaeser, A.; Duarte Campos, D. F.; Weber, M.; Neuss, S.; Theek, B.; Fischer, H.; Jahnen-Dechent, W., Biofabrication under fluorocarbon: a novel freeform fabrication technique to generate high aspect ratio tissue-engineered constructs. *Biores Open Access* **2013,** 2, (5), 374-84.

235. Cui, X.; Boland, T., Human microvasculature fabrication using thermal inkjet printing technology. *Biomaterials* **2009,** 30, (31), 6221-7.

236. Lee, W.; Lee, V.; Polio, S.; Keegan, P.; Lee, J. H.; Fischer, K.; Park, J. K.; Yoo, S. S., On-demand three-dimensional freeform fabrication of multi-layered hydrogel scaffold with fluidic channels. *Biotechnol Bioeng* **2009,** 105, (6), 1178-86.

237. Muller, D.; Chim, H.; Bader, A.; Whiteman, M.; Schantz, J. T., Vascular guidance: microstructural scaffold patterning for inductive neovascularization. *Stem Cells Int* **2011,** 2011, 547247.

238. Villar, G.; Graham, A. D.; Bayley, H., A tissue-like printed material. *Science* **2013,** 340, (6128), 48-52.

239. Ozbolat, I. T.; Yu, Y., Bioprinting toward organ fabrication: challenges and future trends. *IEEE Trans Biomed Eng* **2013,** 60, (3), 691-9.

240. Chiu, Y.-C.; Larson, J. C.; Perez-Luna, V. H.; Brey, E. M., Formation of microchannels in poly(ethylene glycol) hydrogels by selective degradation of patterned microstructures. *Chemical Material* **2009,** 21, 1677-1682.

241. Ashammakhi, N.; Ndreu, A.; Nikkola, L.; Wimpenny, I.; Yang, Y., Advancing tissue engineering by using electrospun nanofibers. *Regen Med* **2008,** 3, (4), 547-74.

242. Boland, E. D.; Coleman, B. D.; Barnes, C. P.; Simpson, D. G.; Wnek, G. E.; Bowlin, G. L., Electrospinning polydioxanone for biomedical applications. *Acta Biomater* **2005,** 1, (1), 115-23.

243. Liang, D.; Hsiao, B. S.; Chu, B., Functional electrospun nanofibrous scaffolds for biomedical applications. *Adv Drug Deliv Rev* **2007,** 59, (14), 1392-412.

244. Hong, Y.; Takanari, K.; Amoroso, N. J.; Hashizume, R.; Brennan-Pierce, E. P.; Freund, J. M.; Badylak, S. F.; Wagner, W. R., An elastomeric patch electrospun from a blended solution of dermal extracellular matrix and biodegradable polyurethane for rat abdominal wall repair. *Tissue Eng Part C Methods* **2012,** 18, (2), 122-32.

245. Jeffries, E. M.; Wang, Y., Incorporation of parallel electrospun fibers for improved topographical guidance in 3D nerve guides. *Biofabrication* **2013,** 5, (3), 035015.

246. Ortega, I.; Ryan, A. J.; Deshpande, P.; MacNeil, S.; Claeyssens, F., Combined microfabrication and electrospinning to produce 3-D architectures for corneal repair. *Acta Biomater* **2013,** 9, (3), 5511-20.

247. Shi, J.; Wang, L.; Chen, Y., Microcontact printing and lithographic patterning of electrospun nanofibers. *Langmuir* **2009,** 25, (11), 6015-8.

248. Dalton, P. D.; Vaquette, C.; Farrugia, B. L.; Dargaville, T. R.; Brown, T. D.; Hutmacher, D. W., Electrospinning and additive manufacturing: converging technologies. *Biomaterials Science* **2013,** 1, 171-185.

249. Bellan, L. M.; Kniazeva, T.; Kim, E. S.; Epshteyn, A. A.; Cropek, D. M.; Langer, R.; Borenstein, J. T., Fabrication of a hybrid microfluidic system incorporating both lithographically

patterned microchannels and a 3D fiber-formed microfluidic network. *Adv Healthc Mater* **2012,** 1, (2), 164-167.

250. Baker, M. I.; Walsh, S. P.; Schwartz, Z.; Boyan, B. D., A review of polyvinyl alcohol and its uses in cartilage and orthopedic applications. *J Biomed Mater Res B Appl Biomater* **2012,** 100, (5), 1451-7.

251. Finne-Wistrand, A.; Albertsson, A. C.; Kwon, O. H.; Kawazoe, N.; Chen, G.; Kang, I. K.; Hasuda, H.; Gong, J.; Ito, Y., Resorbable scaffolds from three different techniques: electrospun fabrics, salt-leaching porous films, and smooth flat surfaces. *Macromol Biosci* **2008,** 8, (10), 951-9.

252. Lee, S. J.; Liu, J.; Oh, S. H.; Soker, S.; Atala, A.; Yoo, J. J., Development of a composite vascular scaffolding system that withstands physiological vascular conditions. *Biomaterials* **2008,** 29, (19), 2891-8.

253. Hakimi, O.; Murphy, R.; Stachewicz, U.; Hislop, S.; Carr, A. J., An electrospun polydioxanone patch for the localisation of biological therapies during tendon repair. *Eur Cell Mater* **2012,** 24, 344-57; discussion 357.

254. Rnjak-Kovacina, J.; Weiss, A. S., Increasing the pore size of electrospun scaffolds. *Tissue Eng Part B Rev* **2011,** 17, (5), 365-72.

255. Herbert, S. P.; Stainier, D. Y., Molecular control of endothelial cell behaviour during blood vessel morphogenesis. *Nat Rev Mol Cell Biol* **2011,** 12, (9), 551-64.

256. Burton, A. C., On the physical equilibrium of small blood vessels. *Am J Physiol* **1951,** 164, (2), 319-29.

257. Dalton, P. D.; Klinkhammer, K.; Salber, J.; Klee, D.; Moller, M., Direct in vitro electrospinning with polymer melts. *Biomacromolecules* **2006,** 7, (3), 686-90.

258. Liu, Y.; Li, X.; Qu, X.; Zhu, L.; He, J.; Zhao, Q.; Wu, W.; Li, D., The fabrication and cell culture of three-dimensional rolled scaffolds with complex micro-architectures. *Biofabrication* **2012,** 4, (1), 015004.

259. Sabir, M. I.; Xu, X.; Li, L., A review on biodegradable polymeric materials for bone tissue engineering applications. *Journal of Material Science* **2009,** 44, 5713-5724.

260. Li, Y.; Thouas, G. A.; Chen, Q.-Z., Biodegradable soft elastomers: synthesis/properties of materials and fabrication of scaffolds. *Royal Society of Chemistry* **2012,** 2, 8229-8242.

261. Rai, R.; Tallawi, M.; Grigore, A.; Boccaccini, A. R., Synthesis, properties and biomedical applications of poly(glycerol sebacate) (PGS): A review. *Progress in Polymer Science* **2012,** 37, 1051-1078.

262. Chen, Q. Z.; Ishii, H.; Thouas, G. A.; Lyon, A. R.; Wright, J. S.; Blaker, J. J.; Chrzanowski, W.; Boccaccini, A. R.; Ali, N. N.; Knowles, J. C.; Harding, S. E., An elastomeric patch derived

from poly(glycerol sebacate) for delivery of embryonic stem cells to the heart. *Biomaterials* **2010,** 31, (14), 3885-93.

263. Redenti, S.; Neeley, W. L.; Rompani, S.; Saigal, S.; Yang, J.; Klassen, H.; Langer, R.; Young, M. J., Engineering retinal progenitor cell and scrollable poly(glycerol-sebacate) composites for expansion and subretinal transplantation. *Biomaterials* **2009,** 30, (20), 3405-14.

264. Wang, Y.; Ameer, G. A.; Sheppard, B. J.; Langer, R., A tough biodegradable elastomer. *Nat Biotechnol* **2002,** 20, (6), 602-6.

265. Mitsak, A. G.; Dunn, A. M.; Hollister, S. J., Mechanical characterization and non-linear elastic modeling of poly(glycerol sebacate) for soft tissue engineering. *J Mech Behav Biomed Mater* **2012,** 11, 3-15.

266. Bettinger, C. J., Biodegradable elastomers for tissue engineering and cell-biomaterial interactions. *Macromol Biosci* **2011,** 11, (4), 467-82.

267. Yi, F.; LaVan, D. A., Poly(glycerol sebacate) nanofiber scaffolds by core/shell electrospinning. *Macromol Biosci* **2008,** 8, (9), 803-6.

268. Sant, S.; Hwang, C. M.; Lee, S. H.; Khademhosseini, A., Hybrid PGS-PCL microfibrous scaffolds with improved mechanical and biological properties. *J Tissue Eng Regen Med* **2010**.

269. Li, Y.; Cook, W. D.; Moorhoff, C.; Huang, W.-C.; Chen, Q.-Z., Synthesis, characterization and properties of biocompatible poly(glycerol sebacate) pre-polymer and gel. *Polymer international* **2013,** 62, 534-547.

270. Ifkovits, J. L.; Devlin, J. J.; Eng, G.; Martens, T. P.; Vunjak-Novakovic, G.; Burdick, J. A., Biodegradable fibrous scaffolds with tunable properties formed from photo-cross-linkable poly(glycerol sebacate). *ACS Appl Mater Interfaces* **2009,** 1, (9), 1878-86.

271. Ravichandran, R.; Venugopal, J. R.; Sundarrajan, S.; Mukherjee, S.; Ramakrishna, S., Poly(Glycerol sebacate)/gelatin core/shell fibrous structure for regeneration of myocardial infarction. *Tissue Eng Part A* **2011,** 17, (9-10), 1363-73.

272. Liu, T.; Teng, W. K.; Chan, B. P.; Chew, S. Y., Photochemical crosslinked electrospun collagen nanofibers: synthesis, characterization and neural stem cell interactions. *J Biomed Mater Res A* **2010,** 95, (1), 276-82.

273. Xu, B.; Rollo, B.; Stamp, L. A.; Zhang, D.; Fang, X.; Newgreen, D. F.; Chen, Q., Non-linear elasticity of core/shell spun PGS/PLLA fibres and their effect on cell proliferation. *Biomaterials* **2013,** 34, (27), 6306-17.

274. Sant, S.; Iyer, D.; Gaharwar, A. K.; Patel, A.; Khademhosseini, A., Effect of biodegradation and de novo matrix synthesis on the mechanical properties of valvular interstitial cell-seeded polyglycerol sebacate-polycaprolactone scaffolds. *Acta Biomater* **2013,** 9, (4), 5963-73.

275. Kharaziha, M.; Nikkhah, M.; Shin, S. R.; Annabi, N.; Masoumi, N.; Gaharwar, A. K.; Camci-Unal, G.; Khademhosseini, A., PGS:Gelatin nanofibrous scaffolds with tunable mechanical and structural properties for engineering cardiac tissues. *Biomaterials* **2013,** 34, (27), 6355-66.

276. Chaouat, M.; Le Visage, C.; Baille, W. E.; Escoubet, B.; Chaubet, F.; Mateescu, M. A.; Letourneur, D., A novel cross-linked poly(vinyl-alcohol) (PVA) for vascular grafts. *Advanced Functional Materials* **2008,** 18, (2855-2861).

277. Hassan, C. M.; Peppas, N. A., Structure and applications of Poly(vinyl alcohol) hydrogels produced by conventional crosslinking or by freezing/thawing methods. *Advances in Polymer Science* **2000,** 153, 37-65.

278. Teo, W. E.; Ramakrishna, S., A review on electrospinning design and nanofibre assemblies. *Nanotechnology* **2006,** 17, (14), R89-R106.

279. LeBlon, C. E.; Pai, R.; Fodor, C. R.; Golding, A. S.; Coulter, J. P.; Jedlicka, S. S., In Vitro Comparative Biodegradation Analysis of Salt-Leached Porous Polymer Scaffolds. *Journal of Applied Polymer Science* **2012**.

280. Jaafar, I. H.; Ammar, M. M.; Jedlicka, S. S.; Pearson, R. A.; Coulter, J. P., Spectroscopic evaluation, thermal, and thermomechanical characterization of poly(glycerol-sebacate) with variations in curing temperatures and durations. *Journal of Material Science* **2010,** 45, 2525-2529.

281. Marsano, A.; Maidhof, R.; Wan, L. Q.; Wang, Y.; Gao, J.; Tandon, N.; Vunjak-Novakovic, G., Scaffold stiffness affects the contractile function of three-dimensional engineered cardiac constructs. *Biotechnol Prog* **2010,** 26, (5), 1382-90.

282. Yeung, T.; Georges, P. C.; Flanagan, L. A.; Marg, B.; Ortiz, M.; Funaki, M.; Zahir, N.; Ming, W.; Weaver, V.; Janmey, P. A., Effects of substrate stiffness on cell morphology, cytoskeletal structure, and adhesion. *Cell Motil Cytoskeleton* **2005,** 60, (1), 24-34.

283. Bruggeman, J. P.; de Bruin, B. J.; Bettinger, C. J.; Langer, R., Biodegradable poly(polyol sebacate) polymers. *Biomaterials* **2008,** 29, (36), 4726-35.